

HISTORIC AMERICAN ENGINEERING RECORD

STRENGTH OF BURR-ARCH TRUSSES

HAER No. OH-138

LOCATION: 10900 Euclid Avenue, Cuyahoga County, Ohio

The Burr-arch truss model was located at latitude 41.502462, longitude -81.606395. The coordinates represent the approximate location of the model when it was installed inside the Vanderhoof-Schuette Structural Laboratory, on the campus of Case Western Reserve University (CWRU). The coordinates were obtained in 2015 by plotting the laboratory location in Google Earth. There is no restriction on its release to the public.

SIGNIFICANCE: Beginning about 1804, Theodore Burr (1771-1822) built wooden covered bridges that combined a multiple-kingpost truss with an arch into one structural form. The Burr-arch truss is now the most common type in the inventory of extant nineteenth-century covered bridges in the United States. However, there is considerable variability in the geometric parameters and details used for actual bridges. Results of a survey of thirty Burr-arch truss bridges were used to design and fabricate a 2/3 scale symmetry model of a Burr-arch truss. This model was load-tested to investigate the behavior of Burr-arch trusses at strength. The overall observations from the tests are that strength is connection-controlled, flaw-controlled, and generally brittle. Some general principles of strength limit state analyses of structural systems are presented in the context of Burr-arch trusses.

AUTHORS: Dario Gasparini, Stacey Hursen, Gregory Willenkin, Kamil Nizamiev, 2015

PROJECT INFORMATION: The National Covered Bridges Recording Project is part of the Historic American Engineering Record (HAER), a long-range program to document historically significant engineering and industrial works in the United States. HAER is administered by the Heritage Documentation Programs Division (Richard O'Connor, Chief), a division of the National Park Service (NPS), U.S. Department of the Interior. The Federal Highway Administration's National Historic Covered Bridge Preservation Program (NHCBP) funded the project (Sheila Duwadi, administrator).

The Strength of Burr-Arch Trusses research project was facilitated through Cooperative Agreement No. P10AC00630, between NPS and CWRU. Christopher H. Marston, HAER Architect, served as project

leader. Prof. Dario Gasparini developed and led the research, with Case Western Reserve University engineering students Stacey Hursen, Gregory Willenkin, and Kamil Nizamiev. Rudy Christian constructed the truss model, assisted by his wife Laura and Andrew Schaeffer. David Simmons, James Cooper, Campbell Fitzhugh, and Linda Gasparini assisted with the survey of Burr-arch truss bridges in Ohio, Indiana, and Pennsylvania.

TABLE OF CONTENTS

INTRODUCTION	4
REVIEW OF STUDIES RELATED TO STRUCTURAL BEHAVIOR OF BURR-ARCH TRUSSES	5
ASPECTS OF STRENGTH LIMIT STATE ANALYSES OF STRUCTURAL SYSTEMS	34
DESIGN OF BURR-ARCH TRUSS MODEL	39
PURCHASE OF WOOD MATERIAL AND FABRICATION OF MODEL	43
SMALL SCALE TESTS TO INFER MATERIAL PROPERTIES	45
LINEAR ELASTIC STRUCTURAL ANALYSES	54
DESIGN AND FABRICATION OF TEST FIXTURE	59
ASSEMBLY, INSTALLATION OF MODEL, AND INSTRUMENTATION	66
STRENGTH TESTS	73
OBSERVATIONS	86
RECOMMENDATIONS	90
ACKNOWLEDGEMENTS	91
REFERENCES	91
APPENDIX – A – DRAWINGS	94

INTRODUCTION

Understanding the structural behavior of Theodore Burr's bridge design has challenged engineers since its first use at the beginning of the nineteenth century. Even its name is problematic; should it be called a truss, an arch, an arch-truss, or a truss-arch? Herein it is simply called a Burr-arch truss. It is an undeniably effective, durable design in view of the fact that it is the most common form in the inventory of extant nineteenth-century covered bridges in the United States. But engineering understanding of the structural behavior and strength of Burr-arch trusses has remained elusive. There are several valid reasons for this. For one, wood is a complex material; it is cellular, inhomogeneous, anisotropic, viscous, and hygroscopic, and contains flaws, principally knots and cracks (or checks, shakes, and splits). Its stress-strain properties are highly variable, even within one species or one grade. Mathematical material stress-strain models that can capture all these features are complex and practically infeasible. There is a paucity of experimental data on the structural performance of wood members, traditional timber joints, and complete systems. This lack of comprehensive experimental structural performance data means that engineers must make very conservative estimates of structural behavior, especially strength. A Burr-arch truss is statically indeterminate, which means that equilibrium equations are not sufficient for performing structural analyses unless some simplifying assumptions are made. In general, a mathematical stress-strain or constitutive model for wood must also be defined. An additional complication is that the diagonal members are "contact" elements; that is, they cannot carry tensile forces. If, in fact, some diagonal members "lose contact" under some load conditions, the system behaves non-linearly. The structural behavior of Burr-arch trusses depends critically on how connections are made. The most important are the arch-to-post, arch-to-chord, post-to-chord, bottom chord tensile splices, and the effective eccentricities of the diagonals relative to the post and chord centerlines.

The history of the Burr-arch truss is well-documented; therefore this report focuses primarily on structural engineering knowledge and understanding. It provides a synthesis of previous studies on the structural behavior of Burr-arch trusses and documents the work performed at Case Western Reserve University (CWRU) as part of NPS-CWRU Cooperative Agreement P10AC00630, funded by the FHWA National Historic Covered Bridge Preservation Program

(NHCBP). The overall objective of this work is to improve engineering understanding of Burr-arch trusses and, in consequence, load rating and rehabilitation technologies.

REVIEW OF STUDIES RELATED TO THE STRUCTURAL BEHAVIOR OF BURR-ARCH TRUSSES

By necessity, individual studies have focused on one or a few aspects of structural behavior and generally fall into the following categories: wood mechanical properties and mathematical modeling; Burr-arch truss conceptual design variations; behavior of members; behavior of connections; structural analysis models and analysis-based observations on system behavior; and experimental studies of Burr-arch trusses.

A brief review of some studies in each of the above areas is as follows.

Wood mechanical properties and modeling – There is a mostly-sublimated conflict among various stakeholders in the process of maintaining the legacy of covered wooden bridges. Some think only solid sawn lumber should be used; others think glued-laminated products are acceptable. Glued-laminated products have better, and less variable, mechanical properties and fewer flaws; but of course were not available in the nineteenth century when most historic wooden covered bridges were built. The brief discussion here is limited to solid sawn lumber, which, as noted previously, is cellular, inhomogeneous, anisotropic, viscous, and hygroscopic, and generally has knots and cracks. Moreover, it is generally observed that nineteenth-century, old-growth, quarter-sawn, seasoned heavy sawn timber sections were better than those currently available for rehabilitation or new covered bridge construction. The most common wood species used for historic covered bridges were Eastern white pine and Southern yellow pine, with some hardwood components. Today, Douglas fir is commonly used for rehabilitation and new designs. Common mechanical properties of most species are given in the *Wood Handbook* of the Forest Products Laboratory.¹ A variety of wood stress-strain or constitutive models may be adopted, of varying complexity and predictive capabilities. The most common is the linear-elastic-isotropic

¹ Forest Products Laboratory, *Wood Handbook—Wood as an Engineering Material*, General Technical Report FPL-GTR-190 (Madison, WI: U.S. Department of Agriculture, Forest Service, Forest Products Laboratory, 2010), available at http://www.fpl.fs.fed.us/documnts/fplgtr/fpl_gtr190.pdf, accessed 1 September 2015.

constitutive model. This model is often used for planar or three-dimensional beam finite element models of entire trusses. Such models generally can provide acceptable predictions of short term global displacements and member forces. Of course the elastic constants are a function of the wood moisture content and there is considerable variability in their values.

Mathematical models of joints or connections generally require anisotropic material models that reflect the axial, radial, and tangential microstructure of wood. For example, Rachel Sangree and Benjamin Schafer used a linear-elastic-orthotropic material model to study stress states in scarf joints.² Linear elastic models, whether isotropic or anisotropic, do not predict redistribution of stresses/forces from wood viscosity or absorption/desorption of moisture (swelling/shrinkage). Temporal changes in member forces or strains may be estimated by using linear viscoelastic material models. Kenneth Fridley provides linear viscoelastic material properties for Douglas fir in the context of prediction of long-term increases in displacements from wood creep.³ Dario Gasparini, Jay Bruckner, and Francesca daPorto used linear viscoelastic models to predict temporal changes in element forces in post-tensioned Howe trusses.⁴ Linear elastic or viscoelastic material models do not predict strength; additional models must be adopted to do so. The strength behavior of a cellular material like wood is complex.⁵ A failure mode can be either ductile or brittle, depending on the stress state, the loading rate, and the moisture content. Failure can occur over time from viscous changes in strains under sustained loading. In addition, homogeneous constitutive and strength models do not capture the presence and effects of flaws such as knots and cracks, which often control the actual strength. These complexities make estimates of wood member or connection or system strength uncertain, with unknown levels of conservatism.

Burr-arch truss conceptual design variations – Joseph Conwill examined the considerable variability in the details used to build Burr-arch trusses in a 2005 article published in *Timber*

² Rachel H. Sangree and Benjamin W. Schafer, “Experimental and numerical analysis of a halved and tabled traditional timber scarf joint,” *Construction and Building Materials* 23 (2009): 615-624.

³ Kenneth J. Fridley, “Designing for Creep in Wood Structures,” *Forest Products Journal* 42, no. 3 (1992): 23-28.

⁴ Dario Gasparini, Jay Bruckner, and Francesca da Porto, “Time-Dependent Behavior of Posttensioned Wood Howe Bridges,” *Journal of Structural Engineering* 132, no. 3 (2006): 418–29.

⁵ Lorna J. Gibson and Michael F. Ashby, *Cellular Solids* (Oxford: Pergamon Press, 1988).

*Framing.*⁶ He discussed typical joint details and common member sizes. As part of this research, to help define a suitable structural model, twenty-one Burr-arch truss bridges in Indiana, Ohio, and Pennsylvania were inspected. David Simmons and James Cooper assisted with the organization and inspection of the Indiana and Ohio bridges. Campbell Fitzhugh and Linda Gasparini assisted with the organization and inspection of the Pennsylvania bridges. The inspected bridges are listed in Table 1.

Name	County	ST	Date	HABS/HAER #	World Guide #
Duck Creek Aqueduct	Franklin	IN	1847	HAER IN-108	14-24-11
Deer's Mill	Montgomery	IN	1878	HAER IN-28	14-54-03
Jackson	Parke	IN	1861	HAER IN-48	14-61-28
Mansfield	Parke	IN	1867	HAER IN-44	14-61-20
Nevins	Parke	IN	1920		14-61-05
Crooks	Parke	IN	1856		14-61-17
Norris Ford	Rush	IN	1916		14-70-08
Offutt's Ford	Rush	IN	1884		14-70-02
Smith	Rush	IN	1877		14-70-01
Bebb Park	Butler	OH	1868		35-09-02
Roberts	Preble	OH	1829		35-68-05
Red	Berks	PA	1867		38-06-06
Griesemer Mill	Berks	PA	1868	HABS PA-1020	38-06-03
Dreibelbis Station	Berks	PA	1869	HAER PA-587	38-06-07
Pool Forge	Berks	PA	1859		38-36-01
Weaver's Mill	Lancaster	PA	1878		38-36-02
Erb's	Lancaster	PA	1887		38-36-34
Ramp	Cumberland	PA	1870		38-21-11
Claycomb	Bedford	PA	1884		38-05-12
Turner	Bedford	PA	1892		38-05-19
Bells Mills	Westmoreland	PA	1850		38-65-01

Table 1 – Inspected Burr-arch truss bridges

In addition, published drawings for the Waterford-Lansingburgh (New York), Pine Grove (HAER PA-586), Barrackville (HAER WV-8), Gilpin's Falls (HAER MD-174), Bartram's (HABS PA-1108), Smith's (HABS DE-1), Johnson's Mill (HABS PA-1173), Zacke Cox

⁶ Joseph D. Conwill, "Burr Truss Framing," *Timber Framing* 78 (December 2005): 4–11.

(Indiana), and Detter's Mill (HABS PA-5184) were reviewed. The inspections and reviews are the bases for the following observations.

Two important global geometric parameters of a Burr-arch truss bridge are the depth-to-span ratio of the multiple-kingpost truss and the rise-to-span ratio of the arches, as shown in Fig. 1.

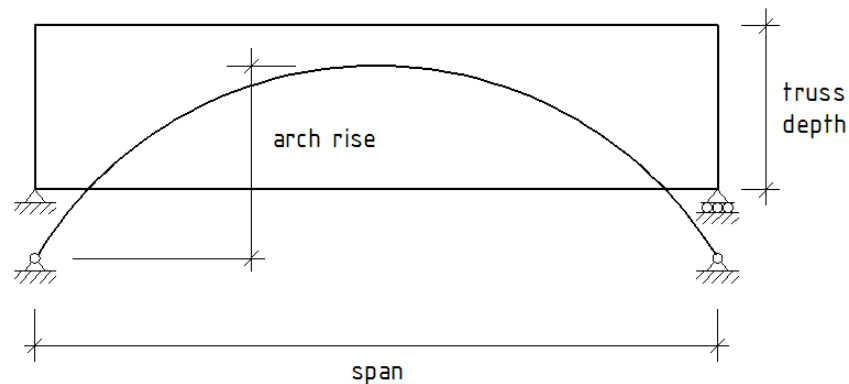


Fig. 1 – Important geometric parameters of Burr-arch truss bridges

Larger values of these two parameters provide larger vertical stiffness. Arch rise-to-span ratios were measured for sixteen bridges; the data are given in Table 2.

Bridge name	Approximate clear span - feet	Approximate arch rise -feet	Rise/span ratio
Roberts	68	15.8	1 / 4.3
Erb's	80	12.8	1 / 6.3
Weaver's Mill	88	13.1	1 / 6.7
Turner	88.3	13.5	1 / 6.5
Pool Forge	99	11.1	1 / 8.9
Bells Mills	107	14.5	1 / 7.4
Crooks	120	17.8	1 / 6.7
Smith	124	18.7	1 / 6.6
Mansfield	125	17.0	1 / 7.4
Ramp	129	13.0	1 / 9.9
Deer's Mill	135	15.5	1 / 8.7
Griesemer Mill	141	14.5	1 / 9.7
Nevins	150	20.2	1 / 7.4
Mansfield	176	19	1 / 9.3
Dreibelbis Station	190	15.8	1 / 12.0
Red	198	16.1	1 / 12.3

Table 2 – Arch rise-to-span ratios

They varied from approximately 1/4.3 for the smallest span to 1/12.3 for the longest span measured. For five spans in the range 100' to 125', the arch rise-to-span ratio varied from 1/6.6 to 1/8.9, with an average of 1/7.4. The truss depth-to-span ratio may in fact be determined by clearance requirements, especially for shorter spans. For spans between 90' and 110', the measured truss depth-to-span ratios varied from 1/6.5 to 1/8.9. A typical Burr-arch truss bridge consists of two trusses, and each truss is “sandwiched” between two arches, one on each side of the truss. However, there are designs that use four or more arches per truss. Although most trusses have posts that are perpendicular to the chords, there are some extant bridges that have inclined posts not perpendicular to the chords. Framing for inclined posts is clearly more complex, and the structural advantages of inclined posts are not self-evident. Given the relative structural complexity of Burr-arch truss bridges, member sizes were historically determined by observation and experience and by geometric constraints imposed by the Burr form. For example, the arches that sandwich the trusses made uniformity in truss member sizes desirable, especially for the dimension perpendicular to the plane of the truss.

The shape of the arch axis also affects structural behavior. It is easiest to lay out a circular arc, if it fits within the geometry of the bridge. However, it is well-known (although perhaps not widely so in the nineteenth century among bridge builders) that, for the particular case of a uniformly distributed vertical load on the horizontal roadway, a parabolic arch is more efficient in the sense that it can satisfy equilibrium with primarily axial forces and smaller bending moments. For non-uniform gravity loads, this advantage of the parabolic shape is no longer present. Detailed measurements to determine whether parabolic or circular arches were used were not made during the inspections for this study. Conwill stated that Burr arches “normally follow a circular arc rather than a parabola,” although in some bridges the arches are “poorly formed.”⁷ Typically, the arches intersect the bottom chord near the end panels as shown in Fig. 1 and then bear on the abutments. In the Zacke Cox Bridge in Indiana, the arches intersect the bottom chord *outside* the end posts.

There is considerable variability in the connection details that were used.

⁷ Conwill, “Burr Truss Framing,” 5.

Arch-to-post – This connection controls the load transfer between the post and the arch. Fig. 2 shows the principal parameters.

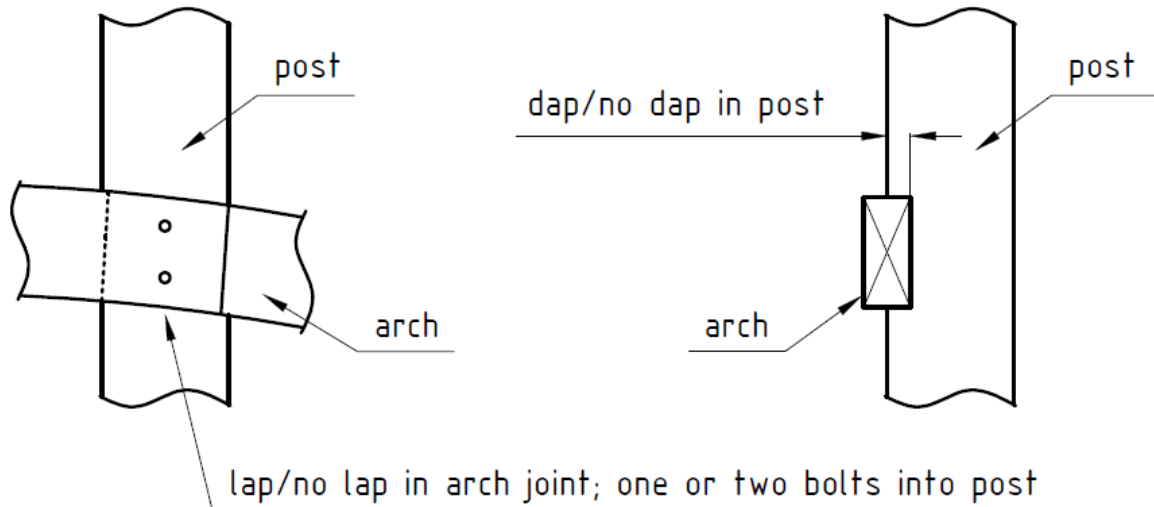


Fig. 2 – Post-to-arch connection

Generally one or two through bolts are used at the arch-post intersection. Splices between arch segments, usually required at every other post, may use laps or the sections may simply abut. The arch may or may not be dapped into the post. If daps are used, the ability of the connection to transfer gravity load into the arches is improved, but daps increase the difficulty of passing the arches by the bottom chord. This framing difficulty is illustrated by Fig. 3, which shows that, in practically all cases, the inner vertical faces of the arches are *inside* the outer vertical faces of the bottom chord.

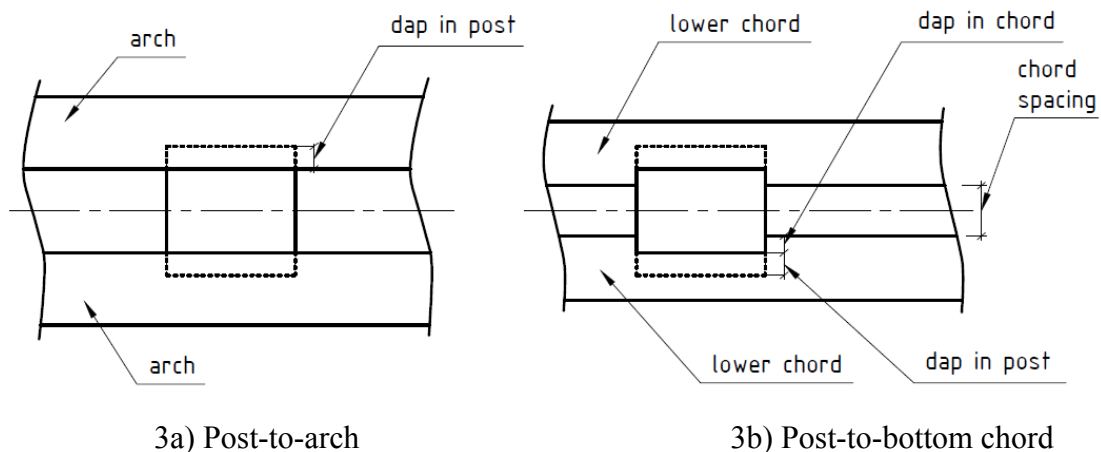
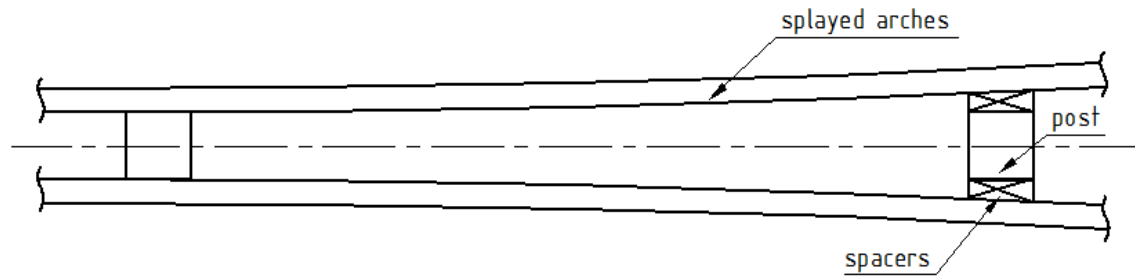
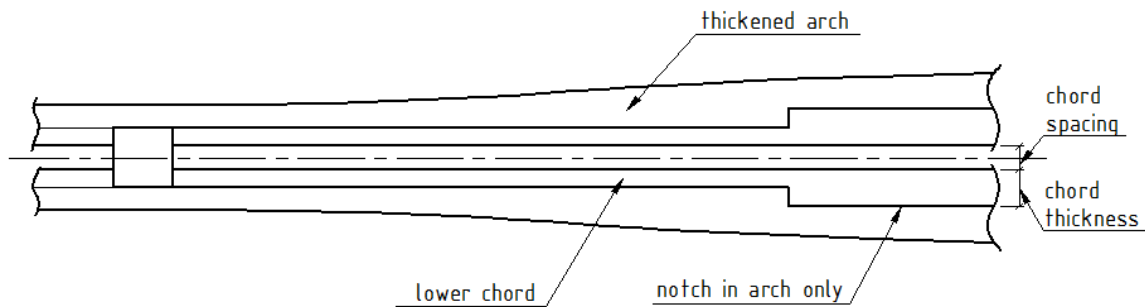


Fig. 3 – Inner vertical faces of arches are generally inside outer vertical faces of chord members

This means that a method must be devised to pass the arches by the bottom chord. Fig. 4 shows three methods builders used for the arch-bottom-chord intersection.



4a) Splay arches



4b) Increase thickness of arches and notch arches only

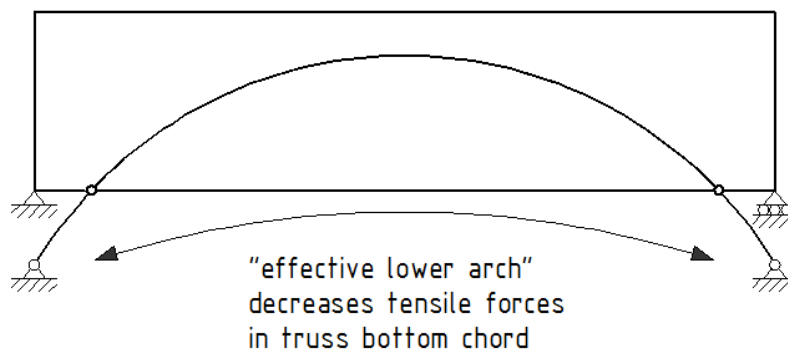


4c) Notch both the bottom chord and arch (Smith Bridge, Rush County, Indiana)

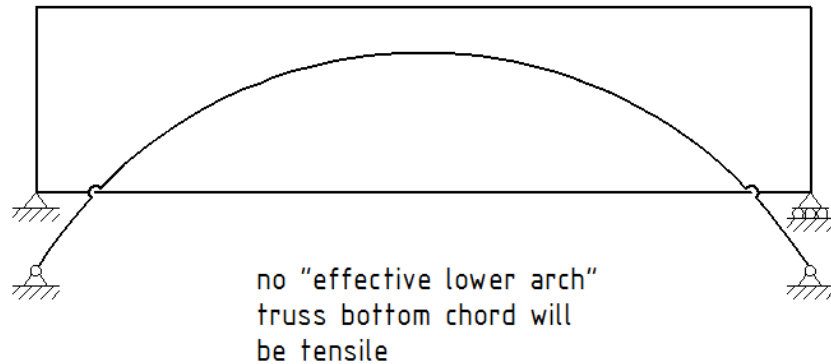
Fig. 4 – Three techniques for passing the arches by the bottom chord

Fig. 4a indicates that some builders simply splayed the arches using spacers on the post nearest the intersection (see, for example, the Mansfield Bridge in Parke County, Indiana). Splaying generally simplifies the framing since no daps are needed. However, the strength of the arches is reduced significantly because they are no longer planar. A second technique, shown in Fig. 4b, is to increase the thickness of the arches in the panels adjacent to the intersection and then use (relatively deep) notches only in the thickened arches. As for the splaying technique, the effective centroidal axis of the thickened arch is no longer planar. The third common technique, shown in Fig. 4c, is to dap or notch both the arch and the bottom chord, a more time-consuming method. In most cases, one or two through bolts are placed at this intersection.

The details used at the arch-to-bottom-chord intersection strongly influence the way live gravity loads are carried by a Burr-arch truss. If it can be assumed that there is no relative movement between the bottom chord and the arch at this intersection, as shown schematically in Fig. 5a, then the bottom chord and the two arch segments below the chord form an “effective lower arch.” This arch-like behavior decreases the normally tensile forces in the bottom chord of the truss, perhaps even causing some to become compressive, especially in the panels immediately inside the arch-bottom-chord intersections.



5a) Pinned connection between bottom chord and arch



5b) No effective connection between bottom chord and arch

Fig. 5 – Bounds on behavior at the intersection of the bottom chord and the arch

If, in fact, relative displacements can occur between the arch and the bottom chord at their intersection, as shown schematically in Fig. 5b, then there is no “effective lower arch” and a uniformly distributed live load causes tension in the bottom chord, as in a conventional simply-supported truss. As discussed later, this change in behavior was noted by Emory Kemp and John Hall in their case study.⁸ How does a typical connection actually behave? This depends on the tightness of the fit between the daps and on the tension force in the through bolts. If the arches are simply splayed, there is certainly greater flexibility at the arch-to-bottom-chord intersection.

Arch-to-single-top-chord connection – Fig. 6 shows the principal parameters of the connection between the post and a single top chord. The mortise-and-tenon are typically “housed” or “shouldered” into the top chord to transfer the horizontal component of the brace force into the chord.

⁸ Emory L. Kemp and J. Hall, “Case Study of Burr Truss Covered Bridge,” *Engineering Issues: Journal of Professional Activities* 101, no. E13 (1975): 391–412.

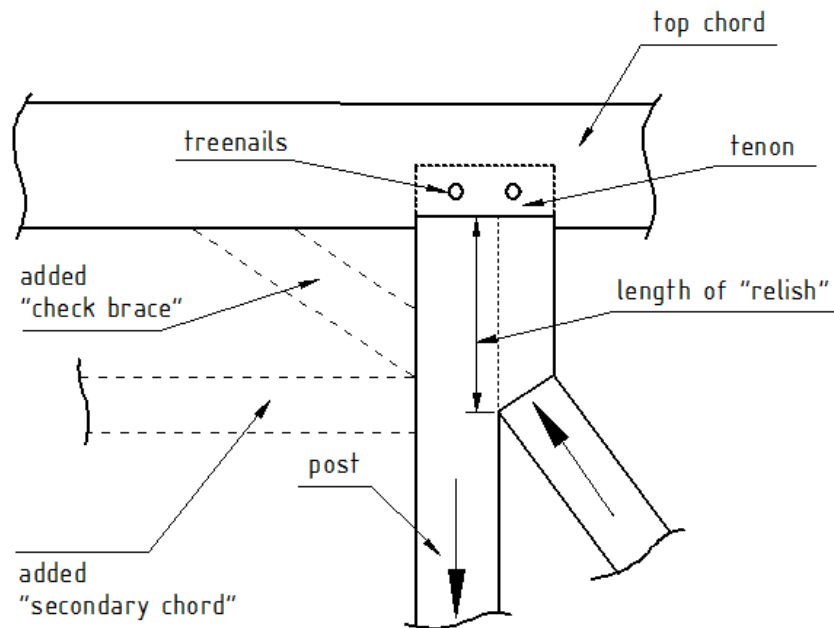


Fig. 6 – Post to single top chord connection

A sufficient “relish” length is required to transfer the vertical component of the brace force into the post. Therefore the brace axis does not meet at the point of intersection of the post and chord axes. That is, there is an eccentricity that produces shear and bending moment in the post. Fig. 7 appears to show shear and bending deformation in the post caused by the eccentricity of the brace.



Fig. 7 - Deformation at the brace-to-post connection, at the Bebb Bridge, Ohio. (The added brace connected to the diagonal is probably unique to the Bebb Bridge.)

These effects of the eccentric brace force were sometimes decreased by adding “check braces” or “secondary chords,” as shown in Fig. 6 (see, for example, the Turner Bridge in Pennsylvania). If the top chord consists of two sticks, as shown in Fig. 8, (see, for example, the Barrackville Bridge in West Virginia) the relish can extend above the top chord and the eccentricity can be made much smaller, as for the post-to-bottom-chord connection. A double top chord is used for longer-span bridges; it effectively increases the lateral stiffness of a planar Burr-arch truss.

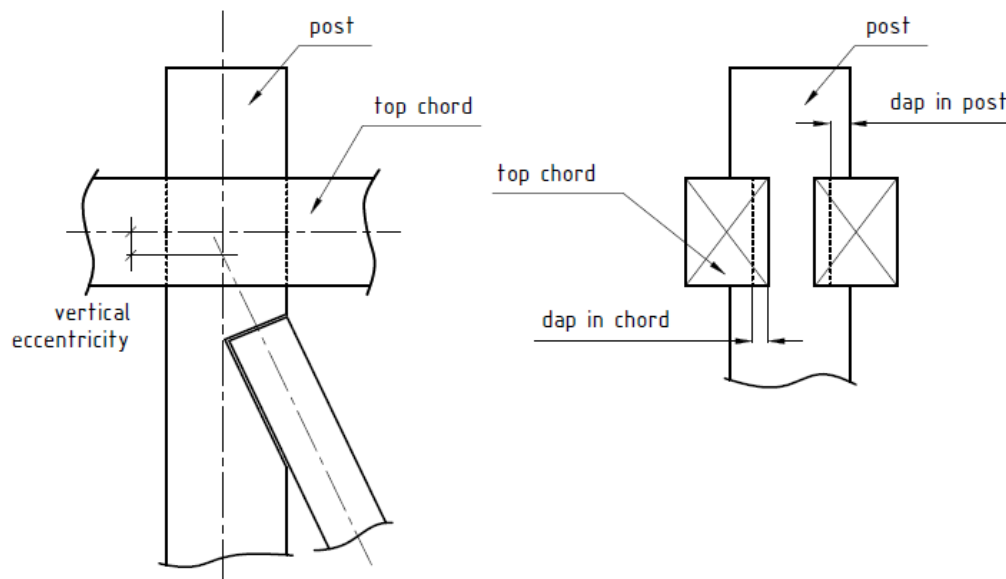


Fig. 8 – Connection between a post and a two-member top chord

As shown in Fig. 9, the bottom chord must consist of at least two members so that floor loads may be transferred into the post by a dap in the post and a “relish” that extends below the bottom chord. Daps must also be cut in the chords to transfer the horizontal component of the brace force into the chords.

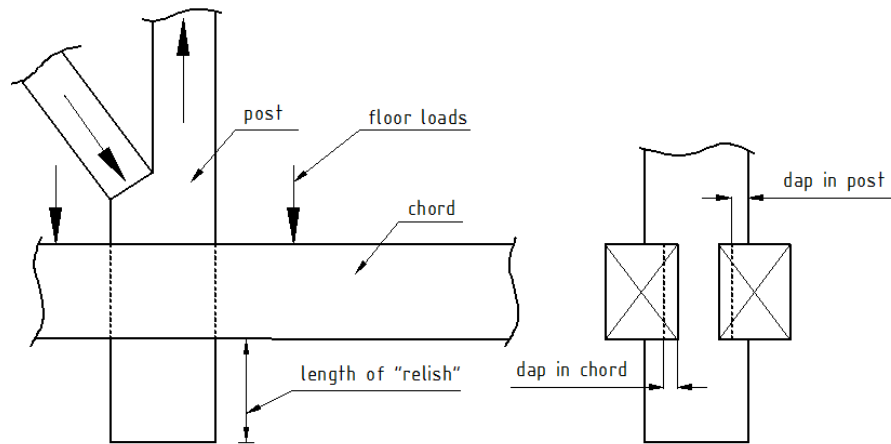
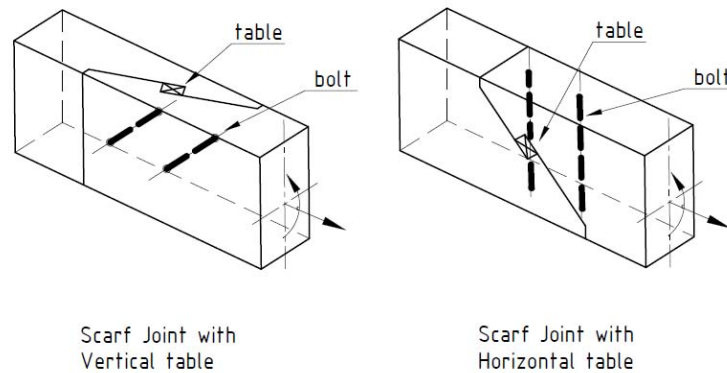
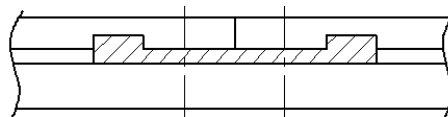


Fig. 9 – Post-to-bottom-chord connection

Splicing of the bottom chord tension members is challenging. “Halved and tabled scarf joints” or “stop-splayed scarf joints with keys” or “fishplates” are typically used.⁹ Fig. 10 shows two scarf joints and a fishplate joint. Typically two or four through bolts are also added.



10a) Tabled scarf joints with key



10b) Fishplate joint

Fig. 10 – Two splices used for bottom chord (tension) members

⁹ Rachel H. Sangree and Benjamin W. Schafer, “Experimental and numerical analysis of a stop-splayed traditional timber scarf joint with key,” *Construction and Building Materials* 23 (2009): 376-385, and Rachel H. Sangree and Benjamin W. Schafer, “Experimental and numerical analysis of a halved and tabled traditional timber scarf joint,” *Construction and Building Materials* (2009): 615-624.

Note that if tabled scarf joints are used to splice chord sticks, the table may be oriented either vertically or horizontally, as shown in Fig. 10a. For the examined bridges (see Table 1) with tabled scarf joints, the most common solution was to use horizontal tables for the top, compressive, chord (Bebb, Ohio; Crook's, Indiana; Bells Mills, Pennsylvania; Dreibelbis, Pennsylvania; Greisemer's Mill, Pennsylvania; Poole Forge, Pennsylvania; Ramp, Pennsylvania) and vertical tables for the bottom, tensile, chord (Bebb, Ohio; Crook's, Indiana; Bells Mills, Pennsylvania; Greisemer's Mill, Pennsylvania; Ramp, Pennsylvania; Weaver's Mill, Pennsylvania). Some builders, for example J. J. Daniels in Indiana, also used iron splicing straps as shown in Fig. 11. The strength of such tensile connections is difficult to predict analytically. For the top chord, the segments are either simply abutted or a tabled scarf joint is used.



Fig. 11 – Daniels' bottom chord splicing detail (Deer's Mill Bridge, Indiana)

Fabrication and erection of Burr-arch truss bridges – To understand framing of historic Burr-arch truss bridges, there is a need to understand dimensional tolerances for heavy sawn wood sections and “square rule framing,” which is adapted to allow for dimensional variations in nominally equal wood sections. Until very recently, detailed dimensions of mortise-and-tenon, scarf, and other connections were based largely on the experience and know-how of heavy timber framers rather than on detailed structural analyses. There's invariably some “looseness” in newly fabricated traditional timber joints. Most connections require “cutouts” or “daps” that form re-

entrant corners with associated stress concentrations; therefore nominal stresses may not represent actual stress conditions.

Burr-arch truss fabrication requires understanding of dimensional changes that occur in wood over time in the axial, radial, and tangential directions. For example, Robert Brungraber explains the fabrication technique called *drawboring*.¹⁰ It consists of intentionally misaligning holes in a mortise and its tenon in an attempt to minimize or prevent the gap that could develop as a function of wood shrinkage over time. The technique essentially prestresses the mortise-and-tenon connection.

Although Burr famously described his daring erection of the record-setting McCall's Ferry Bridge, that process may have been unique, mandated by an exceptionally deep river channel on river ice that was moving, slowly, in three directions!¹¹ In general falsework was used, and the erection typically proceeded by completing the trusses first and then attaching the arches in segments. This sequence raises an important question: should the falsework be (wholly or partially) removed after the trusses are completed, before the arches are engaged? The principal objectives for doing so are to allow the truss joints to tighten and to engage the diagonals in compression as dead load is transferred to the trusses. Timber framer Jan Lewandoski notes: "Any truss, new or restored, will lose some camber immediately when first brought into service by bringing to tight bearing of a great number of joints that merely look tight."¹² In his rehabilitation of Gilpin's Falls Covered Bridge in Maryland, timber framer Tim Andrews partially removed the falsework to allow tightening of the joints, and only engaged the arches as the last erection step by driving folding hardwood wedges.¹³ Of course the falsework can only be (wholly or partially) removed if the trusses are strong enough to carry the dead load and stiff enough such that their vertical displacement is only a fraction of the design camber. The process of transferring part or all of the dead load to the trusses only must be reflected by the analytical

¹⁰ Robert L. Brungraber, "Traditional Timber Joinery: A Modern Analysis" (Ph.D. diss., Stanford University, 1985), 47.

¹¹ Theodore Burr, "McCall's Ferry-Bridge," *Niles' Weekly Register*, 18 November 1815, 200-202.

¹² Jan Lewandoski, review of *America's Covered Bridges*, by Terry Miller and Ronald Knapp, *Timber Framing* no. 117 (September 2015): 2-6.

¹³ Rachel Sangree and Hannah Blum, "Gilpin's Falls Covered Bridge, Engineering Report," HAER No. MD-174, Historic American Engineering Record (HAER), National Park Service, U.S. Department of the Interior, 2012, 51.

models defined by structural engineers to estimate member forces from dead loads. For example, Sangree used a model of the truss only to estimate short-term dead load member forces in the Gilpin's Falls bridge.¹⁴

Is it practical *not* to remove any falsework until the arches are fully engaged? From a structural engineering viewpoint, if the initial tangent vertical stiffness of the arches is much greater than the initial tangent vertical stiffness of the trusses with loose joints, then most of the dead load will be carried by the arches, assuming they have the strength to do so. Conwill and Sangree both state that Archibald M. Kennedy and his son Emmett, the pre-eminent builders of Burr bridges in Indiana, released the falsework only after the arches were fully in place.¹⁵ It appears that this belief is based on statements made by George E. Gould in his 1977 book *Indiana Covered Bridges*. Here Gould states: "In Kennedy bridges the arches were fastened before the falsework was removed."¹⁶ In discussing construction he says: "The falsework was in place until the workmen had finished the siding and roof." But on the same page, Gould also states: "Upon completion of the two *trusses* the structure was raised slightly so that the [bearing] blocks could be removed. Then the span was carefully lowered until it was supporting its own weight."¹⁷ Gould's statements seem ambiguous/inconsistent and need to be corroborated as it does not appear to be certain that the Kennedys did not tighten the truss joints by activating the dead load on the trusses only. The authors' judgment is that an experienced timber framer would not attempt to build a Burr-arch truss bridge without first tightening the joints of the trusses and activating the compression-only diagonals by activating (part or all of) the dead load on the trusses only.

Is it possible to control how the dead load is shared between the arch and truss by, say, a pre-defined sequence of "jacking and shimming" at various locations? Certainly any such sequence will depend on the particular stiffnesses of the arch-truss connections. Verification of the

¹⁴ Sangree, "Gilpin's Falls Covered Bridge," 50.

¹⁵ Conwill, 11; Sangree, "Gilpin's Falls Covered Bridge," 27.

¹⁶ George E. Gould, *Indiana Covered Bridges Thru the Years* (Indianapolis: Indiana Covered Bridge Society, 1977), 15.

¹⁷ Gould, 13.

effectiveness of any such sequence will likely require instrumentation to measure the axial forces in the arches near the bearings. If a desired dead load sharing is achieved, it is only for the relative magnitudes of short-term member forces. Wood viscosity and hygroscopicity will change dead load member forces over time. Generally, over time the arches will bear an increasing share of the dead load, but structural analyses have not been performed to quantify such temporal changes. Moreover, as discussed later in this report, if a Burr-arch truss is a *ductile* system, the way the dead load is shared does not affect the ultimate load capacity of the structure.

Behavior of wood members – Chord, post, and other members of a Burr-arch truss must be sized or rated for design axial forces, shear forces, and moments as determined from structural analyses. It is accepted that the provisions of the *National Design Specification for Wood Construction* may be used for this purpose.¹⁸ It should be kept in mind that shear, tensile, and flexure strength limit states in wood are generally brittle. In addition, actual stress states can be quite different from nominal ones, especially near connections. For example, Fig. 12 shows three principal forces that act near the base of a post, which has several re-entrant corners that cause stress concentrations.

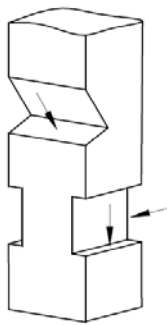


Fig. 12 – Three principal forces acting near the base of a typical Burr-arch truss post

The forces shown cause shear parallel to the grain, compression perpendicular to the grain, and compression at an angle to the grain. The resultant axial tensile force and moment in the post exist on a reduced section at a re-entrant corner. Moreover, knots and cracks commonly occur in

¹⁸ American Wood Council, *National Design Specification for Wood Construction* (Leesburg, VA: ANSI/AWC NDS, 2012).

posts and other members. Similar conditions exist near the mortise-and-tenon connection at the top of a post.

Connection behavior – Following the pioneering modern work of Brungraber, there has been considerable recent engineering research on the physical behavior, mathematical modeling, and design of traditional timber joints. The many dimensions required to define a connection, the orthotropic character of wood, and the variety of possible load conditions constitute a daunting number of parameters or variables to investigate. Therefore studies necessarily involve a limited set of physical experiments, a limited set of numerical finite element studies, and, sometimes, numerical simulation studies. Based on recent engineering studies, some principal observations on mortise-and-tenon and scarf joints are as follows.

Brungraber studied the behavior of pegged, housed and unhoused, mortise-and-tenon joints. He completed both experimental and finite element studies of joints subject to axial tension and compression, shear, and moment. He noted that, without drawboring, the physical joints had an initial slack that is very difficult to model analytically. Drawboring provides joints with an initial tangent stiffness. The behavior of a mortise-and-tenon joint in tension is different from its behavior in compression because different load transfer mechanisms are engaged. Brungraber strongly advocated detailing a joint to preclude two brittle failure modes: tension perpendicular to the grain in the mortised member and shear along the grain in the tenon. Peg behavior depended on its diameter and on the orientation of its growth rings. For his finite element studies Brungraber used a linear elastic orthotropic material model, which does not predict strength. He noted the difficulty of defining appropriate interface elements for his mathematical models.¹⁹ Joseph Miller, Richard Schmidt, and William Bulleit cite and summarize experimental and analytical studies on wood connections performed at the University of Wyoming and at Michigan Technological University. Their own finite element and experimental studies focused on the performance and design of wood dowel or peg connections subject to axial forces and

¹⁹ Brungraber, “Traditional Timber Joinery,” 84.

²⁰ Joseph F. Miller, Richard J. Schmidt, and William Bulleit, “New Yield Model for Wood Dowel Connections,” *Journal of Structural Engineering* 136, no. 10 (October 2010): 1255-1261; and Joseph F. Miller and William M. Bulleit, “Analysis of Mechanically Laminated Timber Beams Using Shear Keys,” *Journal of Structural Engineering* 137, no. 1 (January 2011): 124-132.

shear. They categorized five possible failure modes and derived a design equation for the failure mode in which a dowel fails in shear. They also used Monte Carlo simulation to estimate a reliability index in the context of load and resistance factor design. Miller and Bulleit also studied the performance and design of shear keys used to mechanically laminate timber beams.²⁰

Sangree and Schafer performed analytical and experimental studies of the performance of “halved and tabled” traditional scarf joints. Although only four tension tests were completed on scarf joints with loose clamping bolts, the authors made an important observation on the influence of grain angle (see Fig. 13) on the connection strength.²¹

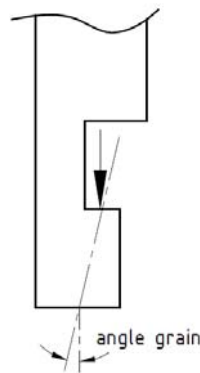


Fig. 13 – Grain angle

For the two specimens with a grain angle close to zero, the failure mode was shear parallel to the grain, whereas for the two specimens with grain angles of approximately 7° and 15° , the failure mode was tension perpendicular to the grain. Both modes were apparently brittle but the strength of wood in tension perpendicular to the grain is much smaller than the shear strength of wood parallel to the grain. This observation underscores the importance of prescribing and enforcing limits on grain angle for grading wood. The authors' linear elastic finite element models predicted the experimentally observed joint stiffness well, and they noted that it was much smaller than that of a solid wood section of equal thickness.

Sangree and Schafer also performed studies of “stop-splayed” traditional scarf joints with keys. Six tension tests were performed, three with tight clamping bolts in oversized holes. They

confirmed the common understanding that tight clamping bolts are necessary to prevent rotation of the key and to develop the strength of the connection. The observed failure limit state was shear parallel to the grain, but the reported load-displacement data showed considerable ductility, apparently from crushing of the key perpendicular to its grain before the shear failure occurred. The connection behavior may not have been ductile if stronger keys, which did not crush, had been used. Again their finite element models predicted the initial stiffness of the scarf joints well.²¹

Structural analysis of Burr-arch trusses – Until the mid 1960s, when computer-based structural analysis programs became widely available, only equilibrium-based manual structural analyses were feasible for Burr-arch trusses, which are highly statically indeterminate. This meant that a sufficient number of assumptions had to be made such that member forces could be estimated using only equilibrium equations. Equilibrium-based structural analyses had been in use in the United States since the 1830s and, in general, led to reliable designs. Two brief articles from *Civil Engineering* magazine, one from 1941 and the other from 1963, indicate levels of understanding of Burr-arch trusses and U.S. engineers' approach toward structural analysis, design, and rehabilitation at those times.

Irving Jelly discussed the Portland-Columbia Bridge, a Burr-arch truss bridge with four 193' spans over the Delaware River between Northumberland County, Pennsylvania, and Warren County, New Jersey (WG#38-48-04x/30-21-03x).²² Charles Kellogg designed and built the bridge, which was completed in 1869. A notable feature, apparently original, was that wedges were used at the lap ends of each arch segment to tighten the arch. Jelly noted that in 1929 steel rods extending between the top and bottom chords were added adjacent to each (tensile) wooden post. In addition, 3' sections of the arches at the abutments had been replaced and spliced using steel plates and bolts. The measured long-term midspan sags were approximately 14" below the horizontal! The author noted that the chord, post, and brace axes were not concurrent at the joints, so as a result, the posts had significant bending moments. Jelly conceptualized that the

²¹ Sangree and Schafer, "Experimental and numerical analysis of a halved and tabled traditional timber scarf joint," 615-624; Sangree and Schafer, "Experimental and Numerical Analysis of a stop-spayed traditional timber scarf joint with key," 376-385.

²² Irving A. Jelly, "Anatomy of an old covered bridge," *Civil Engineering* 11, no. 1 (January 1941): 12-14.

arch and truss were two subsystems that could be analyzed and designed separately. Therefore what was needed was a rational way of assigning fractions of the total uniformly-distributed dead and live gravity load to the arch and truss. Since the two were bolted together at the posts and hence would have the same vertical displacements, he reasoned that each would carry a fraction of the total load proportional to its vertical stiffness. He then estimated the vertical stiffnesses of the arch and truss (by unspecified methods) and concluded that: “the arch should carry 71% and the truss take 29% of the load.”²³ The author did not consider how asymmetric gravity live loads would be carried.

Albert Salkowski wrote on the design and construction of a replica of the Bunker Hill Bridge over the Big Gunpowder Falls river in Baltimore County, Maryland (WG# 20-03-01 #2x).²⁴ The original Burr-arch truss, with a span of 107', was built in 1880, rehabilitated in 1947, and was burned on November 18, 1961. Salkowski stated that to simplify structural analysis, the Burr-arch truss of the replacement bridge was:

Designed as two separate structural systems, as follows:

System 1. The parabolic two-hinged arch was assumed to support the entire dead load.

System 2. The through indeterminate truss was assumed to carry the live load.²⁵

Salkowski discussed an alternate structural analysis, which was similar to that described by Jelly, but it was not used for the redesign. The brief article did not illustrate how most of the joints were detailed, but the designers used high strength bolts, split-ring shear connectors, and steel plates extensively, in sharp departure from traditional timber framing connections.

Very likely the first computer-based linear elastic structural analyses of a Burr system were performed by Emory Kemp and John Hall in the context of assessment and restoration of the Barrackville Bridge (WG# 48-25-02/HAER WV-8).²⁶ Lemuel and Eli Chenoweth completed the nearly 150' span in 1853. The top chord of the bridge consists of *two* sticks and the posts extend

²³ Jelly, “Anatomy,” 14.

²⁴ Albert S. Salkowski, “Reconstructing a covered timber bridge,” *Civil Engineering* (October 1963), 36-39.

²⁵ Salkowski, “Reconstructing,” 37.

²⁶ Kemp and Hall, “Case Study of Burr Truss Covered Bridge.”

above the top chord to carry the roof. In consequence, the eccentricity (see Figs. 6 and 8) between the axis of a diagonal and the axes of the top chord and post is much smaller than in typical Burr-arch trusses. As a result, Kemp and Hall neglected it in their model. They defined three-dimensional frame models of one arch-truss with moment releases at the ends of the diagonals and posts and at the arch bearings. They analyzed three models: one of the arch-truss, another of the truss only, and a third of the arch-truss *without* a connection between the arch and the bottom chord at their intersection. They applied several loadings but, since the (nineteenth century) live load was only about 31 percent of the dead load, they determined that the full dead and live gravity load condition caused maximum load effects in most members. Kemp and Hall made the following important observations that significantly increased engineering understanding of the structural behavior of Burr-arch trusses.

- The connection between the bottom chord and the arch at their intersection is very important. The connection forms an “effective lower arch” (see Fig. 5) that dramatically decreases the tensile forces (some become compressive) in the bottom chord of the truss. This behavior increases the axial force in the arch *below* its intersection with the bottom chord. If this connection is removed, there is no effective lower arch but *member shears and moments at the post-arch intersection nearest the bottom chord are markedly increased.*
- The arch participates (with the diagonals) in carrying shear, especially near the abutments, where the slope of the arch is greater.
- The addition of the arch significantly decreases the (short term) vertical displacements of the system under uniform gravity loads.
- Linear elastic analyses have distinct limitations. Wood viscosity (creep) and hygroscopicity (shrinkage and swelling) change member forces and displacements over time. And connections loosen over time. Similar observations were previously made by Gen. Herman Haupt.²⁷

²⁷ Kemp and Hall, “Case Study of Burr Truss Covered Bridge,” 410; Herman Haupt, *The General Theory of Bridge Construction* (New York: D. Appleton and Co., 1866), 175.

Kemp and Hall also made the observation that: “Conceptually, the arch plays the same role in the Burr system as the cables in a suspension bridge with a stiffening truss.”²⁸ This is not completely correct. It would be correct if the arch and truss were connected as shown in Fig. 14a,

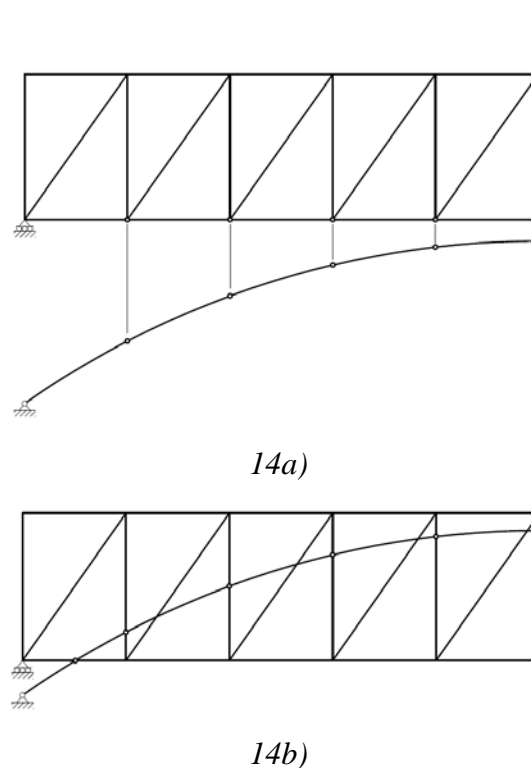


Fig. 14 – Two arrangements of an arch and a truss

but in a Burr system the arch and truss are connected to have the same *horizontal* (as well as vertical) displacements at the arch-bottom chord intersection and at the arch-post intersections, as shown in Fig. 14b. These *horizontal displacement compatibility constraints*, especially the one at the arch-bottom chord intersection, which forms an effective lower arch, make the behavior of a Burr system very different from that of the system shown in Fig. 14a, which is the inverse of a deck-stiffened suspension bridge.

²⁸ Kemp and Hall, “Case Study of Burr Truss Covered Bridge,” 410.

With funding from the National Historic Covered Bridge Preservation Program (NHCBP) of the FHWA, the Historic American Engineering Record (HAER) of the National Park Service (NPS) documented the Pine Grove Bridge in Lancaster County, Pennsylvania, in 2002. As part of the documentation, Benjamin Schafer and Dylan Lamar performed structural studies of the bridge.²⁹ Capt. Elias McMellen, a Civil War veteran, built the Pine Grove Bridge with its two 90' spans in 1884. As in most Burr-arch truss bridges, the Pine Grove Bridge has only one stick for the top chord. Therefore the eccentricity between the axis of the diagonal and the axes of the post and chord is significant and must be included in structural analysis models. Schafer and Lamar considered the effects of a uniform dead load and a concentrated gravity live load applied at midspan and at quarter-span. They defined five principal system models.

- Plane frame model of the truss only, with moment releases at ends of posts, diagonals and arch (called the flexible plane frame model).
- Plane frame model of the truss only without moment releases at ends of diagonals and posts (called the rigid plane frame model).
- Plane frame model of arch only.
- Plane frame model of combined arch-truss system with flexible model of truss.
- Plane frame model of combined arch-truss system with rigid model of truss.³⁰

Schafer and Lamar made the following observations:

Models of truss only – Because of the eccentricity of the diagonals, flexural stiffness is necessary to satisfy equilibrium in such models, therefore there is a considerable difference between the predicted vertical midspan displacement of the flexible and the rigid plane frame models. The predicted vertical midspan displacement of the flexible plane frame model subject to a uniform dead load was 0.96", whereas the corresponding displacement of the rigid plane frame model was 0.74".

²⁹ Dylan Lamar and Benjamin W. Schafer, "Pine Grove Bridge, Engineering Report," HAER No. PA-586, Historic American Engineering Record (HAER), National Park Service, U.S. Department of the Interior, 2003, 19-70; Dylan Lamar and Ben Schafer, "Structural Analysis of Historic Covered Wooden Bridges," *Journal of Bridge Engineering* 9, no. 6 (December 2004): 623-33.

³⁰ Lamar and Schafer, "Pine Grove Bridge."

Models of arch only – When subject to a uniform dead load, the vertical midspan displacement was predicted to be 0.91", very similar to that of the flexible model of the truss only. The authors confirmed the common structural understanding that an arch has very small stiffness when a quarter-span vertical concentrated load is applied.

Models of combined truss and arch – The vertical midspan displacement of the combined system with a “flexible” truss model subject to a uniform dead load was estimated to be 0.25", whereas the combined system with a “rigid” truss model had an estimated displacement of 0.23". Therefore the members’ *axial* stiffnesses dominate the behavior of the combined system; adding flexural stiffness by removing the moment releases does not contribute significantly to a combined system’s stiffness under dead load.

By analyzing separate truss and arch models, Schafer and Lamar demonstrated that the combined system is not simply a parallel arrangement of an arch and truss as illustrated by Fig. 14a. If this were so, then the dead load midspan displacement would be expected to be 0.467" ($1/0.96 + 1/0.91 = 1/0.467$). Combining an arch and truss as shown in Fig. 14b forms a third load path, that is, an effective lower arch (see Fig. 5a) whose stiffness contribution decreases the vertical midspan displacement under dead load to 0.25". Since combining an arch and truss as shown in Fig. 14b effectively creates a new, different system, it seems unproductive to discuss whether the arch stiffens the truss or the truss stiffens the arch, at least for a uniformly distributed gravity load.³¹

Schafer and Lamar also studied the effects of camber and found that it does not change the system’s structural behavior significantly. They also considered the effects of steel rods added between the post-arch intersections and the bottom chord. Although the axial stiffness of the steel rods is generally much smaller than the axial stiffness of the wooden posts, the rods do provide a redundant load path for gravity loads applied to the bottom chord.³²

³¹ Lamar and Schafer, “Pine Grove Bridge,” 56.

³² Lamar and Schafer, “Pine Grove Bridge,” 51-56.

NHCBP funding also enabled Rachel Sangree and Hannah Blum to perform structural studies of the Gilpin's Falls Covered Bridge in conjunction with its rehabilitation by timber framer Tim Andrews in 2009.³³ Joseph G. Johnson built the 98' span in 1860. It has a single stick for the top chord; therefore, the eccentricity of the diagonals needs to be modeled. Each truss has "double arch ribs" with end conditions as shown in Fig. 15.



Fig. 15 – Arch bearings for Gilpin's Falls Covered Bridge. Photo by Christopher Marston, 2010.

Sangree and Blum defined linear elastic plane frame models with moment releases at the ends of the posts, diagonals, and arches. With the objective of predicting effects at the principal stages of reconstruction followed by Tim Andrews, they defined the following models: truss only; truss with arches that are not connected to the abutments; and truss with arches connected to the abutments (condition at completion of reconstruction).

After completing reconstruction of the trusses, Andrews released the falsework except at the first internal post from each end. The action of removal of the falsework caused a midspan vertical displacement of 0.75", as measured by Andrews. The corresponding displacement predicted by Sangree and Blum's linear elastic model with dead load active was 0.29", indicating that the measured vertical displacement of 0.75" was caused primarily by joint tightening rather than from elastic member deformations. Andrews engaged the arches by driving black locust folding wedges, thus inducing some forces in the Burr system, but these forces were not quantified.

³³ Lola Bennett, Rachel Sangree and Hannah Blum, "Gilpin's Falls Covered Bridge," HAER No. MD-174, Historic American Engineering Record (HAER), National Park Service, U.S. Department of the Interior, 2012, 17-71.

Sangree and Blum computed demand-to-capacity ratios for some members for the dead load condition. In general, the posts had the highest ratios, indicating their smaller reserve strength for carrying forces from live loads.³⁴

Sangree and Blum also studied the fault condition corresponding to failure of the arches at the abutments. They determined that such a condition caused very high, probably unsupportable, moments in the bottom chord and arch. Moreover, the system's structural behavior changed to that of a tied arch, in which the horizontal component of the arch thrust caused tension in the bottom chord, assuming the arch-to-bottom-chord connection can affect such a force transfer. Sangree and Blum also quantified the effect of a loss in stiffness of the post-to-arch connection. They defined a three-dimensional frame model of the joint with an element to model the stiffness of the connection. They determined that the force transfer between the post and the arch can be affected even with a small connection stiffness. Sangree and Blum reiterated the comments of Kemp and Hall and Haupt that the short-term member forces predicted from linear elastic models will change with time due to wood viscosity and loosening of the connections.³⁵

Researchers at the National Center for Wood Transportation Structures at Iowa State University, in collaboration with engineers from the Forest Products Laboratory, all funded by NHCBP, have defined analytical models of Burr-arch truss bridges. Fouad Fanous, Douglas Rammer, and Terry Wipf described a three-dimensional linear elastic frame model of the Zacke Cox Bridge in Parke County, Indiana.³⁶ Fanous and Rammer are developing improved analytical models in ongoing research.³⁷ Travis Hosteng, James Wacker, and Brent Phares defined a model of the Cox Ford Bridge in Indiana in the context of improving load rating methods based on analytical

³⁴ Sangree and Blum, "Gilpin's Falls Covered Bridge, 61.

³⁵ Sangree and Blum, "Gilpin's Falls Covered Bridge, 70; Kemp and Hall, "Case Study of Burr Truss Covered Bridge," 410; Haupt, *General Theory*, 175.

³⁶ Fouad Fanous, Douglas Rammer, and Terry Wipf, "Simplified Analytical Model for a Queen-Post Covered Timber Bridge," in James Wacker and J. Krohn, eds., *Proceedings, 2nd International Conference of Timber Bridges* (Washington, DC: WoodWorks – Wood Products Council, 2013).

³⁷ Fouad Fanous, Douglas R. Rammer, *Improved Modeling of Historic Covered Bridges, Phase II*, (Madison, WI: USDA, Forest Service, Forest Products Lab, 2013), Research in progress.

modeling and field testing.³⁸ Allison Machtemes completed a thesis that focused on evaluating different linear elastic models for three Burr-arch truss bridges in Parke County, Indiana: the Zacke Cox Bridge, the Portland Mills Bridge, and the Cox Ford Bridge.³⁹

These recent engineering analytical studies reveal the strengths and limitations of current engineering models and engineering understanding of Burr-arch trusses. Detailed two-dimensional and three-dimensional linear elastic models can: provide estimates for member forces; provide estimates for short-term displacements; identify important members and connections; and provide understanding of short-term linear elastic behavior, including how various live loads are carried and the effects of different construction steps.

However, the results of linear elastic analyses are very sensitive to slight support movements. For example, if one of the arch supports settles, say even a fraction of an inch, the linear elastic member forces will be very different. Potential support settlements are not known *a priori*. Because Burr-arch trusses are statically indeterminate, it is highly probable that stresses will be produced during fabrication and erection. These stresses are not known *a priori*. Wood material properties are highly uncertain, and members in heavy timber frames have daps, mortises, tenons, shoulders, and other changes in cross-section that are difficult to model. These add uncertainty to linear elastic analytical predictions. Although there is a general recognition that time-dependent effects of wood viscosity, hygroscopicity, and the “setting-in” of joints can affect forces and displacements, the capability to model these phenomena is not commonly available. Therefore engineers can only make qualitative estimates of these time-dependent effects.

Experimental Studies of Burr-arch trusses – Field tests have been performed to measure the elastic behavior of existing historic covered bridges. These generally involve instrumenting a bridge with displacement and strain transducers and load testing by driving a truck with known axle spacing and axle weights through the bridge. Of course relatively light vehicles must be

³⁸ Travis Hosteng, James Wacker, and Brent Phares, “Live Load Testing of Historic Covered Timber Bridges,” in James Wacker and J. Krohn, eds., *Proceedings, 2nd International Conference of Timber Bridges* (Washington, DC: WoodWorks – Wood Products Council, 2013).

³⁹ Allison Machtemes, “Investigation of the Structural Behavior of Historical Covered Timber Bridges” (Master of Science thesis, Iowa State University, 2011).

used so as not to cause permanent damage. Measured responses are then used to calibrate or validate analytical models and possibly infer any damage that may exist in a bridge.

Sangree and Schafer measured displacements of the Pine Grove Bridge caused by the passage of a 2-ton pickup truck. The data was used to estimate influence lines for the vertical displacements at midspan and at quarter-span. In general, the measured influence lines agreed with analytical predictions. Sangree and Schafer observed that the four central diagonals of the bridge were partially unseated at their bases. They modified their analytical model by deleting the four diagonals, which improved the match between analytical and experimental results.⁴⁰

Sangree and Blum performed live load tests on the rehabilitated Gilpin's Falls Covered Bridge. They drove a 5,500-lbs pickup truck with an axle spacing of 12' through the bridge, measuring vertical displacements and strains in some members. The vertical midspan and quarter-span displacements were small (0.04" – 0.06") but generally in agreement with linear elastic numerical predictions. Sangree and Blum did not provide a complete interpretation of measured and predicted strains.⁴¹

Perhaps the most extensive field testing of Burr-arch trusses has been performed by researchers from Iowa State University. Allison Machtemes provided a summary of the instrumentation and testing of the Zacke Cox Bridge, the Portland Mills Bridge, and the Cox Ford Bridge, all in Parke County, Indiana. The test results were used to validate/calibrate analytical models and to improve load rating methods. The Iowa State researchers concentrated their strain instrumentation on the posts, diagonals, and arch segments near the midspans of the bridges and at the tension chord splices. The physical measurements provided a reality check for analytically-computed responses. In general, reasonable agreement between measured and predicted displacements (global responses) can be achieved using linear elastic models but measured member strains are much more difficult to predict because they depend on local details. Machtemes gave a frank listing of the three bridges' irregularities that were not included in

⁴⁰ Rachel H. Sangree and Benjamin W. Schafer, "Field experiments and numerical models for the condition assessment of historic timber bridges: Case study," *Journal of Bridge Engineering* 13, no. 6 (November 2008): 595-601.

⁴¹ Sangree and Blum, "Gilpin's Falls Covered Bridge," 59.

numerical models. She noted that the arches of the Zacke Cox Bridge were noticeably out-of-plane and that gaps existed at many connections. The Portland Mills Bridge had some posts that were clearly not vertical and a variety of different conditions existed at the arch bearings. At the Cox Ford Bridge, Machtemes detected “signs of [a shear] failure” in a chord splice. Such irregularities invariably exist in historical covered bridges, making the actual structural behavior more complex than that predicted by typical linear elastic models.⁴²

To observe the behavior of a Burr-arch truss at its strength limit state, the only practical alternative is to perform laboratory tests. Under the supervision of Robert Brungraber, Michael Mileo conducted laboratory tests on a three-dimensional, 1/6 scale, wooden model of the Davidson or Sonestown Bridge over Muncy Creek in Sullivan County, Pennsylvania (WG# 38-57-03). The details of the model and its connections were not given in Mileo’s thesis, but the model seemed to have a type of “secondary chord” (see Fig. 6). Mileo used photoelastic techniques in an attempt to measure member strains. Three tests were performed on two versions of the model.

Test 1 – Performed on the model of the bridge with arches, subject to asymmetric (quarter-point) vertical loading to measure stiffness.

Test 2 – Performed on the model of the bridge with arches, subject to symmetric vertical loading to measure stiffness.

Test 3 – Performed on the model *without* arches, subject to symmetric vertical loading to measure stiffness and ultimate capacity.⁴³

It seems that Test 3 was performed on the bridge model without arches because of limitations in experimental facilities. The following observations were made.

Test 1 – Photoelastic coatings indicated large bending strains in the arch at the arch-bottom-chord intersection. This agrees with the observations of Kemp and Hall.⁴⁴

Test 1 – Loss-of-contact was observed in two diagonals near midspan.

⁴² Machtemes, “Investigation of the Structural Behavior of Historical Covered Timber Bridges,” 67.

⁴³ Michael A. Mileo, “Photoelastic stress analysis of a Burr truss covered bridge” (Master of Science thesis, Bucknell University, April 1982).

⁴⁴ Kemp and Hall, “Case Study of Burr Truss Covered Bridge,” 402.

Test 1 – For the quarter-span asymmetric vertical loading the model deflected *upward* at three-quarter-span, indicating arch-like behavior.

Test 2 – Although nominally the same, the two planes of arch-trusses had different vertical stiffnesses.

Test 3 – Failure occurred at the tension splice (its details were not described) in the bottom chord. The failure was completely brittle.

It is understandable that the failure was brittle, given that a *tensile* failure occurred in a splice and that the bridge model without arches was statically determinate (at least as a true truss). But a Burr-arch truss is statically indeterminate and hence its strength may be greater than the load that causes the first member or connection to fail. Some concepts on estimating strength of structural systems are briefly reviewed in the following section.

ASPECTS OF STRENGTH LIMIT STATE ANALYSES OF STRUCTURAL SYSTEMS

The concepts of statical determinacy/indeterminacy and ductility/brittleness are essential for understanding behavior of structures at the strength limit state. A statically determinate structure is one for which equilibrium equations are sufficient for determining all member forces. If one member or connection breaks, yields, or is removed, equilibrium cannot be satisfied and the system becomes a mechanism. Statically determinate systems are also called series or weak-link systems because their strength depends on the weakest member or connection. A system is statically indeterminate if equilibrium equations are not sufficient (unless assumptions are made) for determining all member forces. In general, more than one connection or member must be at strength before the system becomes a mechanism. Statically indeterminate systems are also called hyperstatic, or parallel, or redundant systems. A statically indeterminate system is said to have multiple load paths.

A material, a member, or a connection is said to be ductile or brittle depending on its force-deformation behavior. If its strength or capacity is maintained through additional deformation as shown in Fig. 16a, the member is said to be ductile. An example is the formation of a plastic (rotational) hinge in a mild structural steel beam.

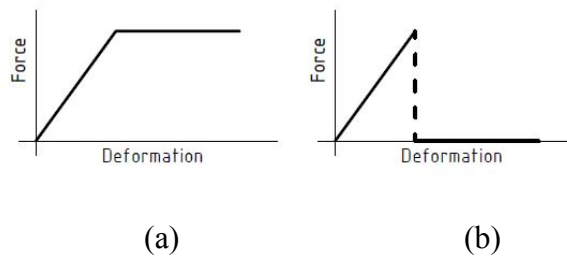


Fig. 16 – Ductile and brittle behavior

If a member breaks and sheds all its force as illustrated in Fig. 16b, it is said to be brittle. An example is the behavior of plain concrete in tension.

The strength behavior of statically indeterminate systems with ductile members/connections (“parallel-ductile” systems) is quite different from the strength behavior of statically indeterminate systems with brittle members/connections (“parallel-brittle” systems). Consider, for example, the simple two-member statically indeterminate system shown in Fig. 17.

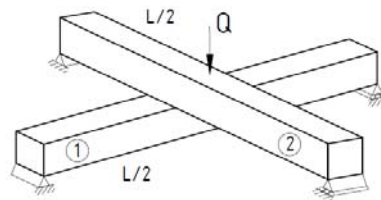


Fig. 17 – A two-member statically indeterminate system

Let M_1 and M_2 be the moment capacities of beams 1 and 2, respectively. Consider only the flexural failure mode (say shear failure is precluded). Then, if the beams are *ductile*, the maximum vertical load that can be applied, that is, the system strength or capacity, is:

$$Q_{\max} = (4/L)(M_1 + M_2) \quad (1)$$

The relative values of the beams’ linear elastic stiffnesses affect the initial load-sharing between the two beams, but *not* the capacity of the system, assuming *ductile* beams. If the beams are

brittle and the two flexural stiffnesses are equal but, say, $M_1 < M_2$, then the system strength is given by:

$$Q_{\max} \text{ is the larger of: } (4/L)(2M_1) \text{ or } (4/L)(M_2) \quad (2)$$

Comparing equation (1) and statement (2) shows that the strength of the parallel-brittle system is smaller than the strength of the parallel-ductile system. The strength of parallel-ductile systems is also independent of initial states of prestress caused by lack-of-fit or small support movements. Say, for example, the two beams had different initial curvatures as shown in Fig. 18.

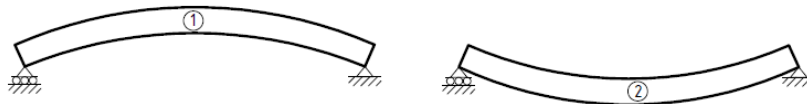
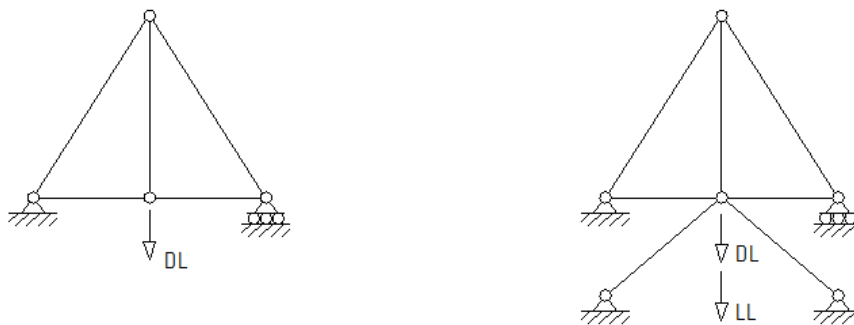


Fig. 18 – Two beams with different initial curvatures

If the two beams were connected as shown in Fig. 17, with all four supports at the same elevation, the system would have a self-equilibrated state of prestress. If the two members are ductile, the strength of the system with an initial state of prestress is the same as the strength of the system without prestress. This is not true for parallel-brittle systems.

Another relevant aspect of the strength behavior of *parallel-ductile* systems is illustrated by Fig. 19.



19a) Truss carries all DL

19b) Arch is added; LL is shared by arch and truss



19c) DL is shared by arch and truss

19d) DL and LL are shared by arch and truss

Fig. 19 – Sharing of dead load and strength of statically indeterminate ductile systems

Fig. 19a shows a simple kingpost truss that carries all the dead load. Fig. 19b shows that an arch is added to the kingpost truss to share in carrying the live load. Fig. 19c shows an arch-truss in which the truss and the arch share in carrying the dead load. Fig. 19d shows a live load applied to the arch-truss of Fig. 19c. If the member/connection strengths are ductile, the way a dead load is carried does not affect the magnitude of the live load that will produce a mechanism in the arch-truss. That is, the live load that will cause a mechanism in the sequence of Fig. 19a and 19b will be the same as that for the sequence shown in Fig. 19c and 19d. Also, as stated previously, the capacity will not be affected by any self-equilibrated state of stress that may be induced during the fabrication and erection of a *parallel-ductile* system.

Engineers are very familiar with analyses to predict the capacity of parallel-ductile systems, especially in the context of ductile rigid frames. In a typical analysis, the load is applied incrementally and checks on member yielding are performed at each increment. If a member yields, its stiffness contributions are removed but its (now constant) forces from yielding are applied to the model. The load is incremented until sufficient members/connections yield to form a mechanism, and no additional load can be applied. The maximum load for which equilibrium is satisfied is then the system's strength.

The strength of parallel-brittle systems can be predicted in a similar way, although many computer structural analysis programs may not have such a capability and therefore it is seldom

done. The load is again applied incrementally and checks on member/connection failures are performed at each step. If a member or connection fails, the failed member/connection is removed, and equilibrium must be satisfied with the remaining members/connections. Sometimes failure of one member/connection leads to other immediate failures. The load at which a cascade of member/connection failures occurs such that equilibrium can no longer be satisfied is the system strength. This process assumes that reliable models for member and connection strength are available and that the brittle failures do not cause dynamic effects.

Burr-arch trusses are statically indeterminate, but not of the pure parallel-ductile type. Both ductile and brittle failure modes can occur, both in a member and in a connection, and diagonal members can lose contact. The ductile modes generally include compression and bearing failures and, possibly, *linear elastic* buckling. The brittle modes generally include shear, tension, and flexure failures. Not considering damage from fire, flood, and foundation subsidence, strength failures are caused by two principal actions: gravity loads and wind. Failure can occur in any of the three principal subsystems: the floor, the lateral bracing system, and the arch-trusses. Four observed failure modes in arch-truss subsystems and their consequences are as follows:

- Compressive failure of the arches, especially near their abutments. This occurred on Gilpin's Falls Covered Bridge and caused a subsequent failure of the lower chord and a partial collapse.
- Shear failures at the relishes (see Fig. 9) that transfer gravity loads from the bottom chord into the post. These cause large bending moments, probably unsupportable, in the bottom chord.
- Failures of bottom chord splices, generally from shear failures in a fishplate or at a scarf. This causes transfer of the total bottom chord tension force to the remaining chord stick.
- Failure at the top-chord-to-post connection (see Fig. 7). This failure may be ductile unless the post fails in flexure.

In general, it can be said that the posts have the most demanding roles and may fail in several modes. In response to the observed failures, some common retrofits are replacement of arch

sections near the abutments, strengthening bottom chord tension splices, and adding steel rods in parallel with the (tensile) posts.

A strength assessment must include floor, lateral, and arch-truss subsystems and must include both members *and connections*. It obviously must begin with a condition assessment based on inspection of the geometry, members, and connections. The most conservative quantitative method for strength assessment or load rating is to consider a Burr-arch truss as a weak-link system. This means performing analyses of linear elastic models and determining the smallest load that causes a demand equal to the estimated capacity of one member *or connection*. This method provides a lower bound for the actual strength of a Burr truss, *conditional* on the estimated member and connection strengths. A final judgment on capacity should be based on an understanding that, for a wooden structure, there is a potential for time-dependent failure, dependence of strength on moisture content, dependence of strength on flaw, and significant variability/uncertainty in estimated member and connection strengths.

Although the above method has unknown conservatism, it seems that alternate strength limit state analyses, which involve applying a load incrementally and following a sequence of member/connection failures until equilibrium can no longer be satisfied, are not yet practical.

To increase understanding of the strength behavior of Burr-arch trusses, a physical model was built and tested at the Vanderhoof-Schuette Structural Laboratory of Case Western Reserve University in 2015. Brief descriptions of the specimen design and fabrication are as follows.

DESIGN OF BURR-ARCH TRUSS MODEL

The intent of the planned physical tests was to observe the strength-limit-state behavior of a “typical” 90'-120' long Burr truss. To minimize issues on scaling of connections and stability of members, it was decided to design a relatively large-scale model with only heavy timber sections with a minimum dimension ≥ 4 ", nominal. The physical constraint was that the Vanderhoof-Schuette Laboratory at Case could accommodate a maximum specimen length of about 40'. A principal design decision was to use a symmetry model (only half a span) representing

approximately a 2/3 scale model of a 90' long Burr-arch truss. Use of a symmetry model implied an important constraint. Since a Burr-arch truss has compression-only diagonals, it cannot be assumed that it will behave antisymmetrically under antisymmetric loads. Therefore the symmetry model cannot be used in conjunction with an antisymmetric load or with an asymmetric load such as an AASHTO-type truck load at the quarter-span only. The research funding allowed only one specimen to be fabricated and tested to failure, under one loading condition (unless repairs could be affected, allowing a retest of the repaired specimen). The model initially proposed is shown in Fig. 20.

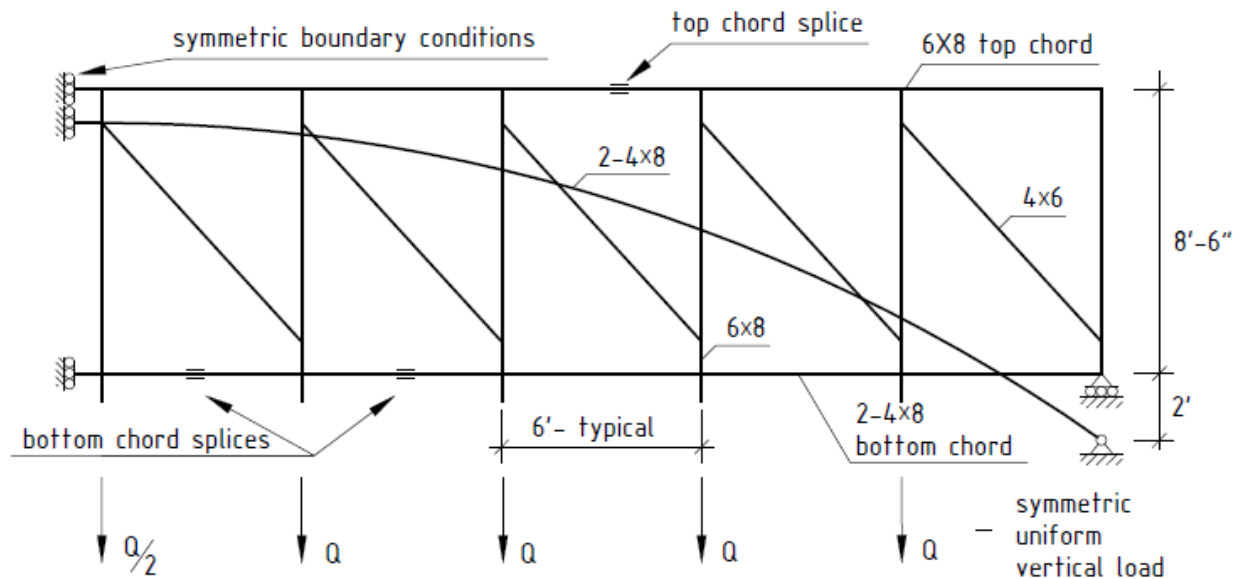


Fig. 20 – Preliminary proposed model design (planed full-size dimensions are given)

It was originally proposed to use Eastern white pine, select structural grade. Additional proposed details were as follows:

Arch

Circular arc – Rise-to-span approximately 1/6.3

Size – 2- 4x8

Length of arch segments – two @ two panels long; one @ one panel long; two splices

Splices – 6" laps at posts

Multiple-kingpost truss - The 8" dimension is perpendicular to the plane of the arch-truss

Top chord – 6x8

Posts – 6x8

Diagonal braces – 4x6

Bottom chord – 2- 4x8

No check braces or “secondary top chords”

Details

Arch-to-post

¾" dap in post

Two 5/8" through bolts

Post-to-top chord

Mortise-and-tenon

¾" dap in top chord

Eccentricity of brace – 8"

Post-to-bottom chord

1-1/2" dap in post

¾" dap in chords

Relish – 8" below bottom chord

Eccentricity of brace – 4" above top of bottom chord

Arch-at-intersection with bottom chord

¾" dap on inside vertical face of arch

1-3/4" dap on outside vertical face of lower chords

One 5/8" through bolt

Splices in bottom chord (two)

First 4x8 member – fishplate with through bolts

Second 4x8 member – oblique tabled (vertical) scarf joint with key and through bolts

Splice in top chord

Oblique tabled (horizontal scarf) joint with key and through bolts

Lateral bracing to be provided at every top chord panel point

The proposed preliminary design was distributed to interested, knowledgeable persons for review and comment. Eight replies were received, four from engineers experienced with heavy timber framing, two from academics, and two from bridge historians. One reviewer thought that the arches should be parabolic, but, in view of the assertion made by Conwill, it was decided to leave the arches as circular arcs.⁴⁵ A relevant observation was that an asymmetric AASHTO-type truck loading near quarter-span was more likely than a uniform gravity load to cause a strength limit state. Several reviewers had reservations about using a symmetry model, preferring a smaller-scale model of an entire span. However, in the judgment of the researchers, a smaller-scale, full-span model, say a 1/3 scale model of a 90' Burr-arch truss, would have introduced issues on scaling of connections (for example, depths of daps) and stability (buckling) of members. Therefore, although an asymmetric truck-type load could not be used, the symmetry model was retained. The preliminary model was, however, changed as follows.

Arches

Normally arch segments span two panels and joints in the two arches are staggered, but the dimensions of a wooden beam from which a two-panel circular arc could be cut were impractically large. Therefore it was decided to fabricate all arch segments to span only one panel, with both arches spliced with radial lap joints at every post.

Multiple-kingpost-truss

The diagonal brace in the second panel away from the arch support was increased to 6x6 to preclude buckling. The end diagonal was also increased to 6x6.

Splice-in-the-top-chord

To decrease fabrication costs, it was decided to use a simple butt connection with a center dowel.

⁴⁵ Conwill, "Burr Truss Framing," 10.

Splice-in-bottom-chord

The splice in one of the chord sticks was moved to the middle panel to decrease the required maximum stick length.

Lateral bracing was used at every top chord panel point and at each post, very near its intersection with the bottom chord. Detailed fabrication drawings of all components are given in Appendix A; conventional detailing was used.

PURCHASE OF WOOD MATERIAL AND FABRICATION OF MODEL

Jim Rice of Lodi Lumber at Lodi, Ohio, and timber framer Rudy Christian of Burbank, Ohio assisted with the order of wood material. The initial intent was to order select structural Eastern white pine (EWP), kiln dried (say MC < 19%), and milled to the prescribed dimensions. It was not specified that the sections had to be quarter-sawn. Obtaining wood that met the above criteria became somewhat of an ordeal. First, select structural EWP in the sizes and lengths required could not easily be obtained. After discussion, it was decided to order Southern Yellow Pine (SYP). The SYP that was shipped did not meet the select structural grading criteria, because the slope of the grain was excessive, and the knots were too big and unsound. The supplier agreed to exchange the material, but when the substitute material arrived, its moisture content varied from 50 percent to 70 percent; it was essentially green. At this point Lodi Lumber offered to replace the green 8x8 sections with some SYP that they had in stock. However the SYP that Lodi Lumber had in stock was Grade 1 rather than select structural. It was this Grade 1 SYP material that was used for several of the posts of the model. As determined later, there was considerable variability in the specific weights of the various members. Afterwards, Rudy Christian remarked that, for the sizes and lengths required, the only *select structural* wood that could be reliably sourced was Douglas fir. However, no Douglas fir was used for the project.

Timber framers Rudy and Laura Christian of Burbank, Ohio, assisted by Andrew Schaeffer, fabricated the members (see Fig. 21). On December 10, 2014, the members were picked up and brought to the Vanderhoof-Schuette Structural Laboratory at CWRU (see Fig. 22).



Fig. 21 – Fabrication of timber sections by Rudy and Laura Christian



Fig. 22 – Fabricated members being picked up at Burbank, Ohio on December 10, 2014

SMALL-SCALE TESTS TO INFER MATERIAL PROPERTIES

Sections of Southern yellow pine (SYP) left over from the fabrication of the Burr truss were sampled to perform the following tests: moisture content, uniaxial compression parallel to the grain, and shear parallel to the grain. Unit weights were determined in conjunction with the above tests. In addition, before the decision to use SYP was made, a section of select structural Eastern white pine (EWP) was purchased and the same tests were performed on EWP during the spring of 2014. Data from those tests are also presented here for comparison.

Moisture content tests – Moisture content tests were performed on thirteen SYP specimens in accordance with ASTM D4442-02 Method B from 8:00AM on February 10, 2015, to 8:00AM on February 13, 2015. The specimens were placed in an oven at 103°C and weighed at approximately 4-hour intervals until the mass no longer decreased. It must be noted that the kiln-dried wood was received at the Vanderhoof-Schuette Structural Laboratory on December 10, 2014. Therefore the moisture content tests were performed after the wood had been in the dry (winter) conditions of the structural laboratory for about two months. Properties of the specimens are given in Table 3.

Specimen	Dimension 1 (in)	Dimension 2 (in)	Dimension 3 (in)	Mass (g)	Volume (in ³)	Unit Weight (lb/ft ³)
1	1.486	1.494	1.489	30.02	3.31	34.6
2	1.540	1.512	1.556	24.08	3.62	25.3
3	1.591	1.496	1.499	30.87	3.57	33.0
4	1.535	1.533	1.525	23.32	3.59	24.8
5	1.501	1.504	1.504	31.18	3.40	35.0
6	1.495	1.489	1.492	30.11	3.32	34.5
7	1.465	1.486	1.489	27.24	3.24	32.0
8	1.555	1.486	1.487	28.10	3.44	31.2
9	1.501	1.523	1.472	22.13	3.36	25.1
10	1.541	1.691	1.520	23.99	3.75	24.4
11	1.505	1.342	1.504	27.91	3.04	35.0
12	1.386	1.384	1.487	26.15	2.85	34.9
13	1.504	1.369	1.500	28.91	3.09	35.7
						Average: 31.2

Table 3 – SYP Moisture content specimens - Dimensions, Volume, Mass, and Unit Weight

The computed moisture contents are given in Table 4; the mean value was 10 percent.

Specimen	Initial Mass (g)	Final Mass (g)	Moisture Content (%)
1	30.02	27.19	10
2	24.08	22.00	9
3	30.87	27.51	12
4	23.32	21.40	9
5	31.18	28.53	9
6	30.11	27.29	10
7	27.24	24.88	9
8	28.10	25.51	10
9	22.13	19.85	11
10	23.99	21.63	11
11	27.91	25.31	10
12	26.15	23.71	10
13	28.91	26.40	10
			Mean: 10
			Std. Deviation: 0.885

Table 4 – SYP Moisture Contents

Uniaxial compressive tests parallel to the grain – Uniaxial compression tests were performed on seven SYP specimens on January 22, 2015. The specimens were all 10" long with cross-sectional dimensions and unit weights as given in Table 5. Five of the seven specimens were clear; specimens 7C and 2C both had small knots near their ends.

Specimen	Dimensions (in)	Cross-Sectional Area (in ²)	Mass (g)	Unit Weight (lb/ft ³)
7C	1.501 x 1.510	2.267	210.56	35.4
6C	1.475 x 1.511	2.229	187.98	32.1
5C	1.507 x 1.502	2.248	203.61	34.5
4C	1.501 x 1.502	2.254	208.38	35.2
3C	1.489 x 1.499	2.232	196.43	33.5
2C	1.493 x 1.503	2.244	200.26	34.0
1C	1.499 x 1.502	2.252	157.83	26.7
				Average: 33.1

Table 5 – SYP Compression Specimens- Dimensions, Mass, and Unit Weight

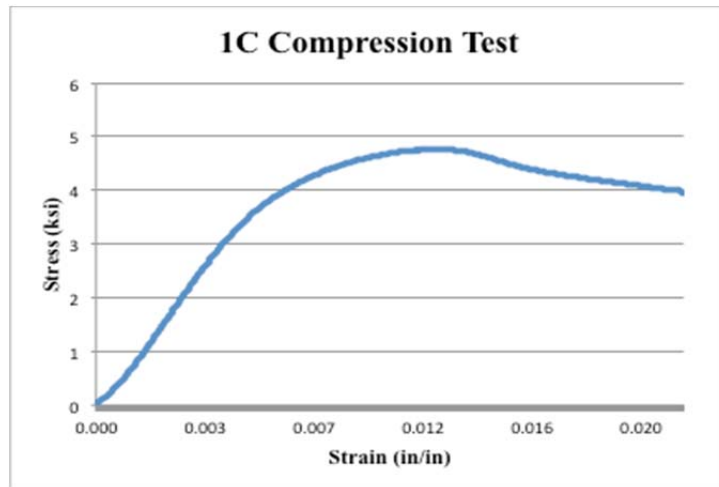
The tests were performed on an MTS servo-hydraulic testing machine in displacement control.

Fig. 23 shows the test setup.

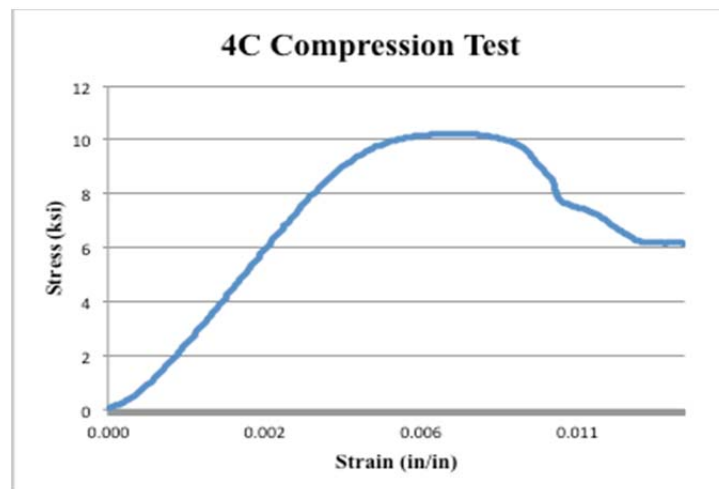


Fig. 23 – Uniaxial compressive test setup

Displacements on two sides of the specimen were measured using direct current differential transformers (DCDTs). The average of the two values was found and divided by the gauge length of 7" to obtain strain values. The stress-strain curves for specimens 4C and 1C are shown in Fig. 24.



24a)



24b)

Fig. 24 - Uniaxial compressive stress strain curves

The modulus of elasticity was computed using linear regression analysis on the data corresponding to the initial (linear) part of the curve. Strengths and moduli for all seven specimens are given in Table 6. The average compressive strength was 7.9 kilopound per square inch (ksi) and the average modulus of elasticity was 1,812ksi. These average values compare well with published values.

Specimen	Compressive Strength (ksi)	Modulus of Elasticity (ksi)
7C	6.97	1806
6C	7.08	1535
5C	9.11	2198
4C	10.24	2510
3C	10.34	1998
2C	6.78	1967
1C	4.77	672
Average	7.90	1812

Table 6 - SYP Compressive Strengths and Moduli of Elasticity

It was observed that properties were correlated with the unit weights and flaws. Specimen 1C had the fewest growth rings, the smallest unit weight and, correspondingly, the smallest strength and modulus. Table 6 shows the variability in properties of wood of the same species and grade. Specimens 7C and 2C, which had small knots, had smaller strengths. Figs. 25(a) and 25(b) show cross-sections and failure modes for specimens 4C and 1C, respectively.

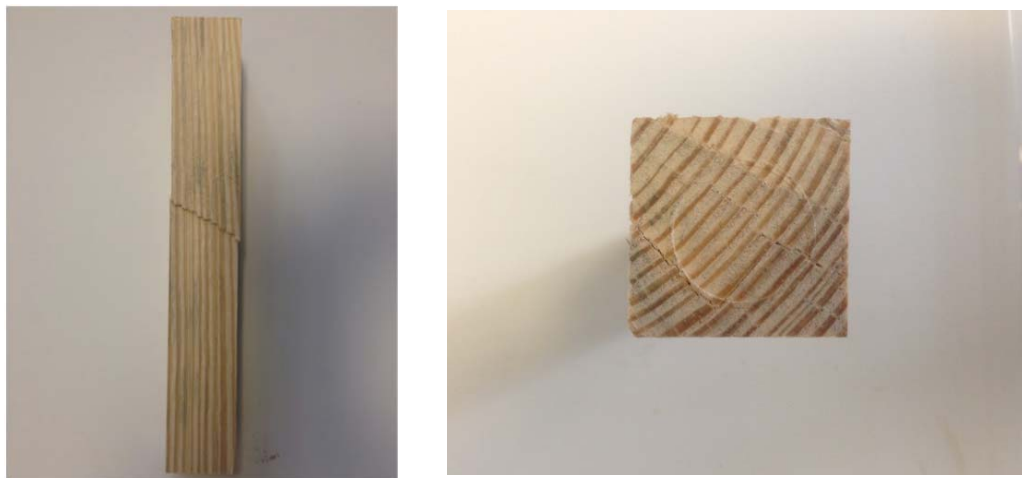


Fig. 25a – Cross section and failure mode for specimen 4C



Fig. 25b – Cross section and failure mode for specimen 1C

Specimens 4C and 1C (as well as 5C) failed in the commonly-observed mode of cell-wall instability and “shear flow” localized at planes of large shear stress (typically at 45° from the axial direction). The stress-strain curves (Fig. 24) show that this mode is ductile. Specimens 2C and 6C failed by crushing outside the gauge length and specimens 7C and 3C displayed longitudinal splitting failures. The corresponding experimental results for the select structural EWP tested in spring 2014 are given in Table 7. As is well-known, the SYP has a significantly larger compressive strength and a slightly larger modulus of elasticity.

Specimen	Compressive Strength (ksi)	Modulus of Elasticity (ksi)
1	5.25	1754
2	5.50	1674
3	6.65	1692
4	6.25	1736
Average	5.91	1714

Table 7 – EWP Compressive strengths and moduli of elasticity

Shear tests parallel to the grain – The shear test specimen that was used and the test set-up are shown in Figs. 26 and 27. Dimensions of the specimens are given in Table 8. All specimens had a nominally zero grain angle.

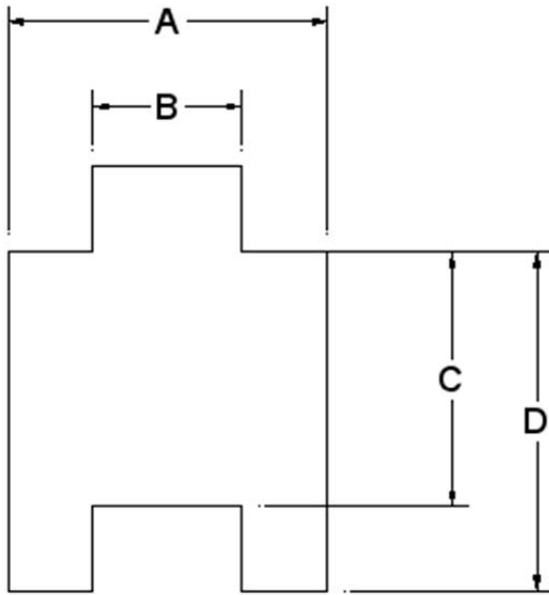


Fig. 26 – Shear test specimen



Fig. 27 – Shear test set-up

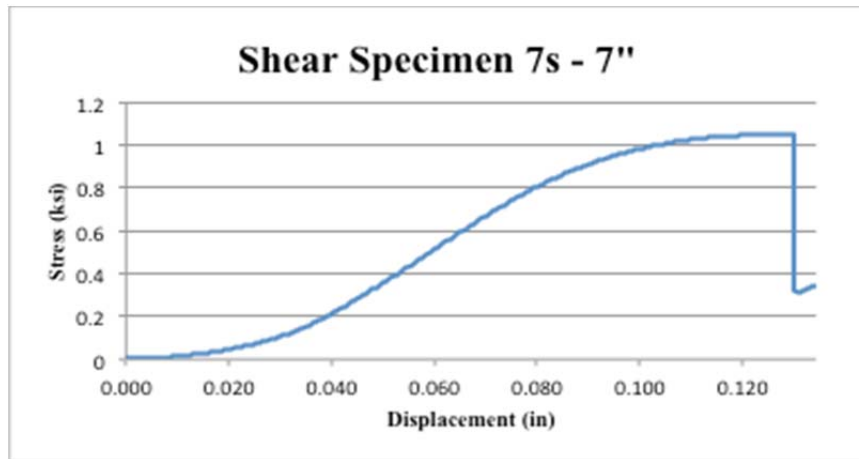
Specimen	A (in)	B (in)	C (in)	D (in)	Depth (in)	Mass (g)	Unit Weight (lb/ft ³)
3S	3.495	1.712	4.031	5.036	3.498	538.91	33.2
4S	3.506	1.731	4.022	4.995	3.489	542.05	33.6
5S	3.493	1.727	5.003	5.700	3.494	649.5	34.5
6S	3.502	1.719	6.022	7.002	3.487	752.77	33.7
7S	3.497	1.730	7.005	7.990	3.491	1065.96	41.6
							Average: 36.2

Table 8 – SYP Shear specimen dimensions, masses, and unit weights

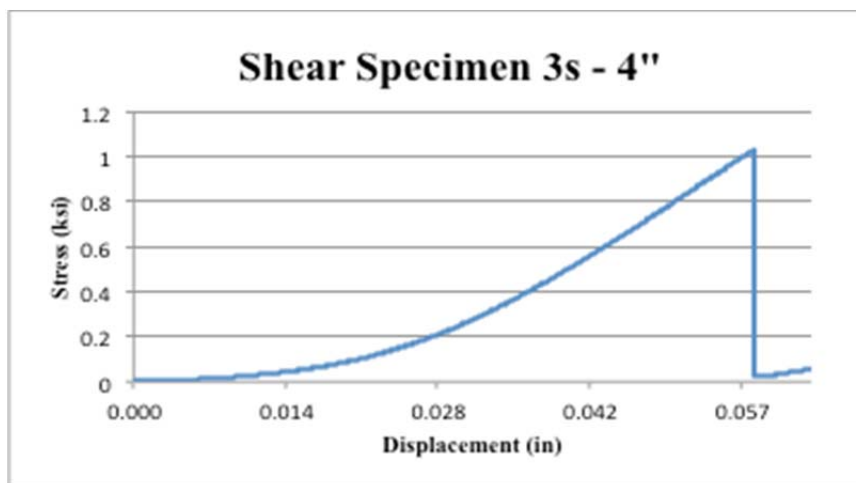
The depth, or the dimension perpendicular to the plane shown in Fig. 26, was maintained constant, approximately equal to 3.5", but the dimension "C" and the corresponding shear area, equal to $2 \cdot C \cdot (\text{depth})$, were varied. Tests were again performed using an MTS servo-hydraulic

testing machine in displacement control. The specimens were loaded with a steel block in the notch as shown in Fig. 27. Two steel blocks, tied horizontally to minimize normal stresses perpendicular to the grain of the wood, were used as bearings at the bottom.

Figs. 28a) and 28b) show the nominal shear stress, computed by $(\text{Load}) / 2 * C * (\text{Depth})$, versus actuator displacement for specimens 3S and 7S.



28a)



28b)

Fig. 28 – SYP Shear stress versus actuator displacement for specimens 3S and 7S

Table 9 shows the computed parallel-to-the grain shear strengths for the five specimens. They are notably consistent, with an average shear strength of 1.00ksi. Fig. 29 shows failed specimen 3S.

Specimen	Shear Strength (ksi)
3S	1.03
4S	1.02
5S	0.958
6S	0.965
7S	1.05
Average	1.00

Table 9 - SYP Shear strength parallel to the grain

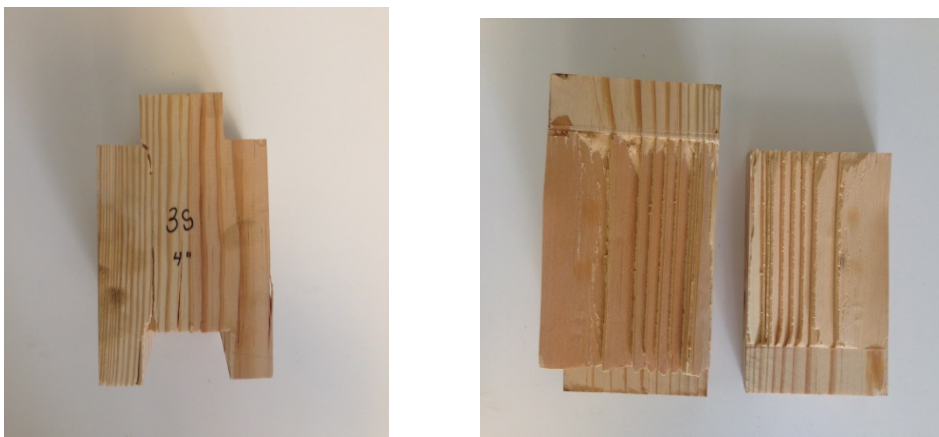


Fig. 29 – SYP failed shear specimen 3S.

Specimens 3S, 4S, 5S, and 6S had a completely brittle shear failure as exemplified by Fig. 28a. Specimen 7S began to fail in compression before ultimately failing in shear. This is demonstrated by Fig. 28b, which shows some ductility before the sudden drop in load due to the shear failure. Therefore the specimen 7S shear area equal to 48.9in^2 caused a transition from a strictly brittle shear failure to a compressive failure over a bearing area equal to 6.04in^2 . The ratio of the two areas, $48.9\text{in}^2/6.04\text{in}^2 = 8.1$, is approximately equal to the ratio of the average SYP (parallel-to-the-grain) compressive strength to the average (parallel-to-the-grain) shear strength, $7.9\text{ksi}/1.0\text{ksi} = 7.9$. This very limited data set suggests that if a SYP specimen has a

ratio of (parallel-to-the-grain) shear area to bearing area ≥ 8.1 , a compressive failure is more likely to occur.

Specimen	A (in)	B (in)	C (in)	Depth (in)	Shear Strength (ksi)
1	3.771	1.749	2.938	3.751	0.575
2	3.765	1.740	4.969	3.768	0.580
3	3.777	1.737	8.938	3.785	compression – crushing failure
					Average Shear Strength: 0.578

Table 10 – EWP parallel-to-the-grain shear strengths

Table 10 contains data for parallel-to-the-grain shear strength measured for the Eastern white pine specimens. The average shear strength is 0.578ksi, smaller than that of the Southern yellow pine. The National Design Specification gives a Reference Design Value for shear parallel to the grain equal to 0.135ksi for select structural EWP. For specimen 3, with $C = 8.938$ in and a shear area equal to $2 * 8.938 * 3.785 = 67.7 \text{in}^2$, a compressive failure was observed over a bearing area $1.737 * 3.785 = 6.57 \text{in}^2$. From Table 7, the average EWP (parallel-to-the-grain) compressive strength was 5.91ksi, giving a ratio of average compressive strength to average (parallel-to-the-grain) shear strength of $5.91 \text{ksi} / 0.578 \text{ksi} = 10.2$, which is approximately equal to the specimen 3 ratio of shear area to bearing area, $67.7 \text{in}^2 / 6.57 \text{in}^2 = 10.3$. This very limited data set suggests that if a EWP specimen has a ratio of (parallel-to-the-grain) shear area to bearing area ≥ 10.3 , a compressive failure is more likely to occur.

LINEAR ELASTIC STRUCTURAL ANALYSES

As discussed previously, beginning with the work of Kemp and Hall, many analytical models have been defined that have illuminated the linear elastic behavior of Burr-arch trusses.

Nonetheless, to determine forces for the particular proposed model geometry and loading condition, a plane frame linear elastic model was defined using SAP2000. The symmetry model has five 6' panels. The geometry of one panel is shown in Fig. 30, which also shows the eccentricities of the diagonals with respect to the post-chord intersections. The radius of curvature was 53.076'. The boundary conditions and the member labeling are shown in Fig. 31.

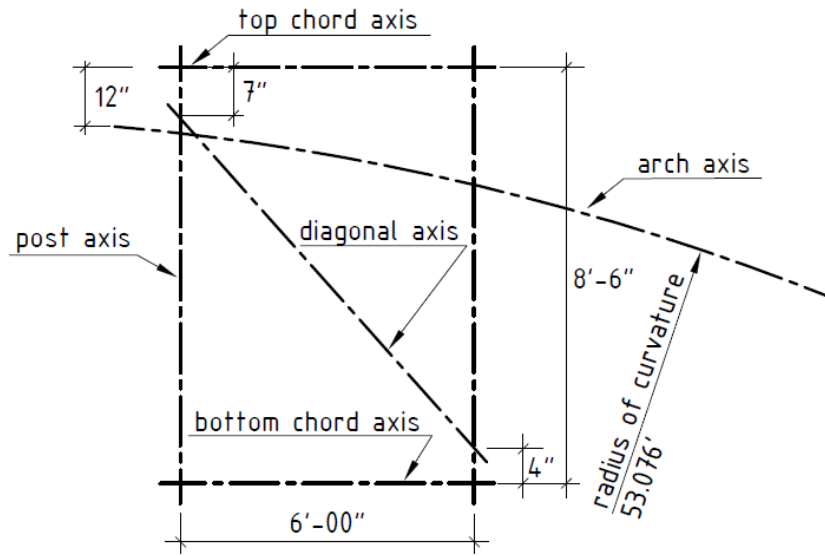


Fig. 30 – Geometry of panel and vertical position of arch at axis of symmetry

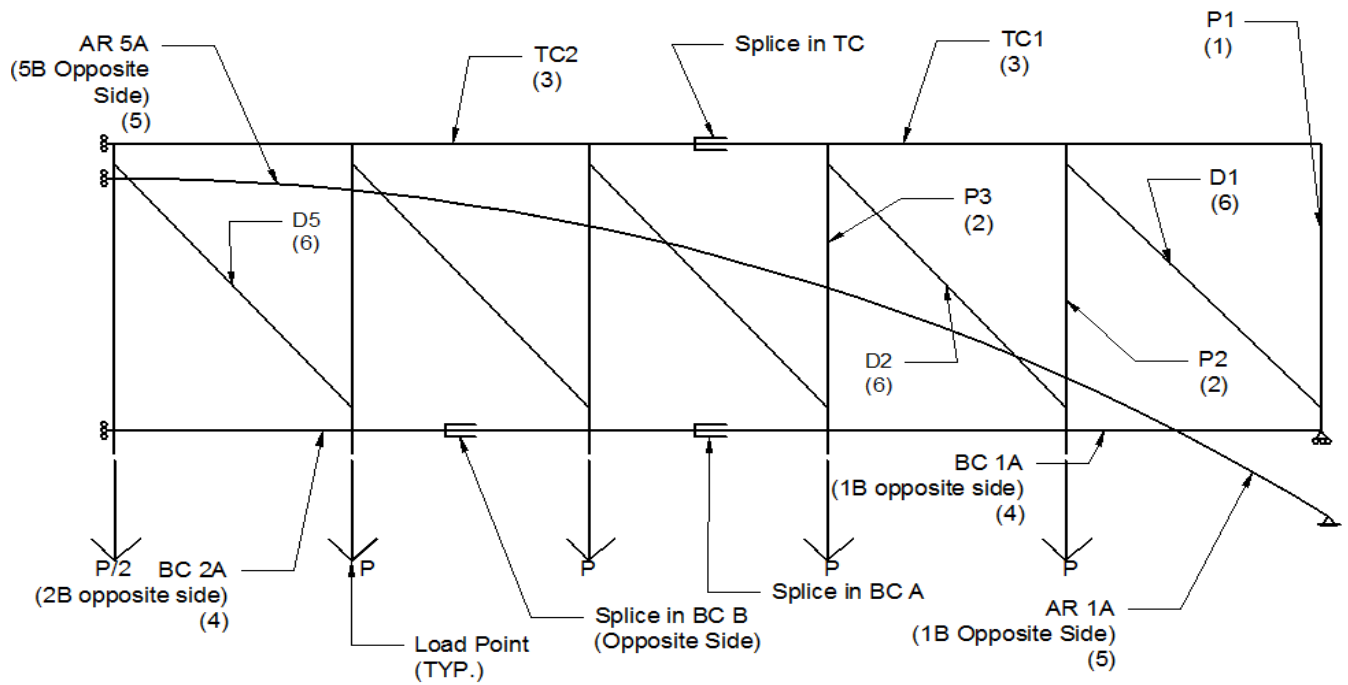


Fig. 31 – Member labeling and symmetry boundary conditions

All members were assumed to be straight and prismatic, with areas and moments of inertia as shown in Table 11. The bottom chord and the arches, which consist of two sticks, were modeled with only one element.

Member	Moment of Inertia (in ⁴)	Cross-Sectional (Axial) Area (in ²)
Bottom Chord/Arch/Posts	341	64
Top Chord	144	48
Diagonals D3, D4 and D5	72	24
Diagonals D1 and D2	108	36

Table 11 – Member properties

The arch segments were assigned moment releases at their ends and the posts were assigned moment releases at their intersections with the top chord. The connection between the arch and the lower chord was assumed to be rotationally rigid. A 1 kip vertical load was applied to each bottom chord panel point ($\frac{1}{2}$ kip at the axis of symmetry). The objective was not to calibrate or verify or refine a linear elastic model, but simply to confirm the expected locations with the largest stress resultants. Therefore, the model was simple; specifically, it did not consider:

- the changes in the cross-section of the posts;
- the scarf and fishplate connections;
- the rotational stiffnesses of the post-bottom chord connections, the post-top chord connections, and the post-arch connections; and
- the continuity in the arch segments provided by the lap splices and the two through bolts.

Considering the butt connection at the top chord to be a rotational hinge, the simple plane frame model as defined was statically indeterminate to the 35th degree. Figs. 32, 33, and 34 show the resultant axial force, shear, and moment diagrams from the analysis. The vertical reaction at the arch thrust bearing is essentially equal to the total vertical load. This vertical reaction would decrease if the bearing had a finite stiffness. There is shear in the arch segment below the bottom chord intersection, which means that the resultant reaction at the thrust bearing is not in the direction of the arch axis at the spring point. Diagonal D1 has a very small compressive axial force.

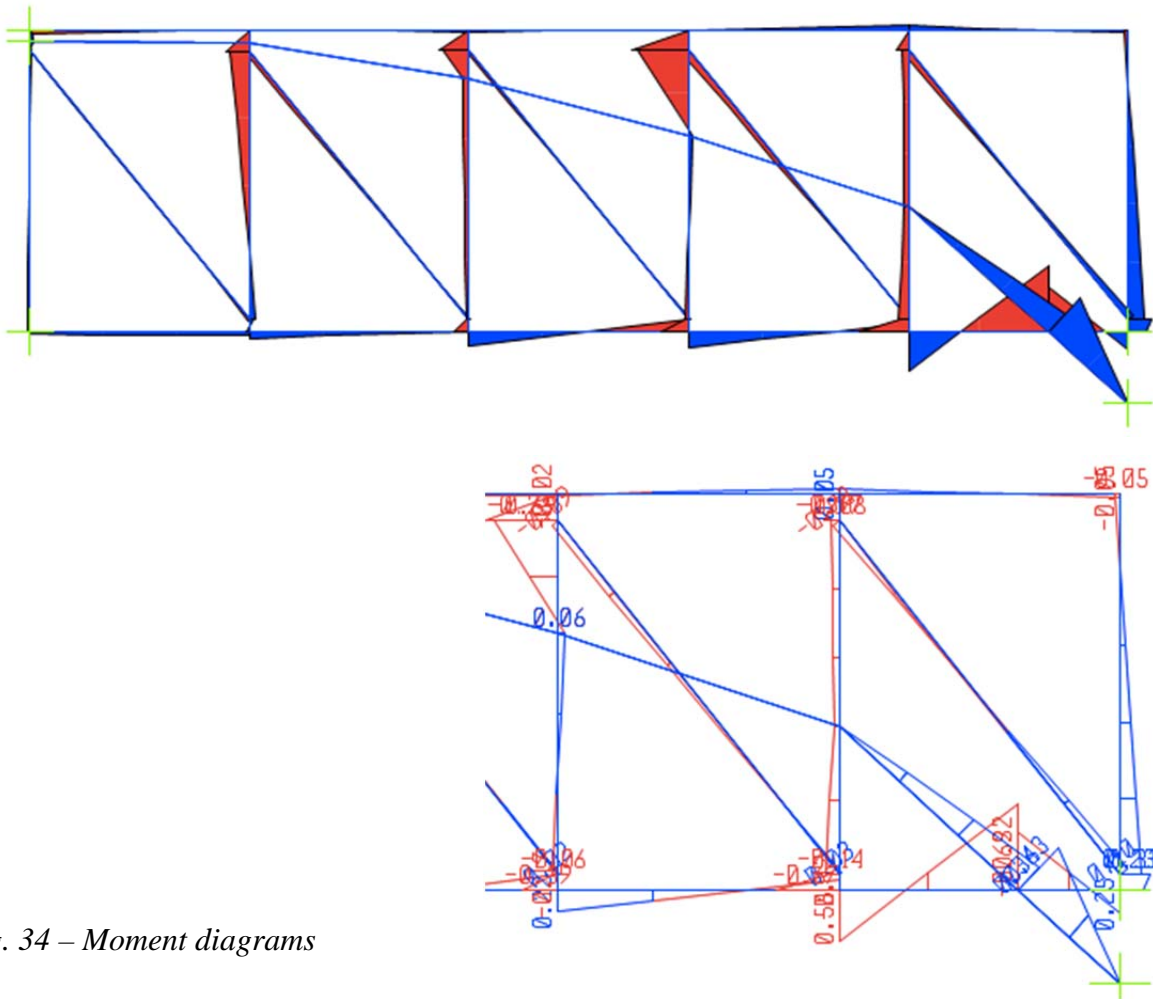


Fig. 34 – Moment diagrams

Figs. 32, 33, and 34 confirm the following locations with large stress resultants (see Fig. 31 and Appendix drawing A-0 for labeling):

Axial forces

- In the arch segment below the arch-bottom chord intersection
- At the scarf joint in the chord in panel 4
- In posts P2, P3, P4, and in diagonal D2

Shear forces

- In post P4 at top, in post P3 at top and bottom, and in post P2 at bottom
- In the bottom chord at the chord-arch intersection

Moments

- In posts P3 and P4 near top
- At the arch-bottom chord intersection, both in the arch and in the chord

Posts P3 and P4 have the largest combined axial force, shear, and moment demands. The linear elastic model with the assumed wood modulus of elasticity of 1800ksi predicted a vertical displacement at midspan (at bottom) equal to 0.052in for the unit vertical loading. However, the actual vertical displacement at the first application of such a load will probably be larger due to “joint tightening.”

DESIGN AND FABRICATION OF TEST FIXTURE

The Vanderhoof-Schuette Structural Laboratory at Case Western Reserve University has both a “strong floor” and a “strong wall.” The L-shaped, cellular strong wall is 8' thick, with 18"- thick flanges with tie-down points at 2' on center. The 10'-deep cellular strong floor also has 18"-thick flanges with tie-downs at 2' on center. The overall arrangement of the Burr-arch truss specimen was as shown in Fig. 35.

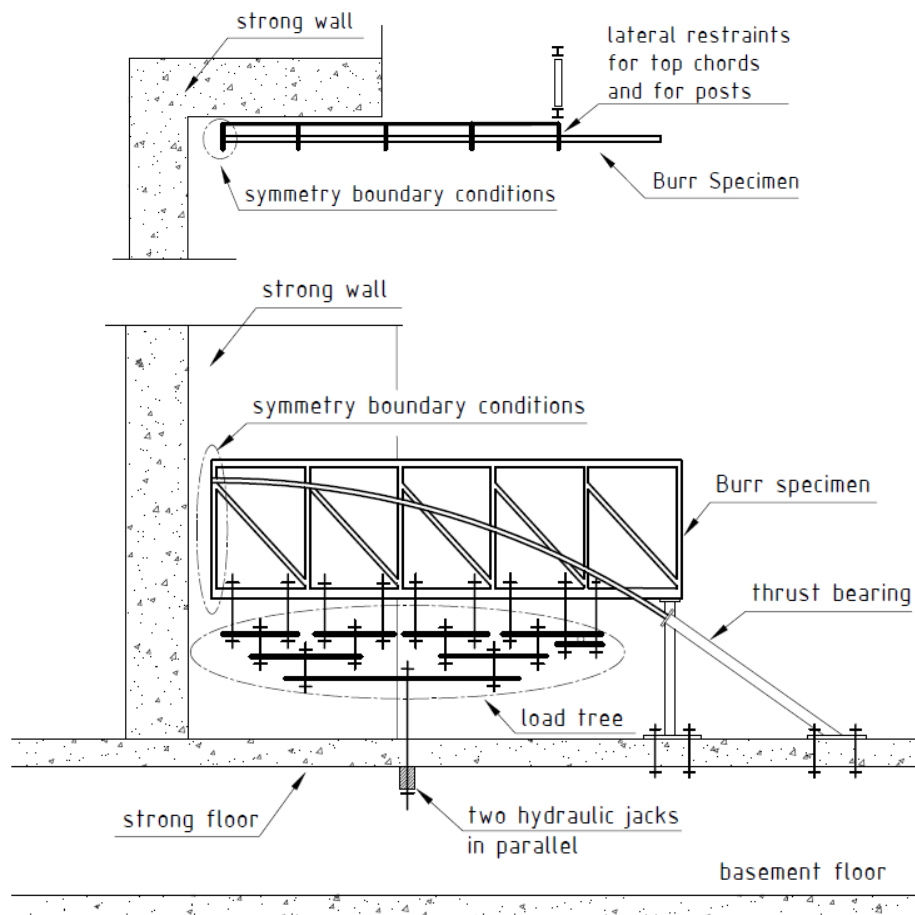


Fig. 35 - Burr specimen layout

Extensive fixturing was required to perform the load tests. All fabrication was performed in-house by Case Civil Engineering department engineers Michael Butler, and Jim Berilla, and students Laura Rendos, Kamil Nizamiev, Stacey Hursen, and Gregory Willenkin. The major components of the test fixture were thrust bearing, lateral bracing, load tree, and boundary conditions at the axis of symmetry.

Thrust bearing – Details of the thrust bearing are given in Appendix drawings A-6 to A-9 and in Figs. 36 and 37.



Fig. 36 – Thrust bearing



Fig. 37 – Arch springing

The estimated horizontal stiffness of the thrust bearing was 2,800 kips/inch, which meant that a horizontal force of 100 kips would cause a horizontal displacement of approximately 1/32 inch. The thrust bearing was attached to the strong floor by four, 2" diameter, steel dowels inserted into the tie down points and posttensioned to the floor. The thrust bearing had a steel bearing plate, perpendicular to the arch axis at the spring point.

Lateral bracing – Ten lateral restraints were installed to preclude out-of-plane motion of the truss. All were custom-fit, U-shaped restraints made of welded steel channel sections. Fig. 38 shows the five lateral restraints at the top nodes. Fig. 39 shows the five lateral restraints placed at accessible locations on the lower half of the posts. The top end node, at post P1, was not braced laterally.



Fig. 38- Lateral restraints at top nodes



Fig. 39 – Lateral restraints on posts

Load tree – To apply a uniform loading, a “load tree” was fabricated as detailed in Appendix drawings A-10 to A-15 and shown in Fig. 40.



Fig. 40 - Load tree

Such a loading system is statically determinate, producing nodal forces that are completely determined by equilibrium. The relative distances between various support and load points at any specific level of the tree were determined such that four equal-magnitude forces were applied to the bottom chord (and a half-magnitude force at the axis of symmetry). Since the applied forces are determined entirely by equilibrium, they are independent of (small) relative vertical displacements of the bottom chord panel points as a load is incremented. Loads were applied to

the bottom chord through bearings as shown in Appendix drawing A-15. The total load was affected by two equal 60-ton hydraulic through jacks connected to a common manifold pressurized by one electric pump. The loading system was effectively displacement controlled. Fig. 41 shows the two hydraulic jacks in the strong floor; extension of the jacks caused tensile forces in two calibrated high-strength Dywidag bars.



Fig. 41 – Two hydraulic jacks in the strong floor

Boundary conditions at axis of symmetry – For a symmetric Burr truss loaded symmetrically, the boundary conditions at midspan must be: zero horizontal displacement, zero rotation, and zero vertical reactive force (shear).

The concrete strong wall of the Vanderhoof-Schuette Structural Laboratory is extremely stiff horizontally, practically rigid for the horizontal forces envisioned during tests of the wooden Burr-arch truss. To preclude rotations, steel channels were fastened with lag bolts at the top and bottom of the chords and arch as shown in Appendix drawing A-2. Because two diagonals frame into the post at the axis of symmetry, there is no shear at the top of this post under a symmetric

load. To preclude shear in this center post a vertical steel plate was inserted between the top chord and the arch as shown in Appendix drawing A-1. In addition, 1½"-diameter steel bars, which were previously welded to the channels, terminated in two bearings restrained between the strong wall and HSS (hollow structured sections) 3x5x1/2 tubes as shown in Figs. 42 and 43. In total, the two chords and the arch had twelve greased horizontal bearings.



Fig – 42 Top bearings at axis of symmetry Fig 43 – Bottom bearings at axis of symmetry

These sliding bearings did not function as expected. The bearings did not allow free vertical motion when large horizontal forces existed, thus providing unwanted vertical reactive forces. Therefore the sliding bearings had to be replaced. A series of small-scale tests were performed to determine a better alternate bearing design. Two steels with different hardness and surface finish were tested with different interfaces. Seven small-scale tests were performed as listed in Table 12. Three had sliding surfaces and three had two sets of four rollers, sold commercially as “dowel pins.”

Small-Scale Test	Bearing type
1	5160 Steel with roller nests
2	4140 Steel with roller nests, ungreased (first replicate)
3	4140 Steel with roller nests, ungreased (second replicate)
4	4140 Steel with PTFE (Teflon)
5	4140 Steel with PTFE and stainless steel
6	4140 Steel with PTFE and stainless steel, greased
7	4140 Steel with roller nests, greased

Table 12 – Small-scale bearing tests



Fig. 44 - Pre-compression of a small-scale bearing assembly

Fig. 44 shows the pre-compression of one bearing assembly using a hydraulic jack. Figs. 45 and 46 show a roller and a sliding bearing assembly placed in the MTS servo-hydraulic testing device. Displacement was applied and the force required to move the plate within the (pre-compressed) assembly was measured.



Fig. 45 – Test of roller bearing assembly



Fig. 46 – Test of sliding bearing assembly

The load versus time curve for the bearing consisting of the 4140 steel with greased roller nests is shown in Fig. 47.

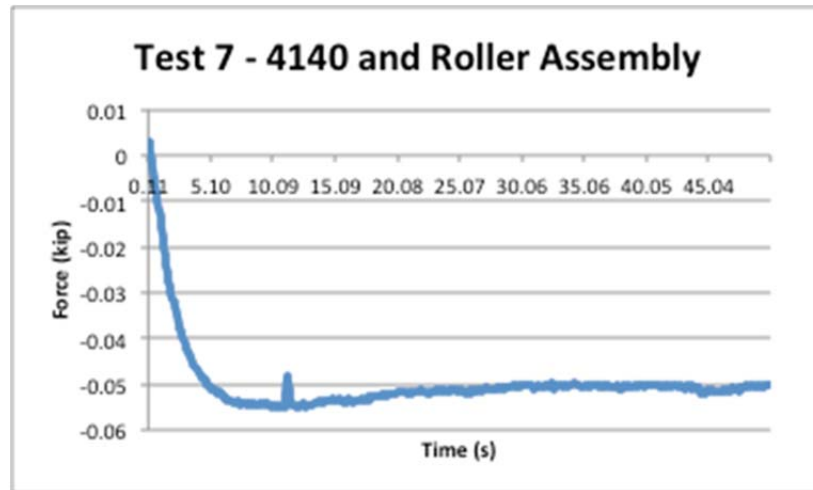


Fig. 47 – Load versus time curve for 4140 steel plates with roller bearing assembly

Results for all seven tests are summarized in Table 13, which shows that the 4140 steel with the greased rollers had the smallest effective coefficient of friction, producing an essentially negligible frictional force in comparison with the envisioned magnitudes of the applied vertical loads. Therefore, nested rollers replaced the sliding bearings. Four nests of rollers were fabricated; the top bearings consisted of twenty-eight dowel-pin rollers in a “cage” while the bottom bearings consisted of seventeen dowel-pin rollers in a cage, as shown in Fig. 48.

Small-Scale Test	Normal (pre-compression) Force (kips)	Maximum Applied Force / 2 (pounds)	Effective Coefficient of Friction
1	15.74	197	0.013
2	15.75	65	0.0041
3	16.25	61	0.0038
4	15.75	1116	0.071
5	16.00	914	0.057
6	15.88	338	0.0213
7	16.25	55	0.0034

Table 13 – Effective coefficients of friction for the seven bearing tests



Fig. 48 – Nested roller bearings

ASSEMBLY, INSTALLATION OF MODEL, AND INSTRUMENTATION

The Burr-arch specimen was assembled on December 11, 2014. Timber framers Rudy and Laura Christian and carpenter Andrew Schaeffer came to the Vanderhoof-Schuette Laboratory to lead and guide the assembly. Case School of Engineering Professor Dario Gasparini, Facilities Manager Neil Harnar, Engineer Michael Butler, and student Kamil Nizamiev assisted them. The overall process consisted of the following steps:

- Layout of posts;
- Assembly of bottom chord sticks with posts;
- Assembly of top chord with posts;
- Rotation of frame to vertical position;
- Insertion of diagonals and activation of truss self-weight; and
- Placement of arch segments, starting from the axis of symmetry and proceeding to the thrust bearings.

The process is illustrated by Figs. 49 through 52.



Fig. 49 – Assembly of bottom chord to posts



Fig. 50 – Assembly of top chord to posts



Fig. 50a – Rotation of frame to vertical position



Fig. 51 – Insertion of diagonals; self-weight partially active



Fig. 52 – Placement of arch segments

The geometry of the daps in arch segments AR-1A and AR-1B at their intersection with the bottom chord was measured in the laboratory and then cut to fit as shown in Fig. 53.



Fig. 53 – Measuring and cutting daps for arch-bottom chord intersection

Arch segments AR -1A and AR-1B (see Appendix drawing A-0) were fabricated approximately 12" longer than required. They were custom-cut later to match precisely with the steel thrust bearings. After the specimen was assembled, considerable time was spent placing the through bolts, installing the lateral bracing, and attaching the steel fittings at the axis of symmetry. In addition, to help transfer tensile force, steel straps and shear plates were installed on the bottom chord sticks at the axis of symmetry as shown in Fig. 54.



Fig. 54 – Steel straps and shear plate to help transfer bottom chord tensile force into bearings

Only limited instrumentation was feasible within the research budget. It consisted of four clip-on strain transducers on the arches near the spring point, displacement transducers at various positions at midspan and at the bottom of post P5, and two calibrated Dywidag bars as force transducers.

To use the Dywidag bars as force transducers, they were instrumented with spot-welded, 350 Ω strain gauges manufactured by Hitec Products, Inc. and then calibrated. The calibration setup is shown in Fig. 55. A calibrated load cell was placed in series and the bars were stretched through the 18" thick face of the strong wall.



Calibrated load cell

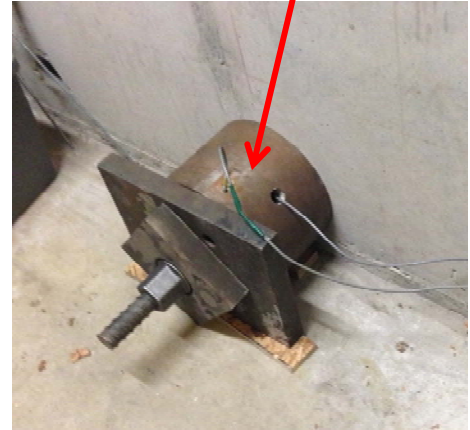


Fig. 55 – Set-up for calibration of Dywidag bars as force transducers

The force versus recorded strain curves are given in Figs. 56 and 57. The slopes of the two calibration curves are given in Table 14.

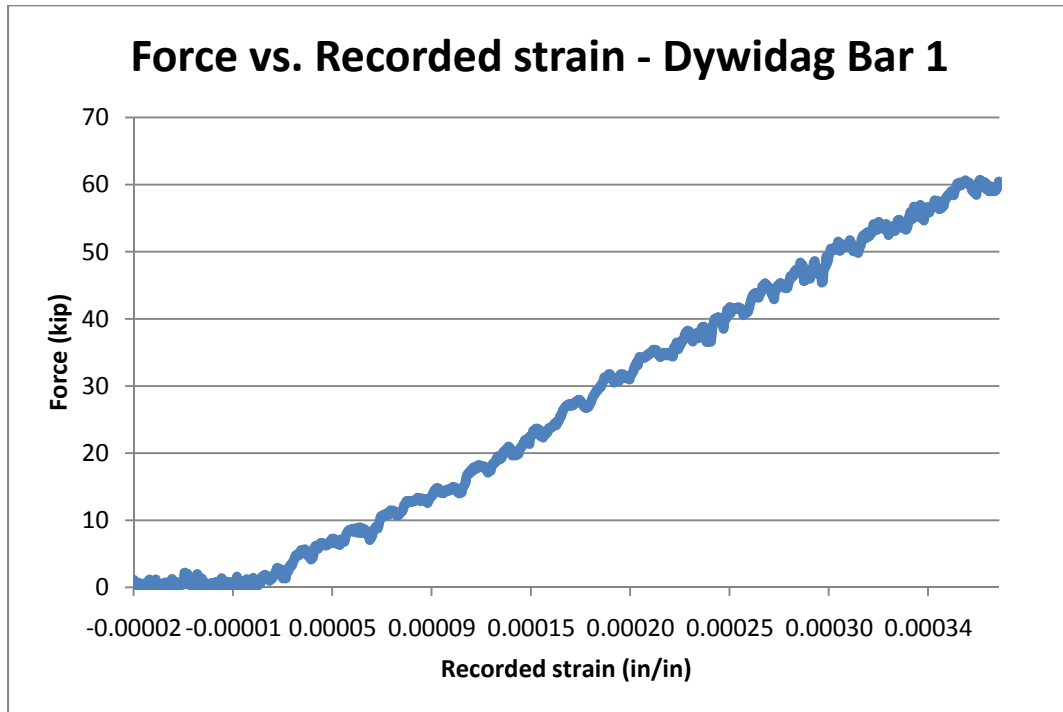


Fig. 56 – Calibration curve for Dywidag bar 1

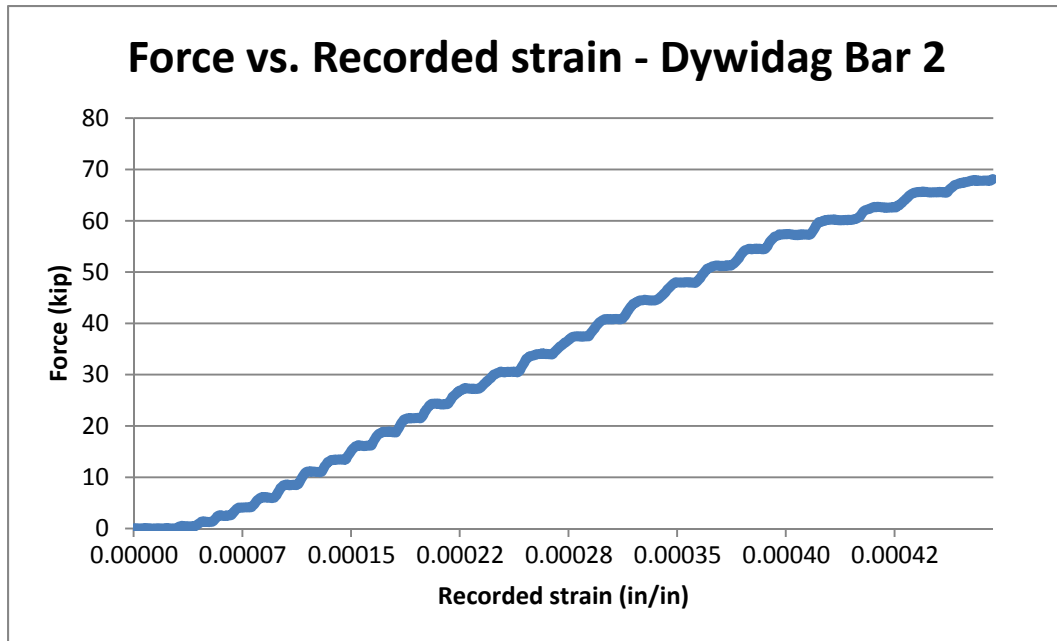


Fig. 57 – Calibration curve for Dywidag bar 2

Specimen	Slope ((μ in/in)/kip)
Dywidag bar 1	5.84
Dywidag bar 2	6.16

Table 14– Calibration curve slopes

Displacement transducers were calibrated by applying a known displacement and verifying that the data acquisition system recorded the correct value. The data acquisition capabilities of the MTS control system in the structural laboratory were used.

Preparations for testing were not completed until the third week of March 2015. Therefore the Burr specimen spent the entire 2014-15 winter in the dry conditions of the Structural Laboratory. As a consequence, extensive shrinkage cracking occurred in the wood sections as the moisture content of the wood decreased. Fig. 58 shows shrinkage cracks (heart checks) in the posts, at the notches for the diagonals and at their bottoms.



Fig. 58 – Cracking (heart checks) in posts after dry (winter) conditions in laboratory

STRENGTH TESTS

In preparation for the strength tests, the weight of the load-tree and the self-weight of the Burr specimen were calculated; they were 4.7 kips and 2.5 kips, respectively, for a total weight of 7.2 kips. From March 24, 2015, to May 21, 2015, the specimen was loaded six times, with the following results.

Test 1 – The first test was performed on March 24, 2015. The load was applied by “jogging” the electric pump and thus extending the hydraulic jacks. After approximately six minutes, at an applied load of 13.4 kips (for a total load of $4.7+2.5+13.4 = 20.6$ kips) the tabled scarf joint in panel 4 failed, as shown in Fig. 59.

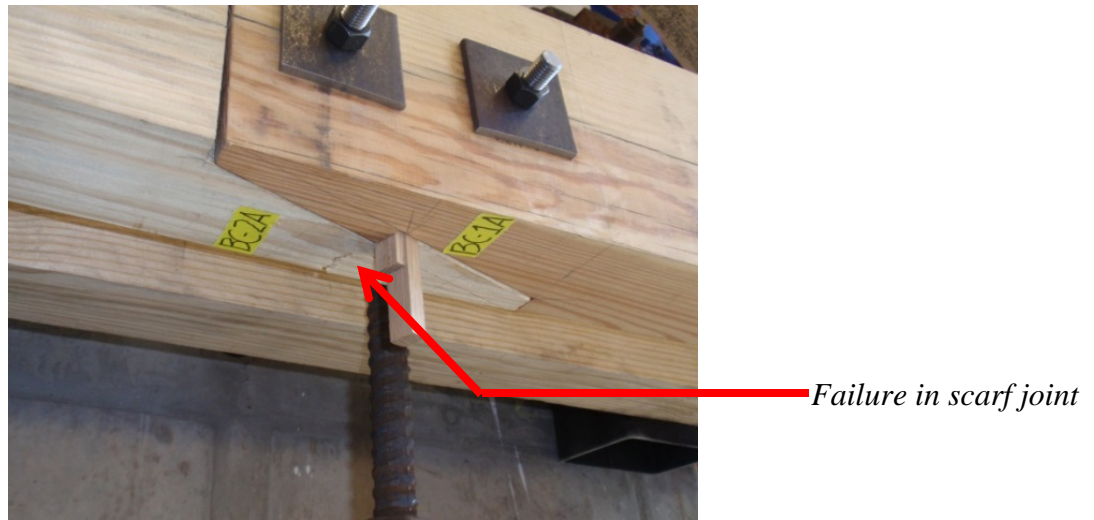


Fig. 59 – Failure in scarf joint in truss panel 4

The failure occurred near the (vertical) scarf table, at the thinnest section. The failure was caused by axial tension in the bottom chord and bending moment produced by applying the load directly on the chord (as commonly done on covered bridges). But the bottom chord consists of two sticks. Each stick carries a fraction of the total axial force and moment proportional to its relative axial and bending stiffness, respectively. Therefore to estimate the axial force and moment carried by the stick with the scarf joint, a model to predict the axial and flexural stiffnesses of the stick with the scarf joint is needed. The stick with the scarf joint certainly has smaller axial and flexural stiffnesses than the stick with a solid section; therefore, it will carry less than half of the

total tensile force and moment. However, there is a stress concentration at the re-entrant corner of the scarf table. It should be noted that after the scarf joint failed, the other chord stick was able to carry the total axial force and moment. That is, the brittle failure and shedding of the load by the scarf joint did not cause an immediate failure in the other stick, and the applied load was maintained.

The scarf joint was repaired as shown in Fig. 60, after a deliberate effort to draw the failed parts together before welding the steel straps.



Fig. 60 – Repair of scarf joint

Test 2 – After the scarf joint repair was completed, the truss was tested again on March 31, 2015. At an applied load of 27.4 kips (total load of 34.6 kips) a localized failure occurred near the bearings of the top chord and arch at the axis of symmetry. A bearing weldment broke, and a separation occurred between the top chord and the post, as shown in Fig. 61. No other damage was observed in the specimen.



Fig. 61 – Localized failure at top chord

Displacement readings and direct observation indicated that the top bearings were not moving freely in the vertical direction. The bearings were “re-greased,” the mortise-and-tenon joint was closed, and steel straps were added to tie the bearings of the top chord and arch together vertically.

Test 3 - The truss was tested again on April 1, 2015. At an applied load of 51.7 kips (total load of 58.9 kips) a tensile-flexural failure occurred in one of the bottom chord sticks as shown in Fig. 63. The wood section at this location was reduced because of the dap; moreover, it had two small knots, one of which is visible in Fig. 62.

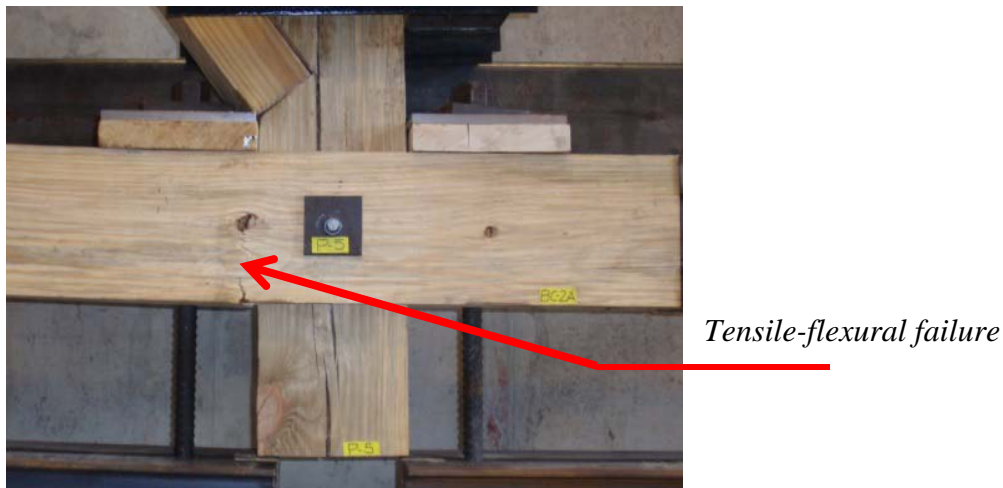


Fig. 62 – Tensile-flexural failure in one of the bottom chord sticks

The brittle rupture of one chord stick did not lead to a significant drop in the applied load, because the second chord stick was able to “take over.” The axial force and moment that caused the failure are uncertain, both because the relative axial and flexural stiffnesses of the two sticks were not measured and because some of the bearings were not moving freely in the vertical direction. Damage also occurred at the mortise-and-tenon joint at the top of post 3. Fig. 63 shows crushing perpendicular to the grain and permanent horizontal displacement. The load that initiated this bearing failure is uncertain because the failure was localized, ductile, and produced no observed loss of system stiffness.



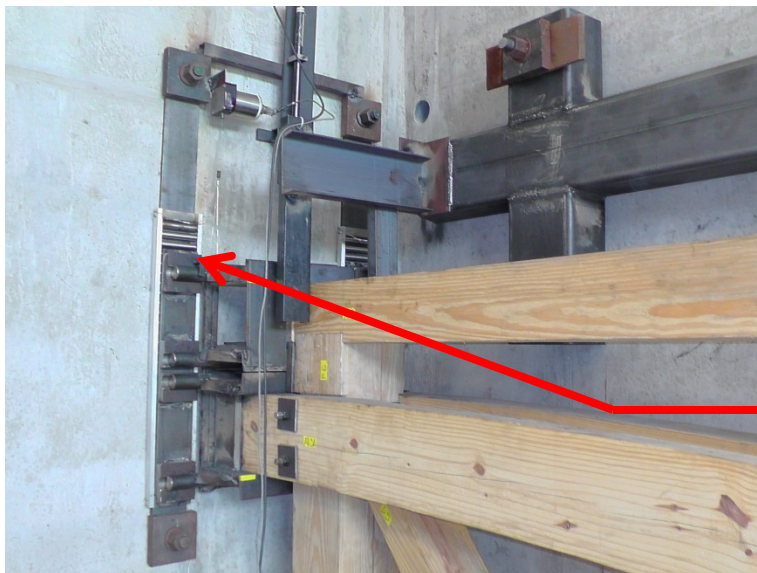
Fig. 63 – Localized bearing failure at mortise-and-tenon joint at top of post 3

The tensile-flexural failure was repaired as shown in Fig. 64, again after a deliberate effort to draw the broken segments together.



Fig. 64 – Repair of tensile-flexural failure in bottom chord stick

Tests 4 and 5 – The truss was again tested on April 8 and 13, 2015. The test on April 8 was stopped because of an observed rotation in the load tree and unequal axial forces in the two Dywidag bars. No damage was observed. The test on April 13 was stopped because the bearings were clearly not displacing freely in the vertical direction. It was then decided to replace the bearings. As described in a previous section, a series of tests was performed to verify the effectiveness of alternate designs. The selected replacement bearings were nested rollers as shown in Fig. 48 and Fig. 65 below.



One of four new roller bearings fabricated to assure free vertical motion at axis of symmetry

Fig. 65 – New roller bearings at wall boundary condition

Test 6 – The final test was performed on May 21, 2015, after the bearings at the axis of symmetry were replaced. Five vertical displacement transducers were installed. Four were at the axis of symmetry, with two at the top and two at the bottom. The fifth was installed at the bottom of post 5. The loading was under displacement control. The electric pump was stopped when loud cracking sounds were heard. During these pauses, at a constant applied displacement, the specimen was briefly inspected. Fig. 66 is a plot of the five measured displacements versus time (the short-duration vertical spikes are electronic noise in one of the displacement transducer channels). The four displacement transducers at the axis of symmetry gave very consistent

results. The vertical displacement under post 5 is very close to the vertical displacements at the axis of symmetry. These displacement data indicate that the bearings at the axis of symmetry indeed allowed the specimen to displace freely vertically at the axis of symmetry. The horizontal portions of the plots reflect times at which the displacement was maintained constant to inspect the specimen. Fig. 66 indicates that the test lasted approximately 27 minutes and 39 seconds. The last constant displacement region began at approximately 26 minutes and 49 seconds and lasted approximately 50 seconds, until failure occurred.

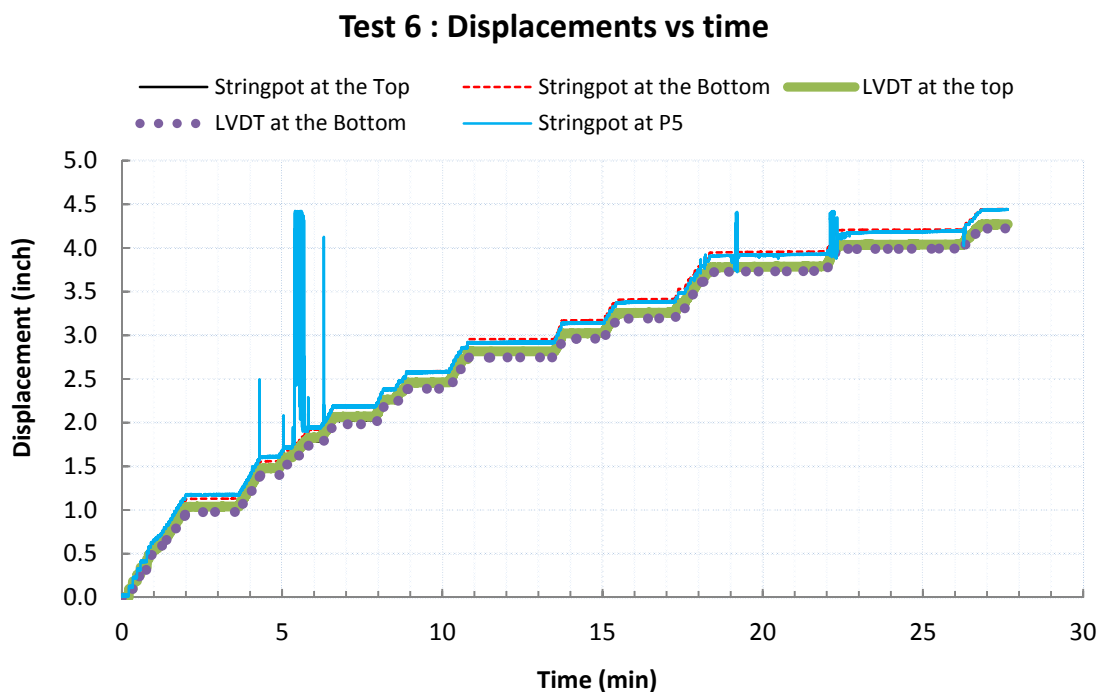


Fig. 66 – Vertical displacements versus time

Fig. 67 shows the applied load versus the vertical displacement at the axis of symmetry. The maximum applied load was 68.8 kips (for a maximum total load of 76 kips). The global truss behavior is generally linear. Some damage, probably cracking, occurred at applied loads in the range 42-48 kips, corresponding to displacements of 2.35" to 2.65", at 8.5–10.5 minutes into the test (see Fig. 66). This damage caused the two decreases in load shown in Fig. 67. With increasing load, additional damage (probably ductile bearing failures perpendicular to the grain) occurred, causing a gradual, relatively small, decrease in truss stiffness until the sudden brittle

failure, which occurred at a midspan displacement-to-span ratio of approximately 1/170, a relatively large value.

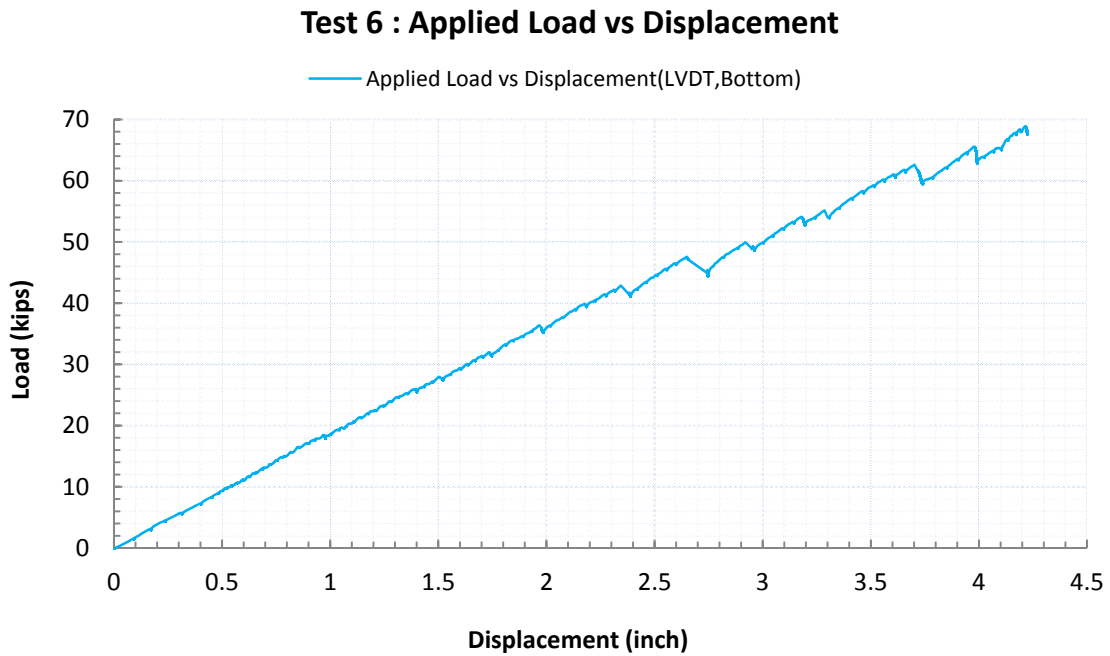


Fig. 67 – Applied load versus vertical displacement at axis of symmetry

Fig. 68 shows time histories of applied load and three strains, two from transducers attached to arch member AR-1A (AA318 and AA316) and one attached to arch member AR-1B (AA317) (the fourth strain transducer did not function). All three strain transducers were near the spring point.

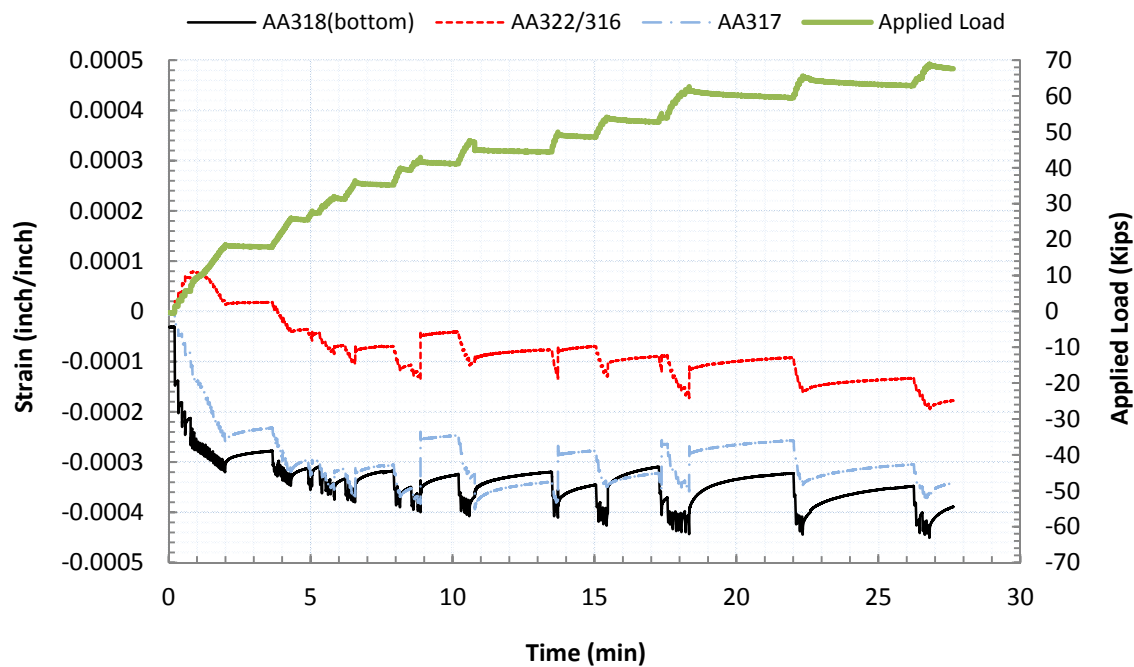


Fig. 68 – Time histories of force and strains

Note that the displacement was maintained constant (see Fig. 66) in the approximate time period from 18.3 to 22 minutes into the test and then again in the period from 22.3 to 26.2 minutes. Fig. 68 shows that in these two time periods there was a slight decrease in applied load, almost surely from wood viscosity. The recorded strain data are not actual total strains, but they do indicate changes in strains as load is increased. Strains increase during the periods when load is increased, and they decrease slightly during periods of constant displacement when the applied load decreases slightly.

During one of the periods at which the displacement was maintained constant, small out-of-plane displacements were observed in the arch sections, specifically in panel 5, as shown in Fig. 69.



Fig. 69 – Small out-of-plane displacements of arch section in panel 5

The failure – As noted, loading was stopped at about 26 mins and 49 secs, and a brittle tensile failure occurred in post P4 approximately 50 seconds later. Therefore it was a delayed, viscous-type failure. The moment of failure was captured in a short video clip, accessible at:

<https://www.nps.gov/hdp/project/coveredbridges/surveys.htm#burr>

In addition, the first twenty frames (approximately 0.67 seconds) have been assembled in a PDF file, also accessible at: <https://www.nps.gov/hdp/project/coveredbridges/surveys.htm#burr>

Fig. 70 shows the origin of the failure at a knot in post P4. Because the failure was sudden, a *dynamic* release of elastic strain energy occurred, principally from the arch, causing the arch and the entire truss to displace vertically upward, which led to several other secondary failures. Figs. 70 and 71 show the splitting failure and the shear failure in bottom chord BC-2B at the fishplate joint.

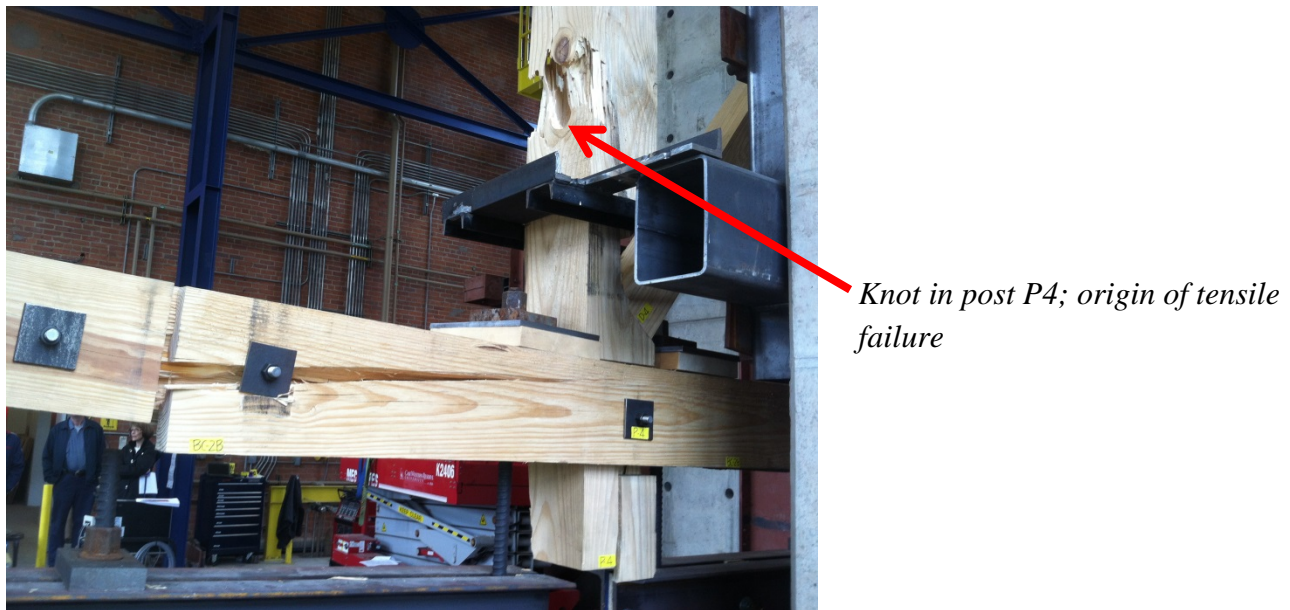


Fig. 70 – Tensile failure in post P4



Fig. 71 – Secondary shear failure in bottom chord BC- 2B at fishplate joint

A secondary shear-tensile failure also occurred at the end of post P3, as shown in Fig. 72.



Location of secondary shear failure

Fig. 72 – Secondary shear failure at bottom of post 3

Bottom chord BC-2A also had a tensile-flexural failure where the cross-section had been reduced to affect a repair, as shown in Fig. 73. An overall view of the failed truss can be seen in Fig. 74.



Fig. 73 – Secondary tensile-flexural failure in bottom chord BC-2A



Fig. 74 – Overall view of failed Burr-arch truss specimen

During disassembly of the truss, observations were made on additional, less-visible damage caused by the total load of 76 kips. Crushing perpendicular to the grain was observed at several locations as shown in Fig. 75 through 77.



Fig. 75 – Crushing perpendicular to the grain in post 3, at its tenon housing



Fig. 76 – Crushing perpendicular to the grain in arch segment at its intersection with post

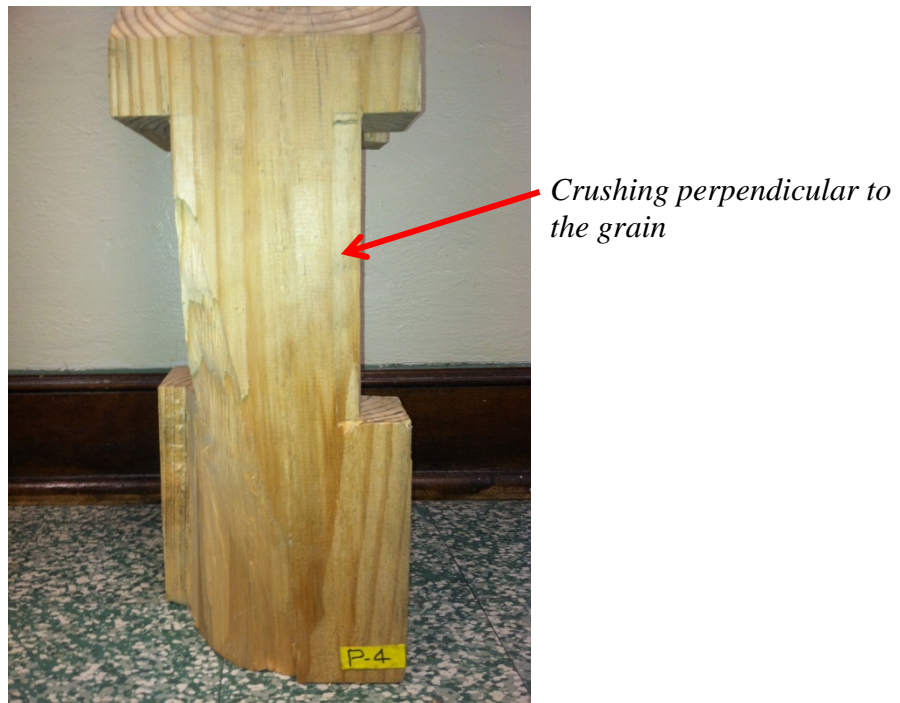


Fig. 77 – Crushing perpendicular to the grain in post P4 at its intersection with the bottom chord

Other than the localized damage at the axis of symmetry caused by the test fixture failure, the top chord had no detectable damage from the tests, although section TC1 warped as its moisture content decreased while in the structures laboratory. The diagonals similarly had no detectable damage. Although some crushing perpendicular to the grain occurred at their intersections with the posts, the arch segments had no other detectable damage. No observable distress occurred at the arch-bottom chord intersection and in the arch segment below the bottom chord.

OBSERVATIONS

The overall objective of the research was to increase understanding of the design and structural behavior, specifically strength, of the Burr-arch truss. To gain a perspective on design variations, twenty-one historic Burr-arch truss bridges in Pennsylvania, Ohio, and Indiana were inspected, and drawings for nine other bridges were reviewed. The observations reported here complement and elaborate on the work of Joseph Conwill.⁴⁶ Two important features of any design are the method used to pass the arches by the bottom chord and the connection between the bottom

⁴⁶ Conwill, "Burr Truss Framing."

chord and the arch. Other important details include the eccentricities of the diagonals, the depths of daps at member intersections, and the length of shear relishes. There is an ongoing discussion on the historic method used to construct Burr-arch trusses. The authors' judgment is that the sensible method is to transfer some or all the dead load to the trusses to tighten the joints prior to engaging the arches. In any case, it is very likely that some (pre)stresses are induced in a Burr-arch truss during fabrication and erection because it is highly statically indeterminate.

A synthesis of previous analytical studies on joint and system linear elastic behavior is presented. Emory Kemp and John Hall completed pioneering linear elastic modeling.⁴⁷ They emphasized the importance of the arch-bottom chord connection in controlling structural behavior. They realistically stated the strengths and limitations of linear elastic modeling in the context of tolerances for actual traditional timber joinery and the viscous, hygroscopic behavior of wood. Additional linear elastic studies should be performed on the effects of a finite stiffness for the arch thrust bearing or the effects of small, prescribed displacements at the thrust support.

There are a limited number of prior experimental studies, possibly because of the daunting number of parameters associated with wood structures. To the authors' knowledge, large-scale experimental studies on the *strength* of Burr-arch trusses have not been previously performed.

Although statically indeterminate, a Burr-arch truss is not a pure parallel-ductile system. Shear, tension, and flexural failures are generally brittle. One such brittle failure does not necessarily lead to system failure, but it seems that a "weak link" model, *applied to both members and connections*, is the only currently-practical approach for estimating system strength. The conservatism of such an approach is, however, unknown.

A primary criterion for the design of the specimen used for the study was that it had to be large scale, using only heavy timber sections and traditional timber joinery. This was to avoid issues of scaling of connections and buckling stability of members. With a large scale, however, the physical dimensions of the laboratory imposed the limitation of having to use a symmetry model,

⁴⁷ Kemp and Hall, "Case Study of Burr Truss Covered Bridge."

loaded symmetrically. Acquiring kiln-dried, select structural, heavy timber sections with long lengths requires research, careful consideration, persistent attention, and verification as it is quite different from ordering A572-steel wide flange sections, for example.

A limited, but informative, set of small-scale, along-grain axial compression and shear strength tests were performed. The results provide insights on the ratios of shear area to compressive area at which there is a transition from a shear failure to a compressive failure, based on actual measured strength data.

Fabrication of the test fixture was performed in-house. The thrust bearing, lateral bracing, and the load tree functioned well. But the sliding bearings at the axis of symmetry did not function as expected and had to be replaced. A series of tests was performed that showed that nested rollers (an old, traditional design!) indeed allowed essentially free vertical motion at the axis of symmetry.

The dry winter conditions in the laboratory caused significant cracking (heart checks) due to decreases in wood moisture content during a two-month period from December 10, 2014, to February 10, 2015. The 8x8 posts, most of which were Grade 1 SYP, experienced the most severe heart checking.

In the context of assessing or load rating existing historic Burr-arch truss bridges, the strength tests that were performed have obvious limitations:

- One specimen, with one set of details;
- One species of wood (SYP), with Grade 1 and select structural newly harvested members;
- One, symmetric, loading;
- No wood degradation (other than shrinkage cracking);
- No large geometric imperfections such as out-of-plane arches; and
- No floor and lateral bracing system models.

Nonetheless, the following observations may be made.

Failure of the scarf joint – The two chord sticks certainly had different axial and flexural stiffnesses; therefore, each carried a different fraction of the total axial force and bending moment. The failure was brittle, but the unbroken chord stick was able to carry the additional forces shed by the broken scarf joint. The authors are not aware of any analytical method for estimating the strength of a scarf joint with a vertical table subject to axial tensile force and bending moment.

Failure of bottom-chord stick – As noted, any pair of sticks invariably have different stiffnesses and hence different demands. The failure occurred at a cross-section that was reduced by a dap, with a re-entrant corner, and at the location of two small knots. The failure was brittle, but again the unbroken stick was able to carry the additional forces shed by the ruptured member.

Failure in post P4 – The failure was primarily from axial tension, although the post also carried moment and shear. The failure originated at a large (2.5" to 3") knot; the capacity would have been larger if the knot had not been there. P4 was not the post with the largest axial, shear, and moment demands. The failure was completely brittle, causing a dynamic release of strain energy and several secondary failures. The failure was time-delayed; it occurred about 50 seconds after the last displacement increment. For an actual bridge subject to a controlled load rather than a controlled displacement, it is very likely that the entire bridge floor would have collapsed. The load at which the failure occurred was very large, corresponding to a total load of 152 kips (2*76 kips), for one complete Burr-arch truss.

Other observed damage/distress – Crushing perpendicular to the grain occurred at several locations. This damage was localized, ductile, and caused relatively small decreases in global stiffness. Some small out-of-plane bending occurred in the arch in panel 5. This was probably caused by non-uniform bearing stresses at the lap splices in the arch but may have been a result of some imperfection at the symmetry boundary.

Practically no damage occurred in the diagonals, arches, and top chord. Similarly, the area around the arch-to-bottom-chord intersection had no observed distress. Of course this would surely be different under an asymmetric quarter-span gravity load.

The overall observations are that the strength was flaw controlled and connection controlled and that the strength behavior was brittle, but augured by audible damage. Because the strength was flaw controlled, the observed capacity of 152 kips under a symmetric load cannot be scaled to Burr-arch trusses of longer or shorter spans.

RECOMMENDATIONS

- Analytical models should reflect the actual construction process used, specifically the sequence of releasing the falsework and engaging the arches.
- Analytical studies with finite thrust bearing stiffnesses and/or prescribed bearing movements, will provide additional insights on structural behavior.
- Analytical studies should model the finite stiffness/flexibility of the connection between the arch and the bottom chord. Experimental studies are needed to verify analytical models.
- Experimental studies on the strength of traditional timber connections, specifically those subject to combined tension and flexure, are needed.
- Strength assessments should include connections, including depths of daps and lengths of relishes, and, possibly, wood imperfections.
- If sawn lumber is used, grading rules must be closely followed. Quarter-sawn wood will probably have better dimensional stability under moisture content changes.

Quantitative analytical studies of the temporal effects of wood viscosity and hygroscopicity would improve understanding of long-term structural behavior, specifically the long-term changes in dead load member forces.

ACKNOWLEDGEMENTS

We thank David Simmons, James Cooper, Campbell Fitzhugh, Linda Gasparini, Laura Rendos, Michael Butler, Rudy and Laura Christian, Andrew Schaeffer, Vincent Marvin, Jim Berilla, and Neil Harnar for assisting with the research. We would also like to thank the following for their peer review: Robert Brungraber, Steven Buonopane, Joseph Conwill, Robert Durfee, Christopher Marston, Philip Pierce, and David Simmons.

REFERENCES

- Brungraber, Robert L. "Traditional Timber Joinery: A Modern Analysis." PhD Dissertation, Stanford University, July 1985.
- Burr, Theodore. "McCall's Ferry-Bridge." *Niles' Weekly Register*, 18 November 1815, 200-202.
- "Burr-Arch Truss Experiment" [video]. Case Western Reserve University, 2015. Available at: <https://www.nps.gov/hdp/project/coveredbridges/surveys.htm#burr>, accessed June 20, 2016.
- Conwill, Joseph D. "Burr Truss Framing." *Timber Framing* 78 (December, 2005): 4-11.
- Fanou, Fouad, Douglas Rammer, and Terry Wipf. "Simplified Analytical Model for a Queen-Post Covered Timber Bridge." Madison, WI: U.S. Department of Agriculture, Forest Service, Forest Products Laboratory, 2013. Available at: http://www.woodcenter.org/docs/ICTB2013/technical/papers/ID_84_Fanou.pdf, accessed March 25, 2016.
- Fridley, Kenneth J. "Designing for Creep in Wood Structures." *Forest Products Journal* 42, no. 3 (1992): 23-28.
- Gasparini, Dario, Jay Bruckner, and Francesca da Porto. "Time-Dependent Behavior of Posttensioned Wood Howe Bridges." *ASCE Journal of Structural Engineering* 132, no. 3, (2006): 418-429.
- Gibson, Lorna J. and Michael F. Ashby. *Cellular Solids: Structure & Properties*. Oxford: Pergamon Press, 1988.

Gould, George E. *Indiana's Covered Bridges Thru the Years*. Indianapolis: Indiana Covered Bridge Society, 1977.

Haupt, Herman. *General Theory of Bridge Construction*. New York: D. Appleton and Company, 1866.

Hosteng, Travis James Wacker, and Brent Phares. "Live Load Testing of Historic Covered Bridges." International Conference on Timber Bridges, Las Vegas, Nevada, 2013. Available at: http://www.woodcenter.org/docs/ICTB2013/technical/papers/ID_124_Hosteng2.pdf, accessed March 25, 2016.

Jelly, Irving A. "Anatomy of an Old Covered Bridge." *Civil Engineering* 11, no. 1 (January 1941): 12-14.

Kemp, Emory L. and John Hall. "Case Study of Burr Truss Covered Bridge." *ASCE Engineering Issues-Journal of Professional Activities* 101, no. E13 (July 1975): 391-412.

Lamar, Dylan and Benjamin Schafer, "Structural Analysis of Historic Covered Wooden Bridges," *Journal of Bridge Engineering* 9, no. 6 (December 2004): 623-33.

Lewandoski, Jan. "Review of *America's Covered Bridges*, by Terry Miller and Ronald Knapp." *Timber Framing* no. 117 (September 2015): 2-6.

Machtemes, Allison. "Investigation of the Structural Behavior of Historical Covered Timber Bridges." Master of Science thesis, Iowa State University, 2011. Available at: <http://lib.dr.iastate.edu/cgi/viewcontent.cgi?article=1179&context=etd>, accessed March 25, 2016.

Mileo, Michael A. "Photoelastic Stress Analysis of a Burr Truss Covered Bridge." Master of Science thesis, Bucknell University, April 1982.

Miller, Joseph F., Richard J. Schmidt, and William M. Bulleit. "New Yield Model for Wood Dowel Connections." *ASCE Journal of Structural Engineering* 136, no. 10 (October 2010): 1255-1261.

Miller, Joseph F. and William M. Bulleit. "Analysis of Mechanically Laminated Timber Beams Using Shear Keys." *ASCE Journal of Structural Engineering* 137, no. 1 (January 2011): 124-132.

National Design Specification, ANSI/AWC NDS-2012. Leesburg, VA: American Wood Council, 2012.

Rammer, Douglas and Fouad Fanous, "Research in Progress: Improved Modeling of Historic Covered Bridges—Phase II." Madison, WI: U.S. Department of Agriculture, Forest Service,

Forest Products Laboratory, 2013. Available at: <http://www.woodcenter.org/docs/fplrrip-4719-018-Rammer-FHWA.pdf> , accessed March 25, 2016.

Salkowski, Albert S. "Reconstructing a Covered Timber Bridge." *Civil Engineering* (October 1963): 36-39.

Sangree, Rachel and Benjamin Schafer. "Experimental and Numerical Analysis of a Halved and Tabled Traditional Timber Scarf Joint." *Construction and Building Materials* 23 (2009): 615-624.

Sangree, Rachel and Benjamin Schafer. "Experimental and Numerical Analysis of a Stop-splayed Traditional Timber Scarf Joint with Key." *Construction and Building Materials* 23 (2009): 376-385.

Sangree, Rachel and Benjamin Schafer. "Field experiments and numerical models for the condition assessment of historic timber bridges: Case study." *Journal of Bridge Engineering* 13, no. 6 (November 2008): 595-601.

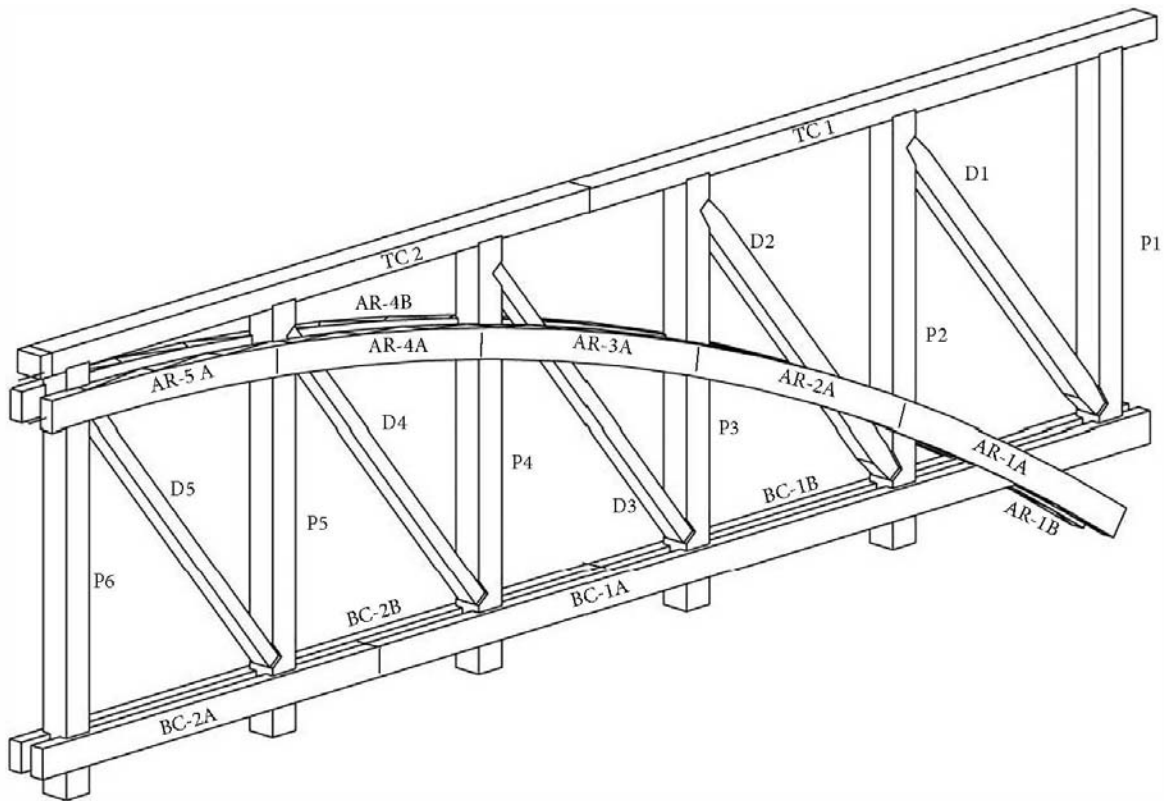
Sangree, Rachel and Hannah Blum, *Gilpin's Falls Covered Bridge*, HAER MD-174, 2009-2012 (<http://www.loc.gov/pictures/collection/hh/item/md1889/>).

Schafer, Benjamin and Dylan Lamar, *Pine Grove Bridge*, HAER PA-586, 2004. <http://www.loc.gov/pictures/collection/hh/item/pa3945/>

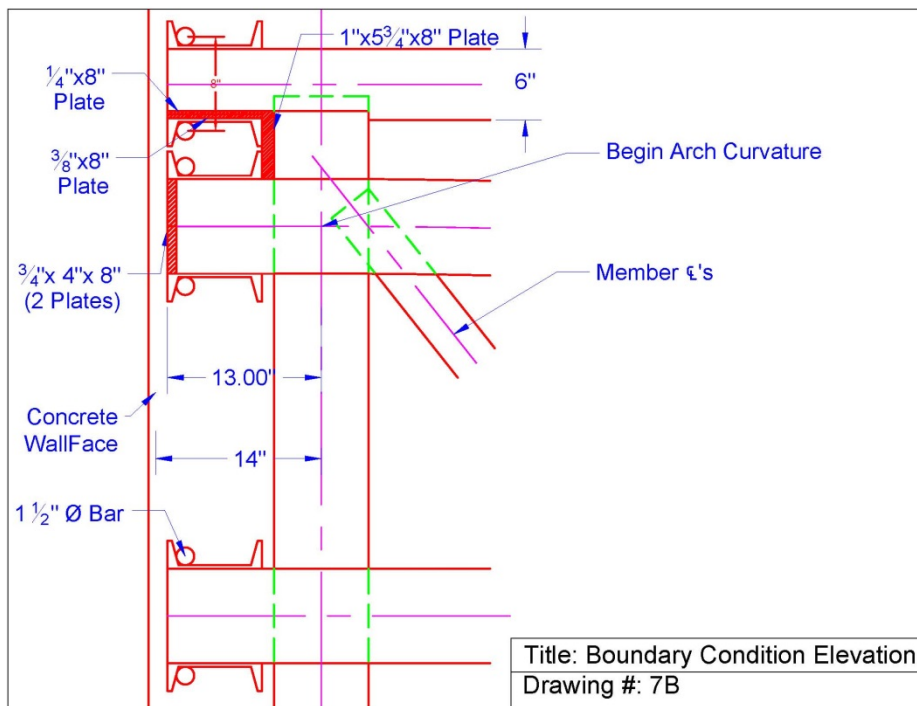
Wood Handbook of the Forest Products Laboratory, Madison, WI. U.S. Department of Agriculture, Forest Service, Forest Products Laboratory, 2010. Available at: http://www.fpl.fs.fed.us/documnts/fplgtr/fpl_gtr190.pdf, accessed March 25, 2016.

APPENDIX A – DRAWINGS

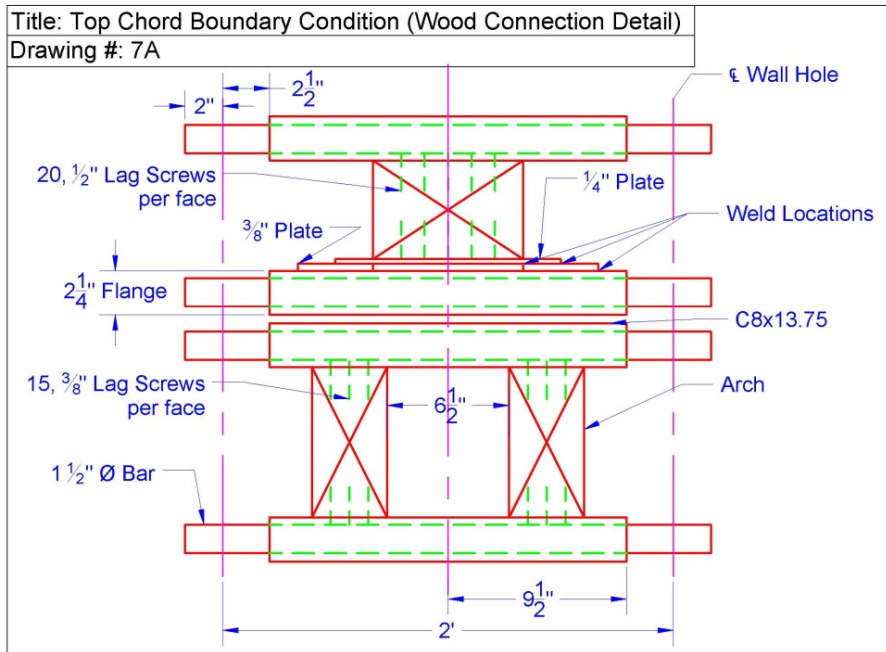
All drawings by the authors: Dario Gasparini, Stacey Hursen, Gregory Willenkin,
and Kamil Nizamiev



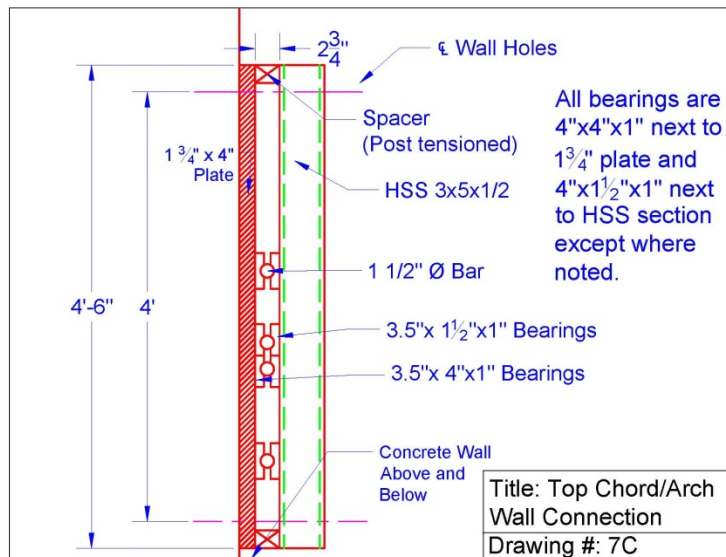
Drawing A-0



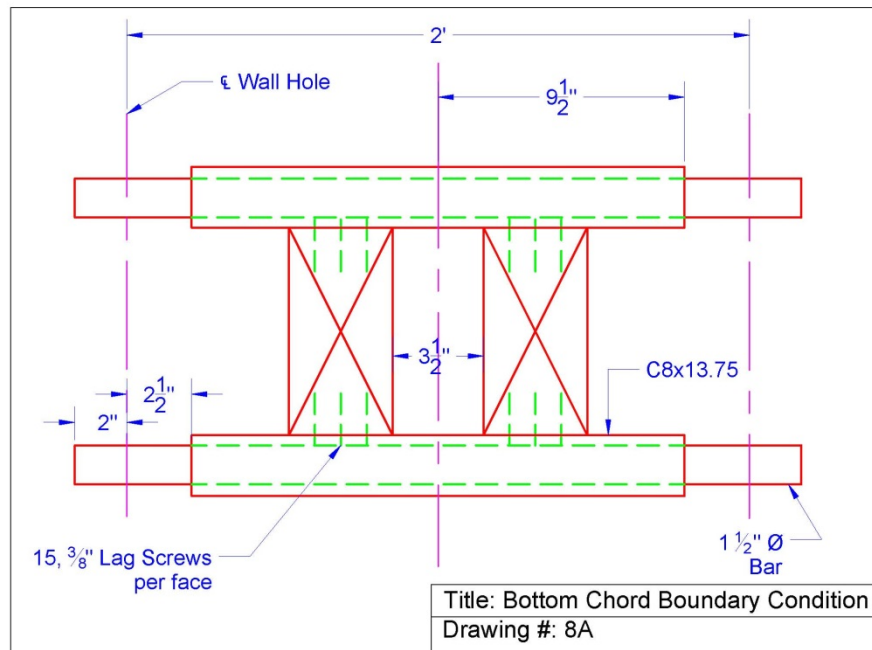
Drawing A-1



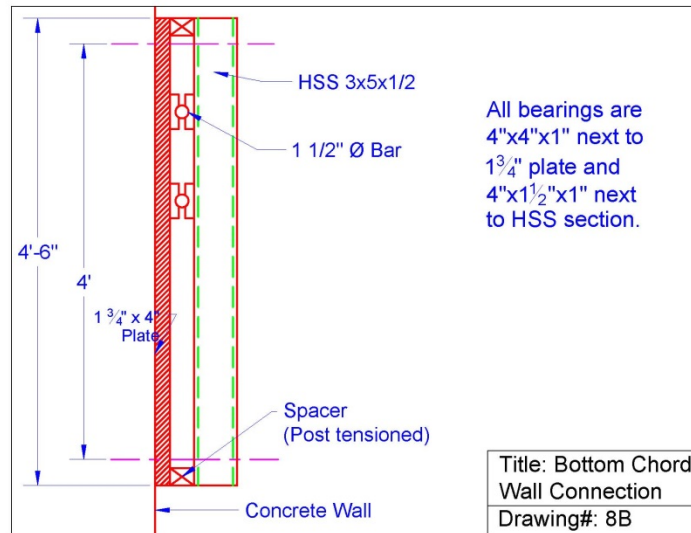
Drawing A-2



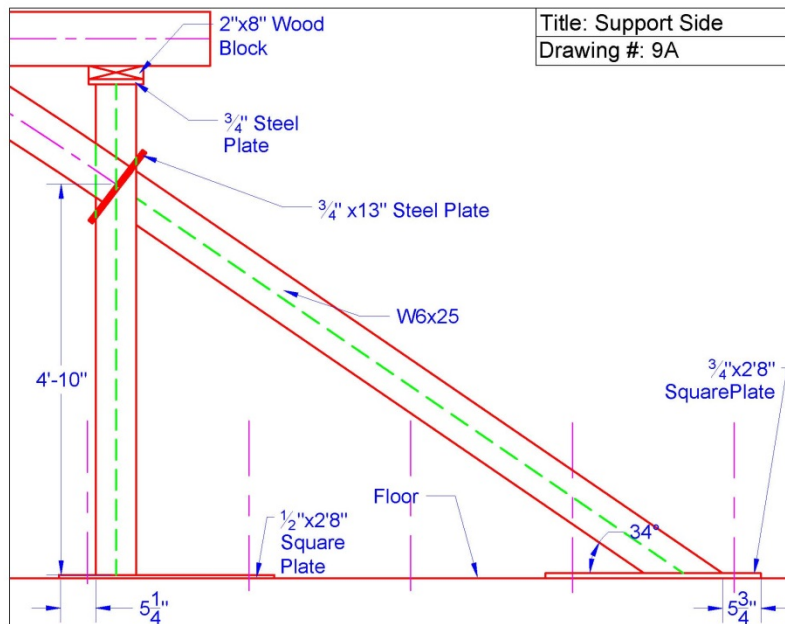
Drawing A-3



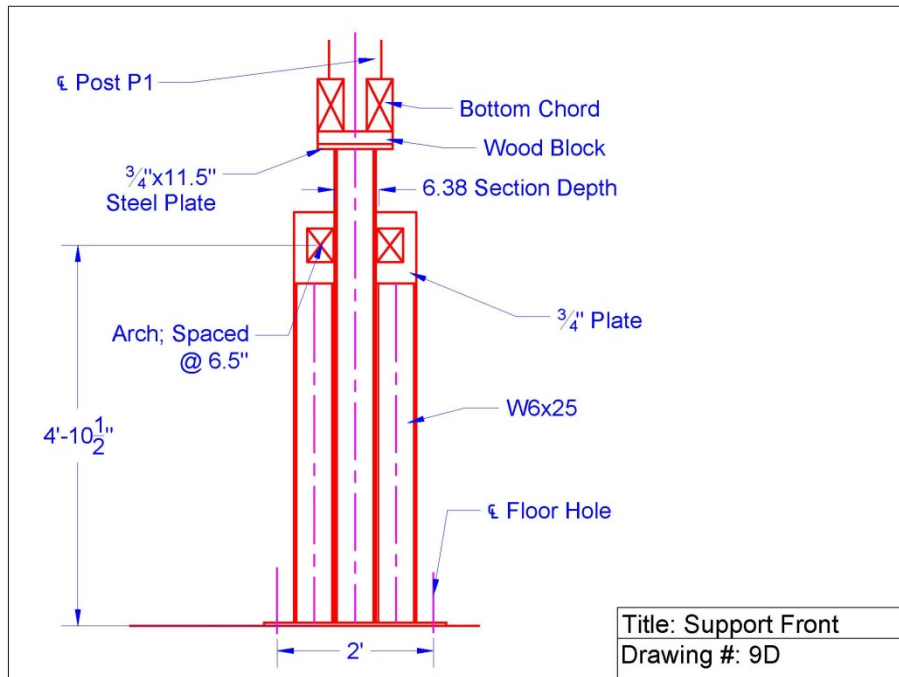
Drawing A-4



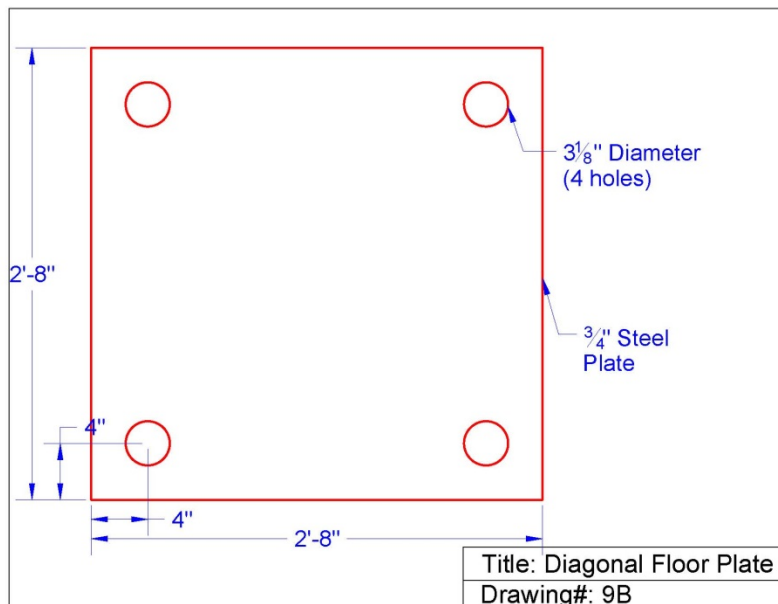
Drawing A-5



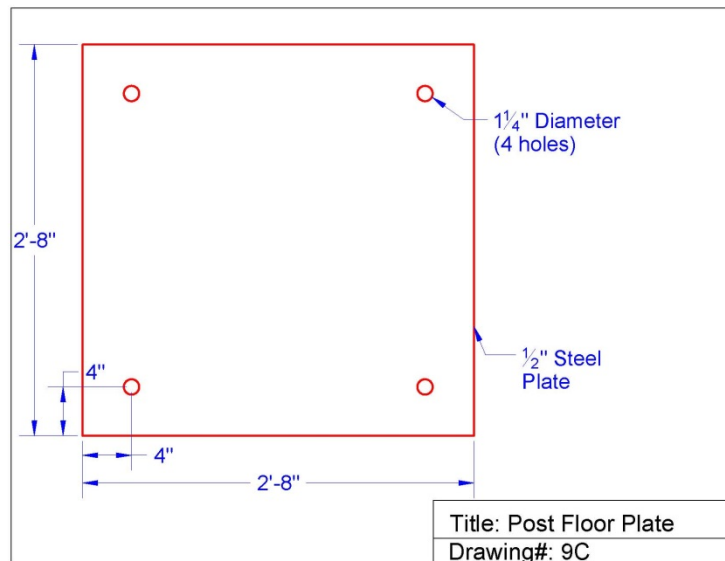
Drawing A-6



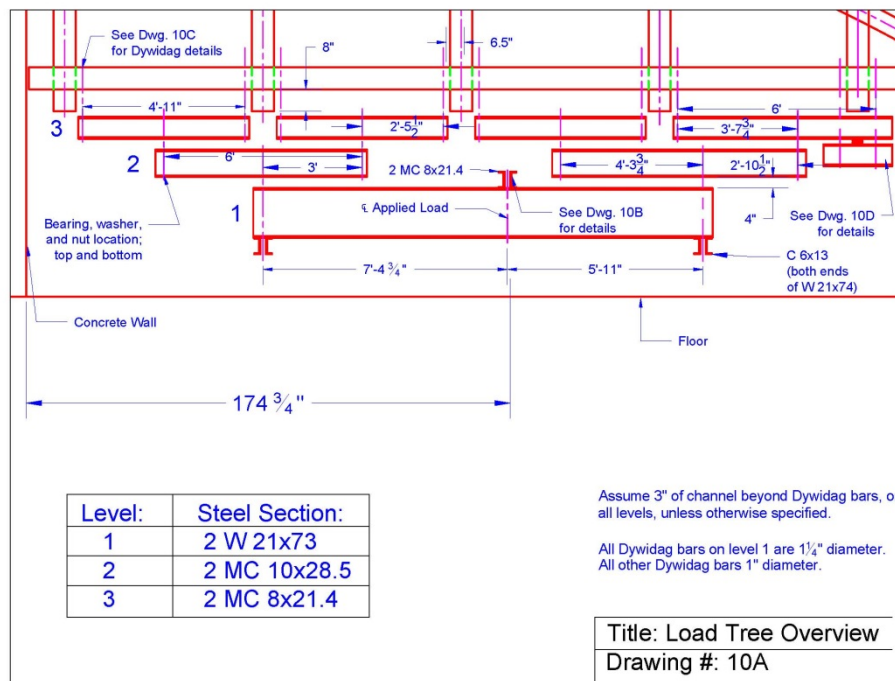
Drawing A-7



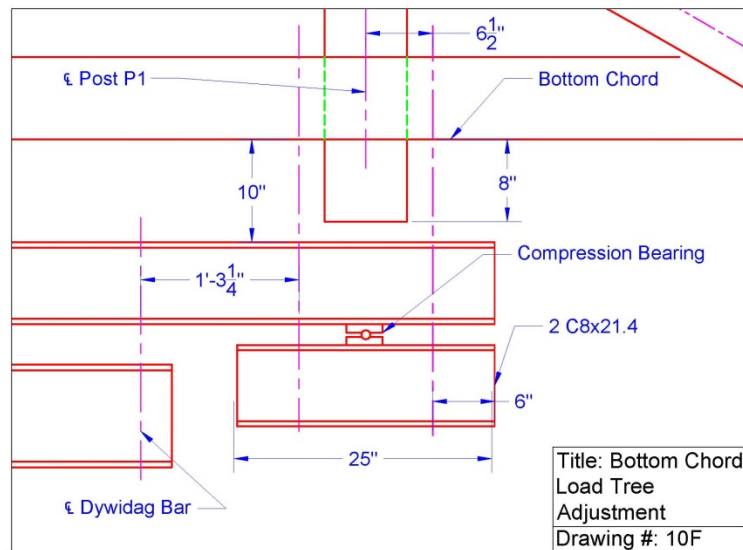
Drawing A-8



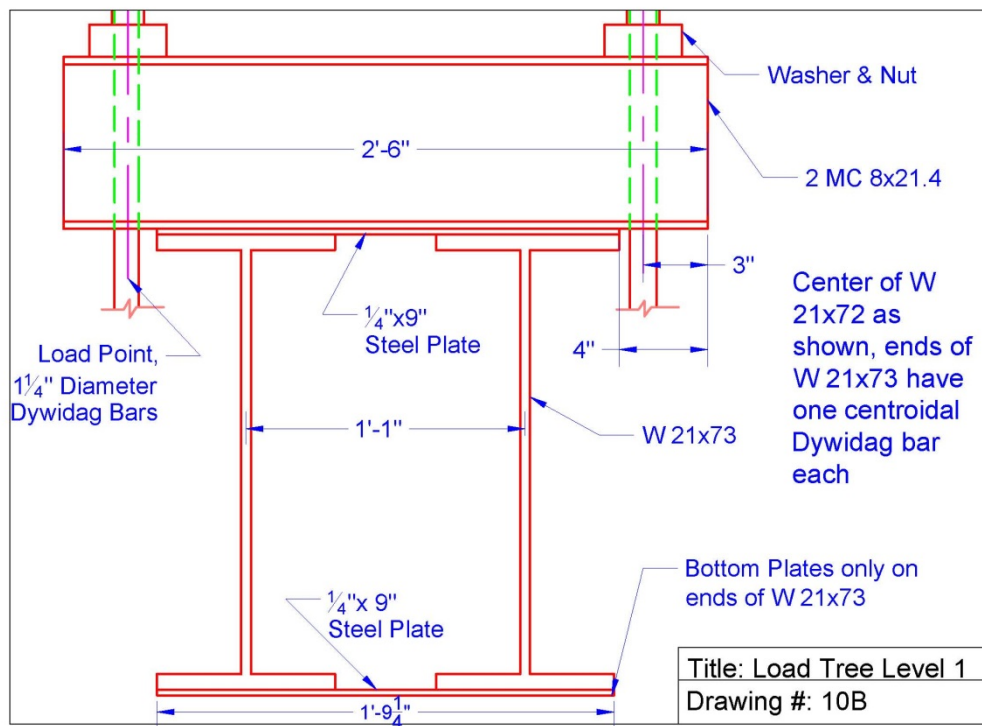
Drawing A-9



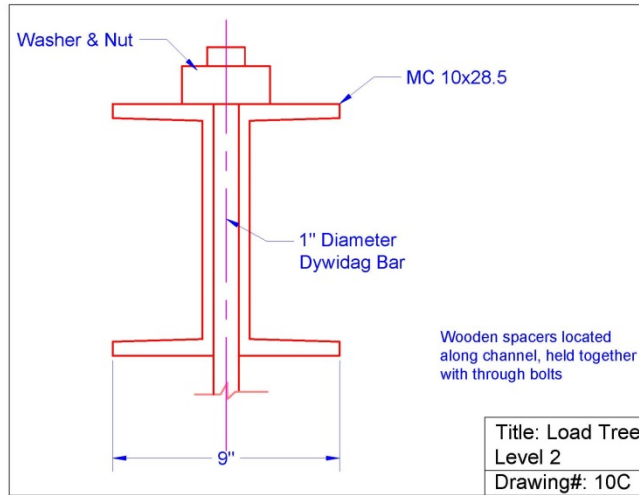
Drawing A-10



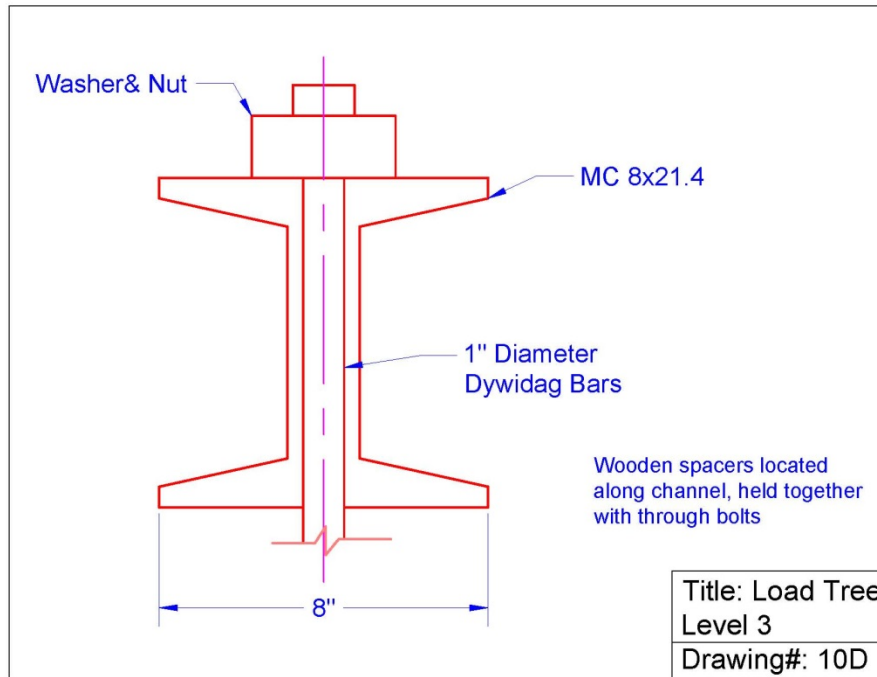
Drawing 11



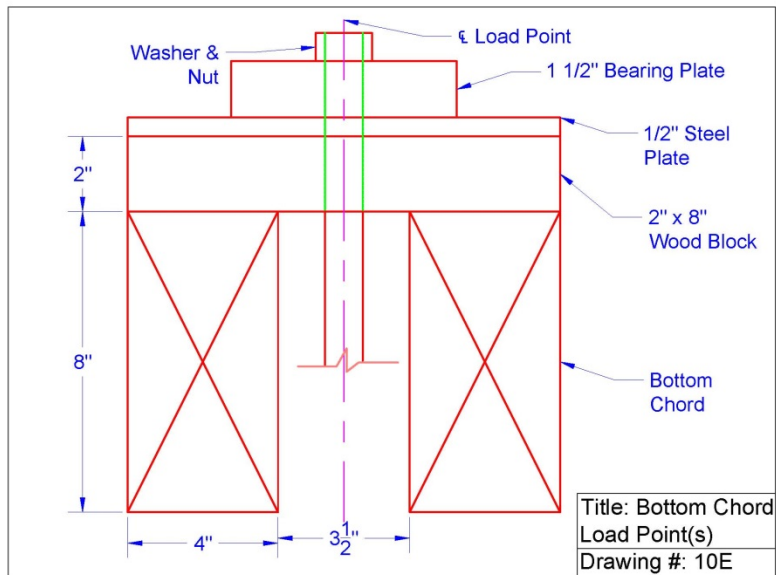
Drawing A-12



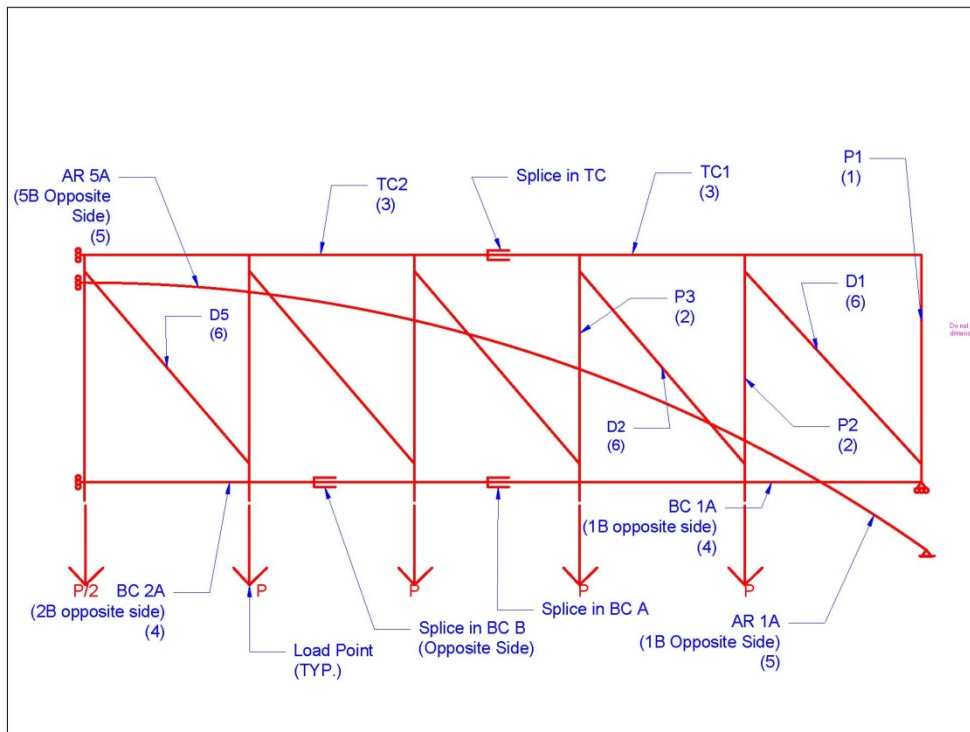
Drawing A-13



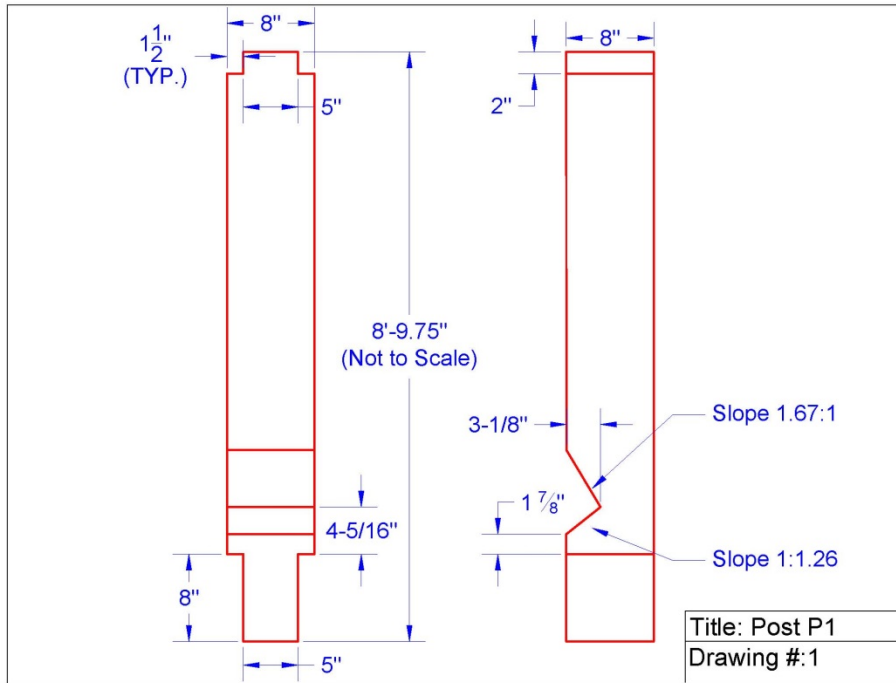
Drawing A-14



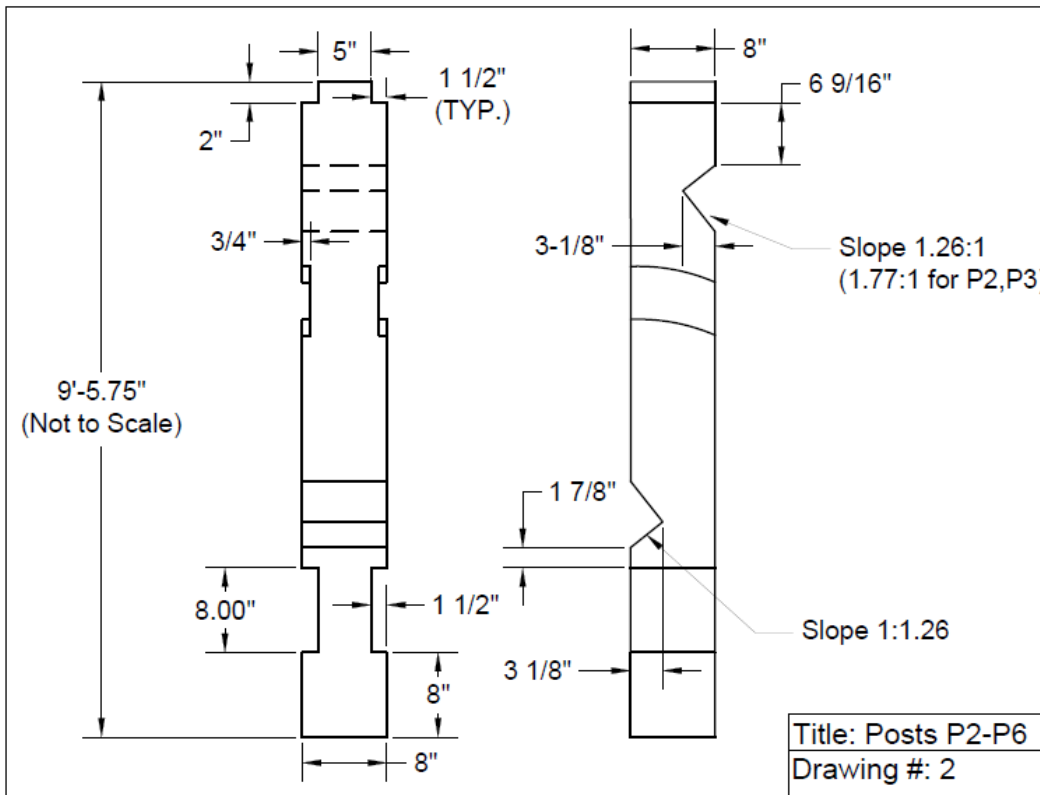
Drawing A-15



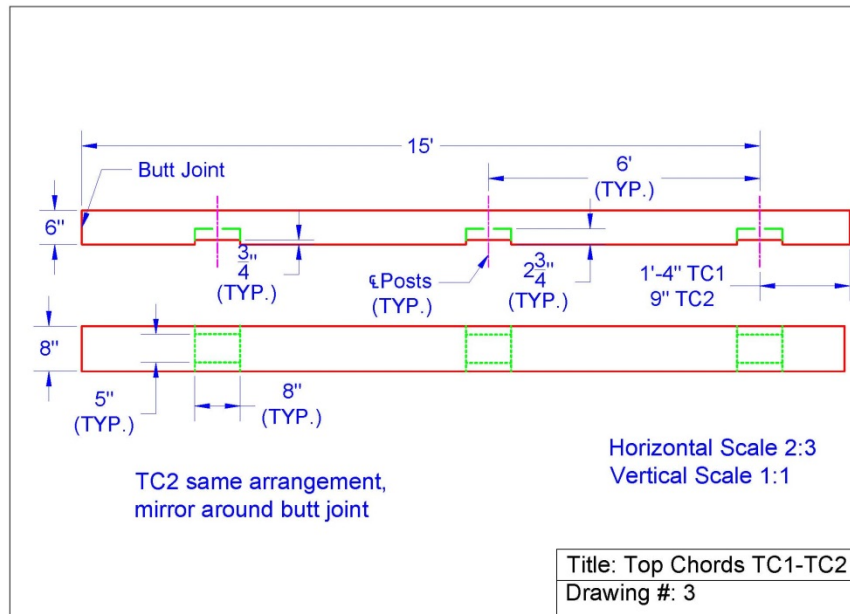
Drawing A-16



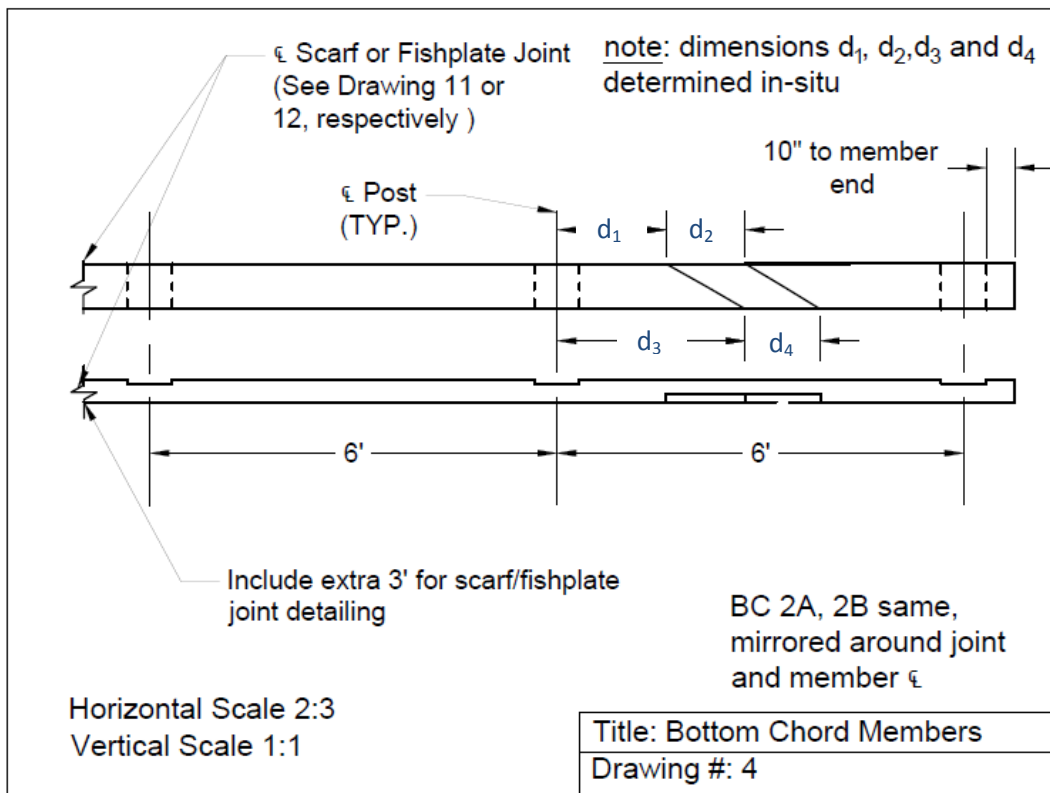
Drawing A-17



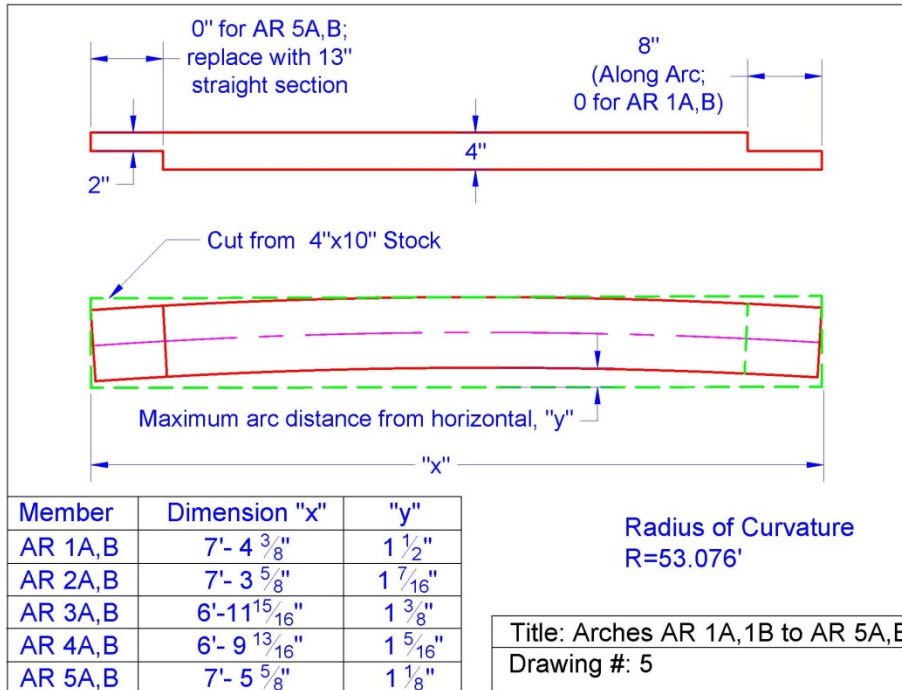
Drawing A-18



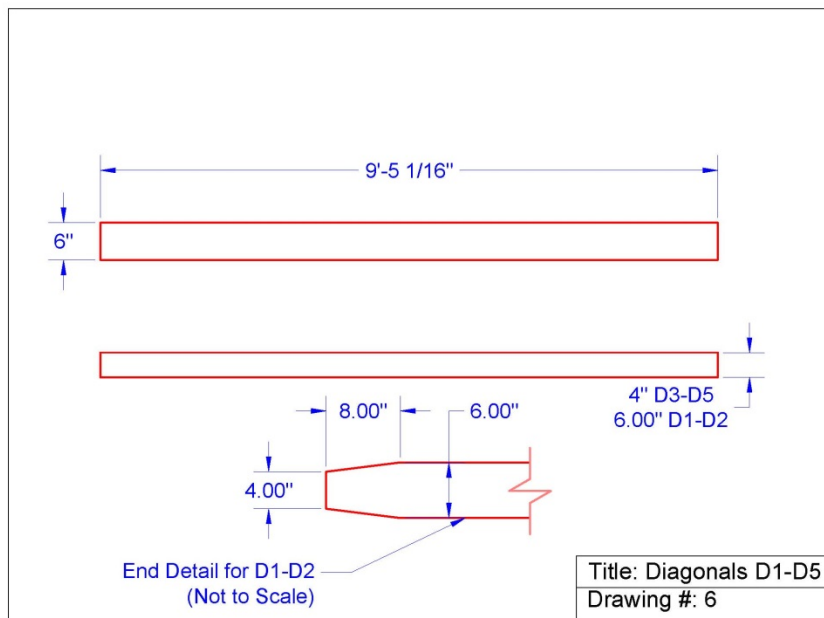
Drawing A-19



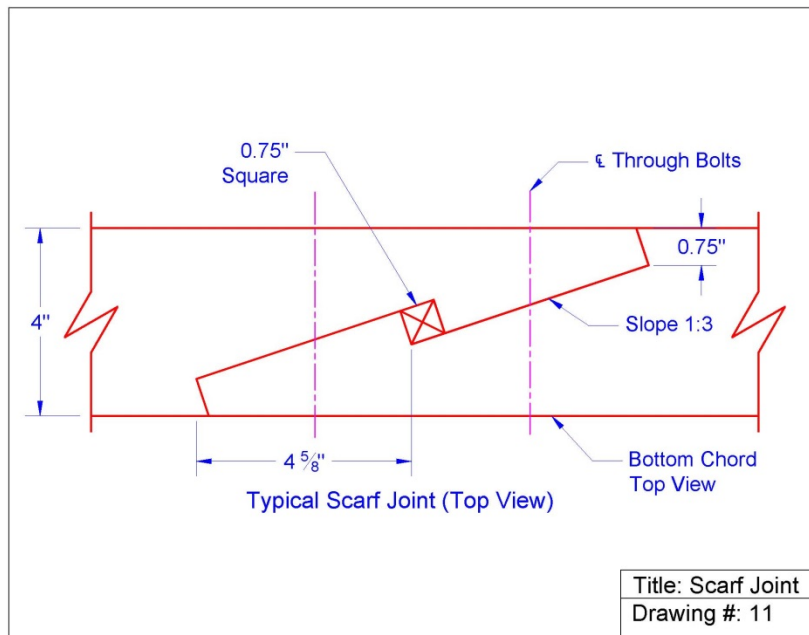
Drawing A-20



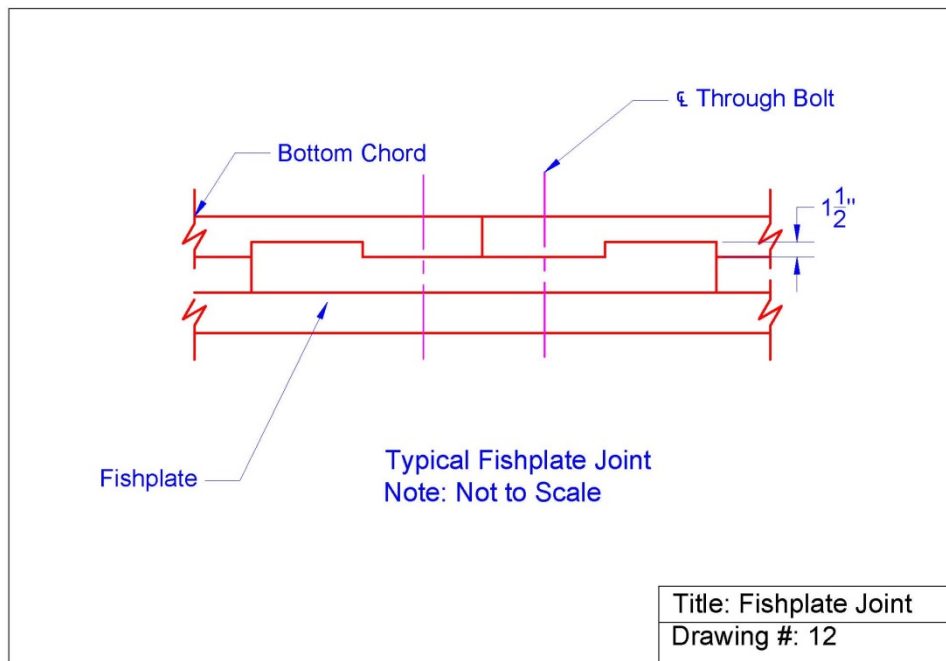
Drawing A-21



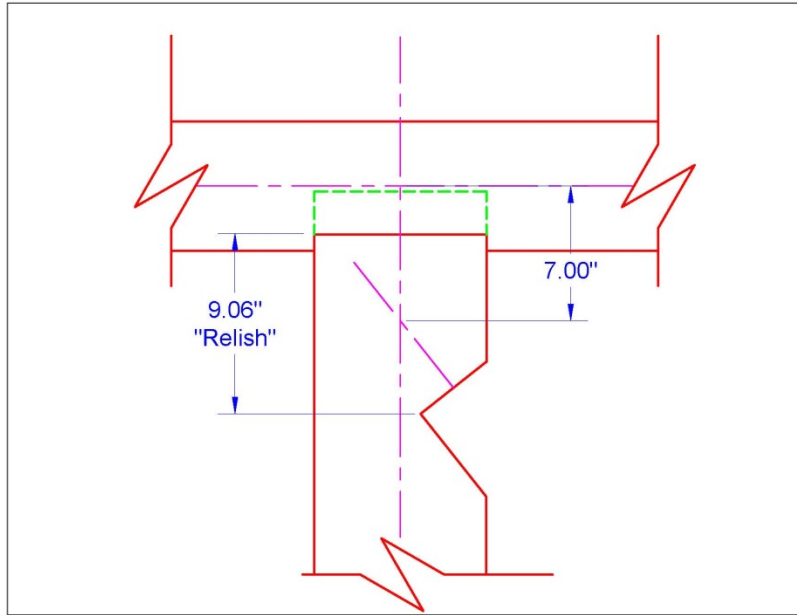
Drawing A-22



Drawing A-23



Drawing A-24



Drawing A-25